Patient-derived cancer cells to dissect the molecular basis of treatment response in primary liver cancer: a mechanistic and functional approach

Dissertation

Zur Erlangung des Grades

Doktor der Naturwissenschaften

am Fachbereich Biologie

der Johannes Gutenberg-Universität Mainz

vorgelegt von Darko Častven

geboren am 24.12.1988 in Sremska Mitrovica, Serbien

Mainz, März 2019

Erklärung

Hiermit erkläre ich an Eides statt, dass ich diese Arbeit selbständig verfasst und keine anderen als die angegebenen Quellen und Hilfsmittel verwendet habe.

Ort, Datum	Darko Častven

Dekan:

1. Berichterstatter:

2. Berichterstatter:

Tag der mündlichen Prüfung:

29.10.2019

Acknowledgements

Abstract

Hepatocellular carcinoma (HCC) and cholangiocarcinoma (CCA) are two major types of primary liver cancers (PLC), ranking among the deadliest cancers worldwide with poor overall survival rates. Lack of clinical symptoms and effective biomarkers for early detection are main causes of late diagnosis. Despite identification of several potentially drugable targets and subsequent development of next-generation targeted therapies, translation of these findings into clinical practice remains challenging. Further, there is a lack of models that truly and accurately represent morphological and molecular heterogeneity of original tumors. Therefore, development of primary culture models that closely recapitulate phenotypic and molecular diversities of PLC is urgently needed to support a translation from laboratory studies to the bedside and improve patient outcome.

In the here presented thesis, we report successful establishment and detailed characterization of seven patient-derived liver cancer cell lines (PDCL) from HCC and intrahepatic CCA. Morphological and histological characteristics of obtained cell lines and xenograft tumors were analyzed and compared to original tumors. Tumor grading and genomic stability were further assessed to determine background setting for successful PDCL establishment. Time course analyses of transcriptomic and genomic changes were performed using next-generation sequencing (NGS) to characterize and generate molecular profiles of newly derived PDCL and investigate how accurately they recapitulate original cancer tissue. Key oncogenic alterations were identified by targeted NGS and cell lines carrying potentially actionable mutations were treated with corresponding specific inhibitors. Long-term cultivation effect on treatment response to classic chemotherapeutics was monitored.

Our results show that PDCL fully resembled morphological features of the primary cancers *in vitro* and *in vivo* over extended period in culture. We also provide evidence that less differentiated tumors with higher genomic instability possess a higher likelihood of successful PDCL establishment. Genomic analyses confirmed that PDCL retain similar profile as corresponding primary tumors during long-term culturing. Targeted-NGS demonstrated that key oncogenic alterations such as *TP53, KRAS, CTNNB1* as well as actionable mutations (e.g. *MET, KIT, KDR*) were highly conserved in PDCL and amenable for individualized therapeutic approaches. Integrative genomic and transcriptomic approaches further demonstrated that PDCL more closely resemble molecular and prognostic features of PLC than established cell lines.

Our integrative analysis demonstrates that PDCL represents refined model for discovery of relevant molecular subgroups and exploration of precision medicine approaches for the treatment of primary liver cancer.

Zusammenfassung

Primäre Lebertumore (PLC) zählen zu den häufigsten und tödlichsten Krebsarten weltweit. Klinisch werden PLCs in Hepatozelluläre Karzinome (HCC) und Cholangiokarzinome (CCA) unterteilt. Fehlende spezifische Symptome und verlässliche Biomarker für eine Früherkennung sind Hauptgründe für eine späte Diagnose, so dass die Möglichkeit von kurativen Therapieverfahren meist begrenzt ist. Trotz der Identifizierung mehrerer potenzieller Zielmoleküle und Entwicklung zielgerichteter Therapien bleibt die Translation dieser Ergebnisse in die klinische Praxis eine Herausforderung. Zudem gibt es keine verlässlichen Modelle, die morphologische und molekulare Heterogenität der ursprünglichen Tumore umfänglich und präzise widerspiegeln. Die Entwicklung von Primärkulturmodellen, welche die phänotypischen und molekularen Eigenschaften von PLC rekapitulieren, ist dringend erforderlich für eine erfolgreiche Übertragung der Ergebnisse von Laboruntersuchungen in die klinische Praxis.

In der hier vorliegenden Arbeit wurden sieben neue Patienten-abgeleitete Leberkrebszelllinien (*patient-derived cell lines*; PDCL) erfolgreich generiert und umfassend charakterisiert. Die morphologischen und histologischen Eigenschaften der Zelllinien sowie der entsprechenden Xenograft-Tumore wurden analysiert und mit den ursprünglichen Tumoren verglichen. Tumor-Grading und die genomische Stabilität wurden erfasst, um die Voraussetzungen für eine erfolgreiche PDCL-Etablierung zu bewerten. Zur Erstellung von molekularen Profilen der neu etablierten PDCL wurden Zeitverlaufsanalysen von Genexpression und genomischen Veränderungen wurden mittels Next-Generation Sequenzierung (NGS) durchgeführt. Zudem wurde untersucht, ob die PDCL Eigenschaften des ursprünglichen Krebsgewebes zuverlässig rekapitulieren können. Darüber hinaus wurden potentiell behandelbare Mutationen mittels NGS hochauflösend nachgewiesen und in Folge mit spezifischen Inhibitoren behandelt. Weiterhin wurde der Effekt einer Langzeitkultivierung auf die Behandlungseffektivität klassischer Chemotherapeutika bewertet.

Die morphologischen Merkmale der primären Krebsarten blieben in PDCL sowohl *in vitro* als auch *in vivo* über einen längeren Zeitraum in Kultur stabil. Die Ergebnisse dieser Studie erbrachten zudem den Nachweis, dass schlecht differenzierte Tumore mit höherer genomischer Instabilität eine vermehrte Rate an erfolgreicher Etablierung von PDCL aufwiesen. Genomanalysen bestätigten zudem, dass das molekulare Profil der Primärtumore während der Langzeitkultivierung in den PDCL konserviert wurde. Mittels zielgerichtetem NGS konnte verifiziert werden, dass wichtige onkogene Veränderungen wie TP53, KRAS, CTNNB1 sowie behandelbare Mutationen (z. B. MET, KIT, KDR) in PDCL nachgewiesen und für individualisierte therapeutische Ansätze genutzt werden können. Integrative Analysen zeigten weiterhin, dass PDCL den molekularen und prognostischen Merkmalen von PLC stärker ähneln als etablierte Zelllinien und somit ein wertvolles Werkzeug für die Bewertung von potenziellen Therapiezielen darstellen. Unsere integrative Analyse zeigt, dass PDCL ein geeignetes Modell für die Untersuchung relevanter molekularer Untergruppen und die Erforschung von präzisionsmedizinischen Ansätzen für die Behandlung von primärem Leberkrebs darstellen.

Table of content

List of figures

List of tables

List of abbreviations

5-FU	fluoruracil
AFP	alpha-fetoprotein
ASBT	apical sodium bile acid cotransporter
BSA	bovine serum albumin
CCA	cholangiocarcinoma
CCLE	cancer cell line encyclopedia
CK19	cytokeratin 19
CNA	copy number alteration
COX2	cyclooxygenease-2
CSC	cancer stem cells
CTLA-4	cytotoxic T-lymphocyte-associated protein 4
DAPI	4′,6-diamidino-2-phenylindole
DMEM	dulbecco's modified eagle's medium
DMSO	dimethyl sulfoxide
DN	dysplastic nodules
DNA	deoxyribonucleic acid
DNMT	DNA methyl-transferases
EDTA	ethylendiamintetraacetat
EGF	epidermal growth
EGFR	epidermal growth factor receptor
EMT	epithelial-mesenchymal-transition
EpCAM	epithelial cell adhesion molecule
FBS	fetal bovine serum
FDA	US Food and Drug Administration
FGF	fibroblast growth factor
GSEA	gene set enrichment analysis
HBV	hepatitis B virus

HBsAg	hepatitis B surface antigen
HBx	hepatitis B virus protein
HCC	hepatocellular carcinoma
HCV	hepatitis C virus
HGDN	high-grade dysplastic nodules
HGF	hepatocyte growth factor
Hh	hedgehog
HIV	human immunodeficiency virus
HPC	hepatic progenitor cells
HSC	hepatic stellate cells
IGF	insulin-like growth factor
IL-6	interleukin-6
IPA	ingenuity pathway analysis
JAK	janus kinase
KCs	kupffer cells
KRAS	kristen rat sarcoma
LGDN	low-grade dysplastic nodules
lncRNAs	long non-coding RNAs
LRR	log R ratio
LSECs	liver sinusoidal endothelial cells
MAPK	mitogen-activated protein kinase
Mcl-1	myeloid cell leukemia-1
miRNAs	micro-RNAs
mRNA	messenger RNA
mTOR	mammalian target of rapamycin
N	surrounding liver tissue
NAFLD	non-alcoholic fatty liver disease
NASH	non-alcoholic steatohepatitis

NGS	next-generation sequencing
NK	natural killer cells
NKT	natural killer T cells
NOD/SCID	nonobese diabetic/severe combined immunodeficiency
NSCLC	non-small cell lung carcinoma
p53	tumor protein 53
PBS	phosphate-buffered saline solution
PCA	principal components analysis
PD-1	programmed cell death-1
PD-L1	programmed death ligand 1
PDCL	patient-derived cell lines
PDGF	platelet-derived growth factor
PDGFR	platelet-derived growth factor receptor
PDX	patient-derive xenograft
PFA	paraformaldehyde
PI3K	phosphatidylinositol-3-kinase
PIP_3	phosphoinositol triphosphate
PLC	primary liver cancer
PTEN	phosphatase and tensin homolog
RNA	ribonucleic acid
RT	room temperature
shRNA	short hairpin RNA
SD	standard deviation
SL	tumor-surrounding liver tissue
SNV	single nucleotide variance
SOCS1	suppressor of cytokine signaling 1
SSI-1	stress survival islet-1
STAT	signal transducer and activator of transcription

TERT	telomerase reverse transcriptase
TGF-α	transforming growth factor alpha
TGF-β	transforming growth factor beta
VEGF	vascular endothelial growth factor
VEGFR	vascular endothelial growth factor receptor

1. Introduction

1.1 General aspects of liver physiology

1.1.1 Morphology, histology and liver function

Liver is the second largest organ and the largest exocrine gland in the human body. It accounts for approximately 2,5% of body weight, or about 1,5 kg in average adult human.[1] The organ is made of soft, reddish-brown tissue, encapsulated by connective tissue and divided into two lobes with eight segments of unequal size and shapes. The liver is one of the most biochemically and metabolically complex and active organs in the body. It receives oxygen-poor and nutrient-rich blood from the portal vein, comprising approximately 70-80% of total blood supply in the liver. In parallel, liver receives oxygenated blood with low nutrient content from hepatic artery, comprising approximately 20-30% of total liver blood supply. Portal vein and hepatic artery enter the liver and divide into smaller vessels of the liver lobules. Blood further continues through the small blood vessels called sinusoids, characterized by high permeability and fewer tight junctions, towards the central vein of each lobule. The central veins drain into hepatic vein and next into *vena cava inferior* (Figure 1).[2]

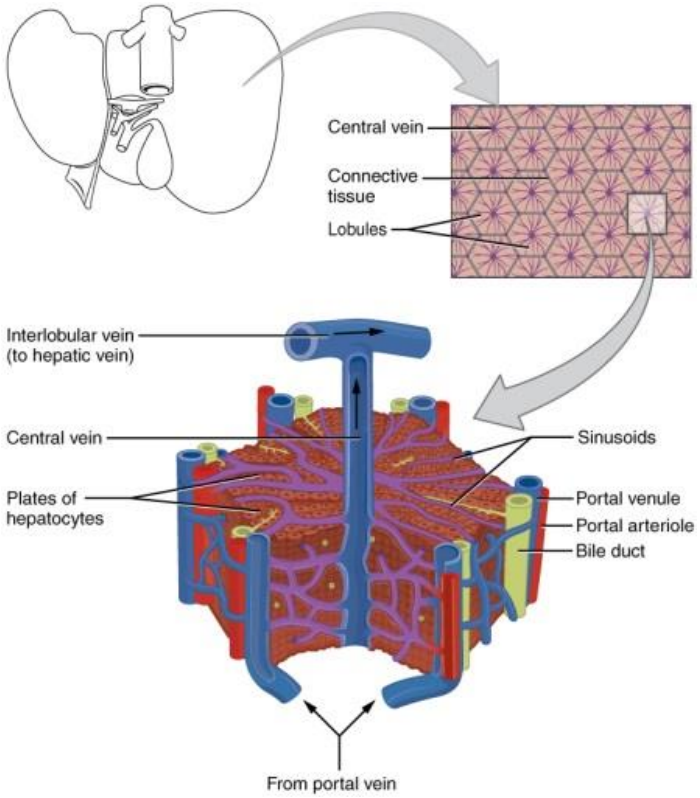

Figure 1 Illustration of the microscopic anatomy of the liver.

Figure shows cross-section of the liver with uniformly organized hexagonal liver lobules. Further in the lower part is shown cross-section of the single liver lobule, with details on the blood vessels, bile ducts and liver parenchyma mostly composed of the hepatocytes. (Downloaded from: Illustration from Anatomy & Physiology, Connexions; Web site: http://cnx.org/content/col11496/1.6/, Sept 2018)

1.1.1.1 Liver lobule and liver acinus

The basic structural unit of the liver is the liver lobule, which is a cylindrical structure between 0,8 and 2 millimeters in diameter. It forms a hexagonal region within liver parenchyma bordered by six portal triads and a central vein in the middle. Portal triads consist of branches from the portal vein, hepatic artery as well as bile ductules. The lobule is composed of many cellular plates that radiate from the central vein. Each hepatic plate is usually two cells thick, where in between the adjacent cells lays small bile canaliculi that empties into bile ducts. The basal side of the cells is facing perisinusoidal space (space of Disse), an area between liver sinusoidal endothelial cells and hepatocytes. This particular region is important for transport of lipoproteins, small chylomicron particles and other macromolecules to the hepatocytes. Efficient transfer of these compounds from the blood into the space of Disse is facilitated by fenestrated sinusoidal epithelium and lack of a basement membrane (Figure 2).[2-4]

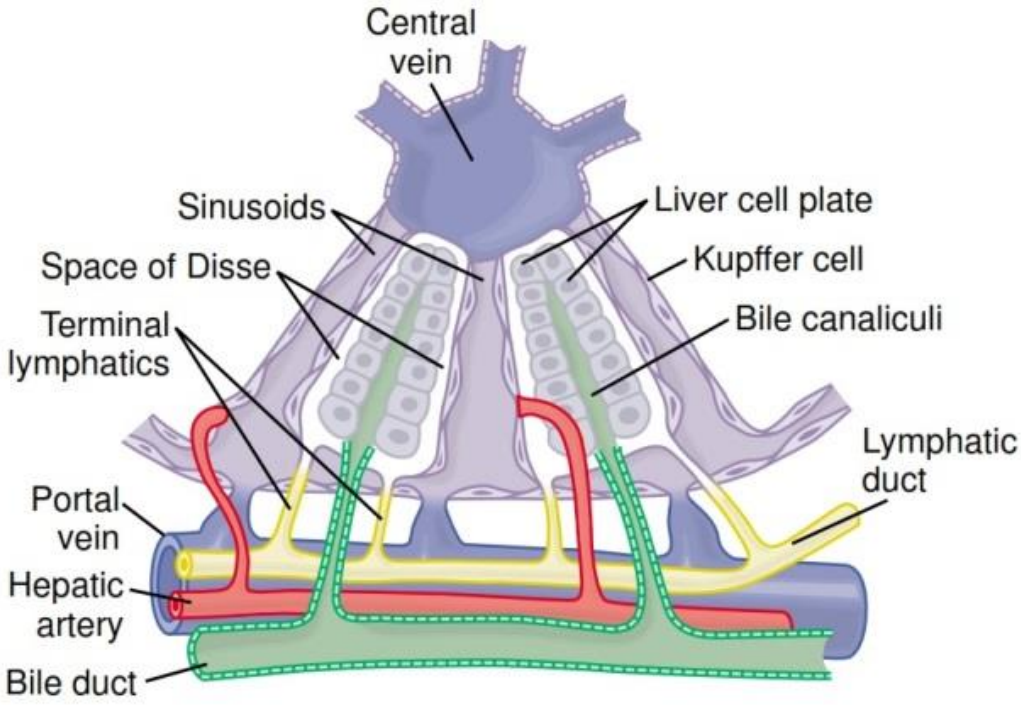

Figure 2 Illustration of the microscopic anatomy of the single liver lobule.
Illustration shows anatomical structures within a single liver lobule as well as cellular composition (Guyton *et al.* 2006[3]).

Despite a relatively homogenous composition on histological level, liver lobules show an excessive heterogeneity in biochemical and physiological functions.[5] This is a consequence of specific blood flow from the portal triad to the central vein, where oxygen and nutrients are consumed and concentration gradient is formed. Therefore, hepatocytes located in close proximity to the central vein receive less oxygen and nutrients than hepatocytes surrounding portal triads. As a result, three metabolic zones can be distinguished (zone I-III) with a differential distribution of key enzymes involved in numerous metabolic pathways.[6] Such specific functional and zonal organization of the liver can be defined and recognized as a liver acinus.

Borders of the acinus are not morphologically clearly delineated, however, it can be visualized by connecting two portal triads with a line from which it further extends in direction of two adjacent central veins in a triangular shape (Figure 3).[7] Zonation and acinar organization of the liver provide several advantages. For instance, it allows spatial separation between opposing anabolic and catabolic pathways and favors more efficient way of xenobiotic metabolism and biotransformation of endogenous metabolic byproducts.[8] It is important to indicate that many molecules and signaling pathways regulate liver zonation, and the most prominent are Wnt/β-catenin, hepatocyte growth factor (HGF) and Hedgehog (Hh) signaling.[4]

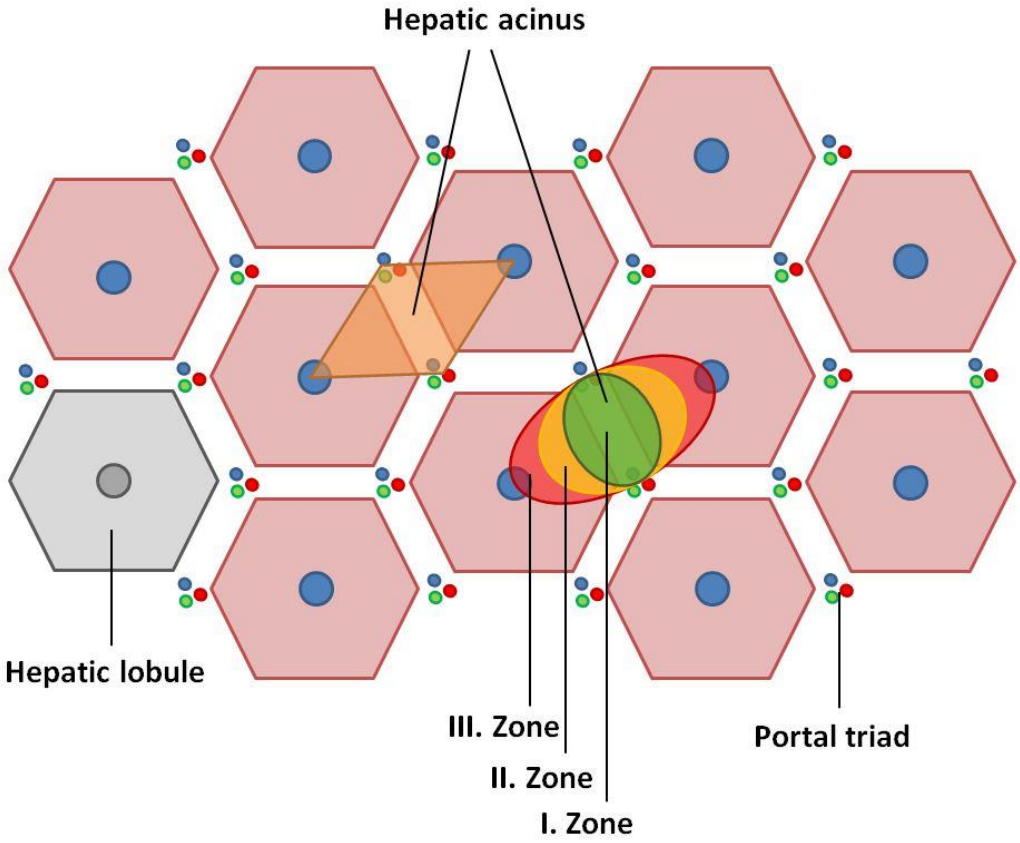

Figure 3 Illustration of structural and functional subunits of liver.
Figure shows hexagonal liver lobules as a structural and acinus as a functional subunit of the liver. Orange rhombus delineates liver acinus, while metabolic zones (I-III) are represented as colored ellipses.

1.1.1.2 **Liver function**

There are several key functions of the liver which can be divided into distinct categories: digestive function (bile liquid), metabolic function (carbohydrate, fat and protein metabolism), synthesizing function (plasma proteins, hormones and nutrients), storage function (glycogen, lipid, cholesterol, vitamins and iron), immunological function (production of the circulating innate immunity proteins and host for large number of immune cells) and biotransformation (drugs and toxins). Substances produced by the liver are secreted to the bloodstream and further

distributed through the hepatic vein, or excreted through the bile and biliary system (Figure 1).[4, 9]

1.1.1.3 **Liver cells**

Liver complexity is also evident on a cellular level, where many different cell types are organized in a sophisticated cellular network, which orchestrates metabolic processes and keeps the physiological balance of an organism. These cell types include: hepatocytes, cholangiocytes, liver sinusoidal endothelial cells (LSECs), Kupffer cells (KCs), lymphocytes (e.g. natural killer (NK) cells), hepatic stellate cells (HSC), and hepatic progenitor cells (HPC).[4]

1.1.1.3.1 **Hepatic progenitor cells**

HPC are about 10 μm in size and express markers of immature liver cells such as alpha-fetoprotein (AFP) as well as markers of biliary epithelium - cytokeratin 19 (CK19) and hepatocyte lineages (albumin).[10] Moreover, there are certain indications that epithelial cell adhesion molecule (EpCAM) plays a role in liver cell plasticity and liver regeneration, by modulating HPC differentiation status.[11] EpCAM is usually highly expressed in immature progenitor cells and low in differentiated hepatocytes.[11] The most important role of HPC is differentiation into mature hepatocytes or cholangiocytes. During the course of differentiation, progenitor cells that reside in the canals of Hering initially form strands of cells that further expand in liver parenchyma and differentiate into hepatocytes, or shape branching ducts that move from the canals of Hering to the center of the portal space and form bile ducts.[10, 12]

1.1.1.3.2 **Hepatocytes**

Hepatocytes are the most abundant cell type in liver parenchyma and account for 60% of total cell number and comprise 80% of liver volume.[1] During development, hepatocytes differentiate from bi-potent hepatoblasts, while in adult liver, during intensive regenerative processes, hepatocytes differentiate from bi-potent HPC. The bi-potent nature of HPC suggests that they originate from fetal hepatoblasts that remain undifferentiated in a stem cell niche.[13] Differentiated hepatocytes are relatively large polygonal cells between 20–30 μm in diameter with a larger number of organelles such as endoplasmic reticulum, golgi apparatuses, large mitochondria, as well as lysosomes and peroxisomes.[4] Cells are arranged in a specific pattern inside hepatic parenchyma, where double-cell thick layers of hepatocytes are building up characteristic plate-like architecture.[14] As a consequence of a specific arrangement, hepatocytes show structural and functional polarity with existence of two major domains: 1) basal domain - exposed to sinusoidal endothelial cells and space of Disse; 2) apical domain - exposed to a narrow lumen between two hepatocytes (site of bile secretion).[15] Functional polarity of the hepatocytes can be recognized by specific spatial distribution of receptors, pumps, transport channels and other proteins across the cell membrane. Consequently, apical part of the cell is specialized for bile excretion, while basal segment is functionally adapted for extraction of many molecules carried by blood, but also for secretion of final

products synthesized or modified by the cells.[4, 15] Biochemical machinery of hepatocytes has a capability of maintaining homeostasis and physiological balance of an organism by synthesizing many essential blood components and by biotransformation of xenobiotics and endogenous metabolic byproducts.[16, 17] Such a complex machinery is mainly involved in amino acid metabolism, protein production (e.g. albumin, clotting factors etc.), cholesterol, bile salts, lipoproteins, phospholipids and glycoproteins. Other important functions carried by hepatocytes include conversion and storage of carbohydrates and proteins, formation and secretion of bile and urea, and the detoxification of toxic substances.[18] It is important to highlight significance of several proteins synthesized in hepatocytes, such as albumin and AFP, as level variations can indicate presence of liver injury and potential malignant transformation.[19-21] Albumin is the most abundant circulating protein with diverse roles in metabolism, tissue fluid distribution, transport of substrates, antioxidant function etc.[22] Studies have shown that level of albumin, as well as structural alterations in the protein, correlate with level of liver injury, particularly with advanced liver cirrhosis.[23, 24] AFP is a fetal plasma protein proposed to be the analog of serum albumin during fetal development. Significant amounts of this protein are produced by the yolk sac and liver of the fetus, however, total amount is significantly reduced after birth.[20] In adults, reactivation of AFP production usually occurs during liver regeneration and hepatocarcinogenesis.[25] Therefore, AFP blood concentration has been used to monitor chronic liver disease, onset and progression of hepatocellular carcinoma (HCC), effectiveness of curative treatment and predicting the outcome.[20]

1.1.1.3.3 **Cholangiocytes**

Cholangiocytes are a heterogeneous population of epithelial cells which line the biliary epithelium. They build a complex network of ducts responsible for bile acid transport and ductal bicarbonate secretion.[26] Cholangiocytes can be found in both, intra- and extrahepatic ducts of the biliary tree, however, those two cell groups show developmental heterogeneity. Cells within intrahepatic biliary tree derive from hepatoblast, whereas cholangiocytes lining the extrahepatic biliary tree derive directly from endoderm.[27] Intrahepatic cholangiocytes comprise relatively small volume of the liver, about 3 to 5%, but still play an important role in physiologic processes.[28] Shape and size of the cells can vary, where in small bile ducts (lumen diameter <15 µm), cells are either flattened or cuboidal, while in large bile ducts (lumen diameter >15 µm), cholangiocytes are columnar and significantly more abundant. Accordingly, the size of cells is also heterogeneous and ranges from 6 - 15 µm in diameter.[26, 29, 30] Along with morphological heterogeneity, cholangiocytes demonstrate biochemical and functional diversity with differential expression of some key proteins.[31] By expressing variety of transporters on both, basolateral and apical plasma membrane, they play a role in bile acid modification via processes of secretion and absorption. These processes occur as the bile is transported along the biliary tree to the intestine. Primary bile is modified predominantly by secretion of water, Cl^- and HCO_3^- into the duct, and extraction of glucose, bile acids and amino acids. These complex tasks are performed by several transporters, channels

and exchangers, which activity depends on the content of the bile and intracellular space.[26] Important characteristic of cholangiocytes is high expression of CK19 on plasma membrane, a common marker expressed in biliary epithelium, which has also been shown to be associated with intrahepatic cholangiocarcinoma (iCCA).[32, 33] In iCCA, the expression of CK19, as well as some other members of cytokeratin family (CK7, CK20), is much more pronounced than in HCC, allowing distinction of these two tumor entities as well as recognition of combined HCC/iCCA type.[34]

1.1.1.3.4 **Non-parenchymal cells**

Non-parenchymal cells of the liver include liver sinusoidal endothelial cells, Kupffer cells, lymphocytes, biliary cells and hepatic stellate cells.[35]

1.1.1.3.4.1 **Liver sinusoidal endothelial cells**

Liver sinusoidal endothelial cells constitute a sinusoidal wall, which is also known as the liver endothelium, or endothelial lining.[36] The liver sinusoids represent a unique type of capillaries with the existence of open pores or fenestrae which connects them with the space of Disse. This unique property distinguishes them from other capillaries in the body.[36] Such specific structure of the cells allows free access of fluid, solutes, droplets, and particles from the lumen toward the space of Disse and hepatocytes, as well as re-circulation in the opposite direction.[4]

1.1.1.3.4.2 **Kupffer cells**

Kupffer cells comprise about 2% of the liver mass and account for about 20% of non-parenchymal cells in the liver.[4, 37] They derive from circulating monocytes, and once localized within the liver, they reside in the lumen of sinusoids.[38] Major roles of Kupffer cells are to clear endotoxins from passing blood and to phagocytose debris and microorganisms, as well as to pass through the space of Disse and phagocytose apoptotic hepatocytes.[37]

1.1.1.3.4.3 **Lymphocytes**

Lymphocytes are dispersed in the liver parenchyma and in the portal tracts.[39] Human liver hosts approximately 10^{10} lymphocytes, and they can be divided into conventional and unconventional lymphocyte subpopulations, namely adaptive immune systems (T and B cells) and innate (NKT and NK cells). Lymphocytes play an essential role in the first line immune defense against pathogens, modulation of liver injury and recruitment of circulating lymphocytes.[37]

1.1.1.3.4.4 **Hepatic stellate cells**

These cells are located in the space of Disse and comprise around 1,5% of the total liver mass.[4] Stellate cells have many roles, and together with hepatocytes, they take part in the metabolism of vitamin A. They also synthetize, secrete, and degrade components of the perisinusoidal extracellular matrix.[4] Hepatic stellate cells are quiescent in normal healthy livers (quiescent HSCs); however, they undergo morphological changes during liver injury. They gradually become activated and

differentiate into myofibroblastic cells, characterized by a loss of vitamin A and increased collagen expression, overall contributing to liver fibrosis.[35]

1.2 Primary liver cancers

Primary liver cancers (PLC) are a heterogeneous group of benign and malignant solid tumors. Clinically, they are characterized by ethnic, etiological, geographical and gender diversity.[40-43] There are two major subtypes of primary liver cancers, HCC and iCCA. Together, they comprise more than 1 million newly diagnosed cases annually. Over the recent years, raising incidence of PLC has been observed globally, thus, PLC represent an increasing health care problem worldwide.[44] These malignancies are the second most common cause of cancer-related death after lung cancer and rank among the few solid tumors with increasing mortality rates worldwide.[45] Due to lack of clinical symptoms and biomarkers for early detection, the majority of cancers are identified at late stages when curative treatment options are limited. In addition, the majority of the patients present with an underlying liver disease and a compromised liver function.[40] For HCC, main etiological agents are well known and characterized. Specific background, such as viral infections (hepatitis B virus (HBV) and hepatitis C virus (HCV)), ethanol abuse, non-alcoholic fatty liver disease (NAFLD), non-alcoholic steatohepatitis (NASH) and other metabolic disorders, contribute to a great extent to the development of HCC.[46] Development of iCCA is associated with parasitic liver flukes infection (*Opisthorchis viverrini* and *Clonorchis sinensis*) in many parts of the world, conditions resulting in chronic biliary tract inflammation. Development of the cancer can also be affected by different drugs and toxins, as well as congenital disorders.[47] Notably, new evidence delineates that inflammatory diseases, such as human immunodeficiency virus (HIV), HBV and HCV, are associated with iCCA.[47] Overall, disruption of hepatic microenvironment and constant remodeling of diseased liver parenchyma, as well as activation of immune-cell mediated inflammation, creates an adverse milieu that promotes PLC development.[48]

Carcinogenesis is a complex process that can be initiated as the consequence of genetic and/or epigenetic alterations in different cell types. Therefore, the cellular origin of PLC is diverse, and tumors can arise from both stem and progenitor cells as well as terminally differentiated cells, such as hepatocytes and cholangiocytes. The relative contribution of each cell type to tumorigenesis may depend on diverse factors related to inflammation, structural changes in the hepatic microenvironment and principal oncogenic events (Figure 4).[40]

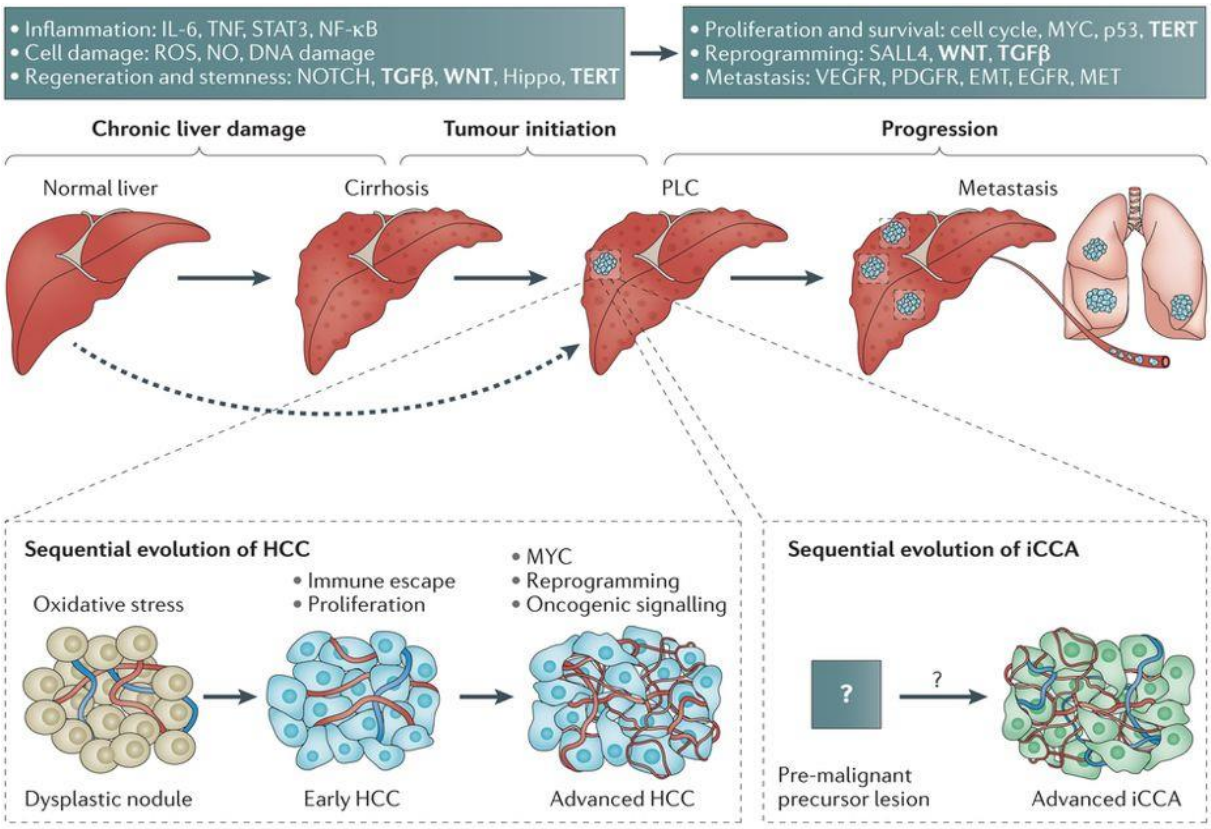

Figure 4 Sequential evolution of liver disease leading to PLC.
Majority of chronic liver diseases develop liver cirrhosis as an end stage, which is one of the most important predisposing factors for development of PLC. During the sequential evolution of PLC, from chronic liver damage and tumor initiation to tumor progression and metastasis, many of the signaling pathways and genes are dysregulated and altered. Evolution of HCC is accompanied with increased neovascularization to sufficiently provide nutrient and oxygen supply to the progressing tumor. For iCCA, the sequential evolution and underlying phenotypic features are not well known, and yet to be precisely defined (Marquardt *et al.* 2015[40]).

1.2.1 Hepatocellular carcinoma

HCC is the most common primary liver cancer, representing approximately 90% of all PLC cases. Prevalence of HCC is reported to be highest in Africa and Southeast Asia, but with steadily increasing incidence in western countries as well as Japan over past several decades.[49] In all geographical regions, males have a higher incidence of HCC than females.[41, 43] As such, HCC has become one of the most rapidly developing cancers and the 6th most common malignancy worldwide as well as third leading cause of cancer related death.[45, 50] High mortality of liver cancer partially originates from its resistance to existing anticancer agents, a lack of biomarkers that allow detection of surgically resectable tumors, and underlying chronic liver disease that limits the application of operative, interventional and chemotherapeutic approaches.

1.2.1.1 Risk factors

Development of HCC involves multistep process, where hepatocytes or hepatic progenitor cells proliferate in the setting of chronically altered and inflammatory microenvironment. Aberrant intracellular signaling and dysregulated genetic and

epigenetic events, induced by constant cellular damage and turnover, subsequently progress into dysplastic nodules (DN) and ultimately lead to formation of HCC.[51]

Liver cirrhosis is the strongest and most common risk factor for development of HCC.[52] More than 85% of HCC develop on the basis of advanced hepatic fibrosis and/or cirrhosis. The cumulative risk of HCC development is significantly influenced by the underlying etiological condition.[40] Several different risk factors have been associated with liver cirrhosis and HCC. The most prominent are chronic HBV and HCV infections, alcoholic liver disease, NAFLD/NASH, aflatoxin B1, metabolic disorders (e.g. hereditary haemochromatosis, α1 antitrypsin deficiency, hereditary tyrosinemia), diabetes mellitus and several others with lower frequency (Figure 5).[53]

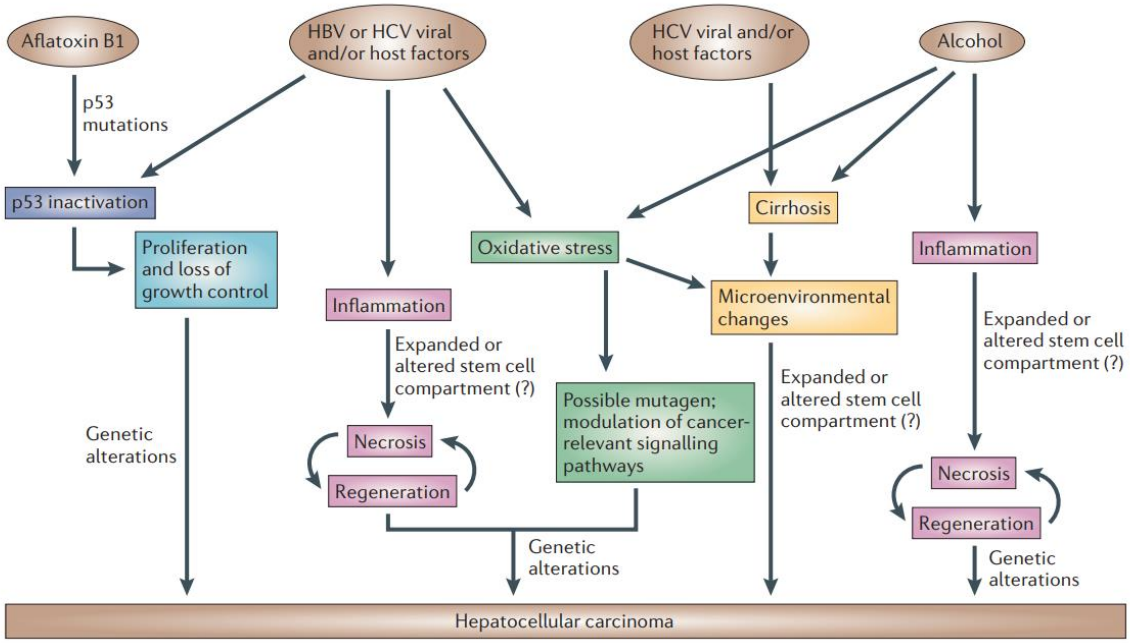

Figure 5 Different predisposing risk factors that can lead to the development of HCC. In the figure different risk factors (e.g. Aflatoxin B1, viral infections and alcohol), and affected cellular processes and genes that could lead to development of HCC are represented (Farazi *et al.* 2006[53]).

1.2.2 **Cholangiocarcinoma**

Cholangiocarcinoma is the second most common primary liver cancer originating from the epithelial lining of the biliary tree.[54] It accounts for about 3% of all gastrointestinal tumors. The epidemiology of CCA is heterogeneous with the rising incidence over the past three decades.[55] Gender-related distribution of CCA is more homogeneous than for HCC, being very similar for male and female.[42] Although 1-year mortality has improved over time, 5-year survival is still as low as 10%. This is a direct consequence of considerably low number of CCA patients diagnosed at stages when curative treatments are available.[55] Globally, hepatobiliary cancers account for 13% of total cancer-related deaths, whereas, 10–20% of these are attributable to CCA.[56]

1.2.2.1 **Classification of CCA**

Cholangiocarcinoma is classified based on anatomical location. Intrahepatic cholangiocarcinomas are located within hepatic parenchyma, while extrahepatic cholangiocarcinomas are separated by the second order bile ducts and categorized as perihilar (pCCAs) and distal tumors (dCCAs) (Figure 6). Majority of CCAs, 60–70%, are perihilar, 20–30% are located distally and intrahepatic CCA accounts for 5–10%. The classification of CCA is of clinical relevance for management and prognosis of CCA, due to different epidemiological features between pCCA and dCCA.[55] Incidence rates for CCA show high geographical variation, which is partly related to variations in risk factors. However, an increased risk for iCCA development has been recently observed in patients with chronic viral hepatitis (HBV and HCV) and cirrhosis.[40]

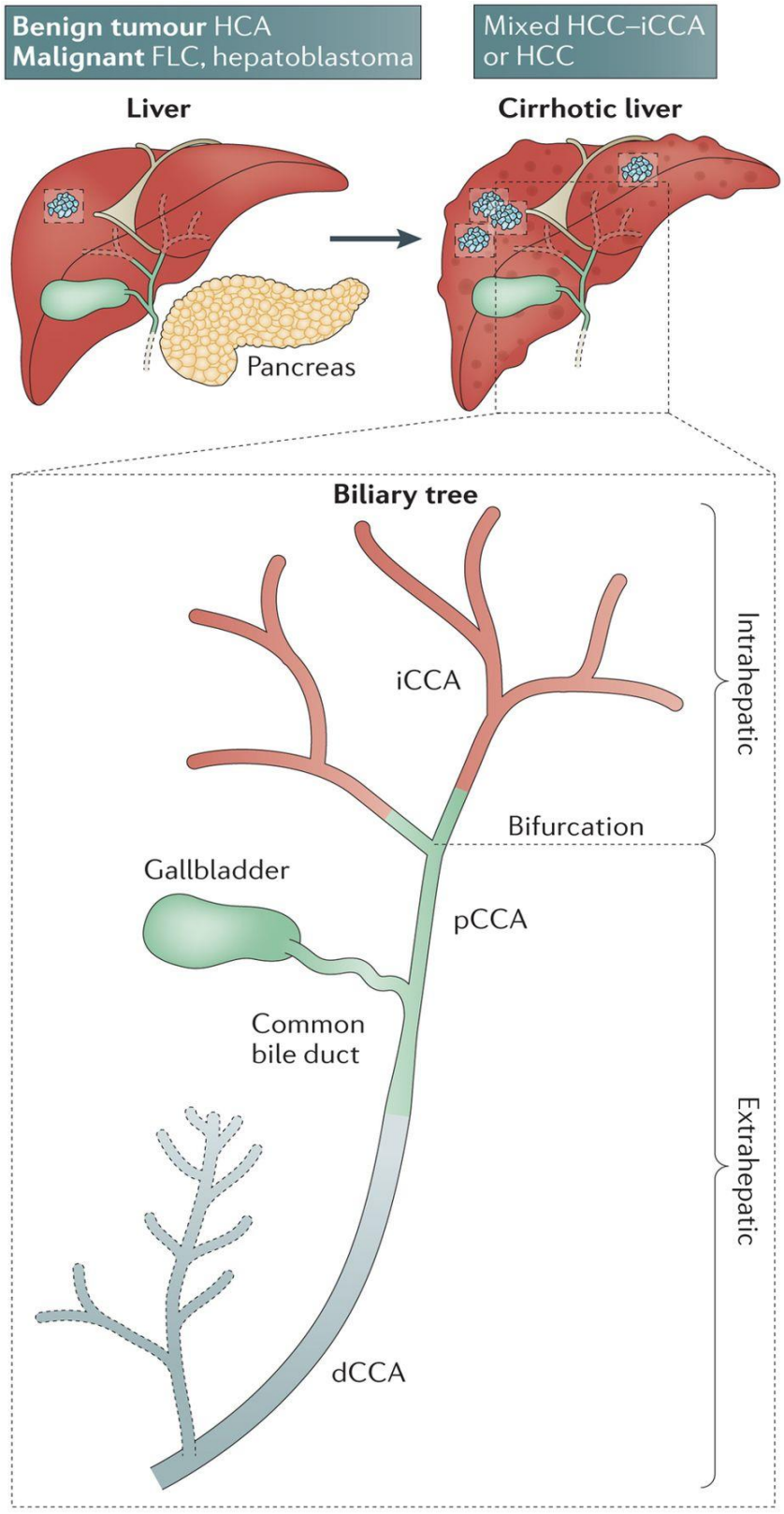

Figure 6 Overview of different parts of the biliary tree in which tumor can develop. CCA can be divided into three categories according to its anatomical location in the biliary tree. Intrahepatic cholangiocarcinomas (iCCAs) is located in hepatic parenchyma and derived from intrahepatic ducts, while perihilar CCA (pCCA) and distal (dCCA) are located outside live parenchyma in the second order bile ducts (modified from Marquardt *et al.* 2015[40]).

1.2.2.2 **Risk factors**

Despite most iCCAs arise sporadically, there are several reported risk factors that have been assigned to development of iCCA: biliary duct disorders, parasitic infections, toxins, as well as chronic liver diseases such as viral infections with HBV and HCV. Potential risk factors with less evidence are inflammatory bowel disease, diabetes, obesity, gallstone disease, alcohol, smoking and polymorphisms in some genes encoding drug metabolizing enzymes and biliary transporter proteins (e.g. *NAT2, ABCB11*, *ATP8B1*).[55, 57, 58] Parasitic infections with the liver flukes *Opisthorchis viverrini* and *Clonorchis sinensis* are mostly dominant causes of iCCA in Southeast Asia, by causing chronic inflammation of biliary epithelial cells further increasing the risk of iCCA.[55] Inherited biliary disorders can contribute to malignant transformation of the cells in the biliary tract. Bile duct cysts are rare congenital anomalies characterized by cystic dilatation of the bile ducts, where most patients (60%) are diagnosed in their first decade of life but up to 20% are diagnosed in adulthood.[59] Furthermore, hepatolithiasis or intrahepatic stones are thought to predispose to malignancy by causing bile stasis, recurrent cholangitis and chronic inflammation.[60] In addition, HBV and HCV, as well as liver cirrhosis are associated with iCCA. The pathogenesis of iCCA in these conditions is not clear, but undoubtedly chronic inflammation and increased cell proliferation could play a role in tumorigenesis.[55]

1.2.3 **Molecular pathogenesis of PLC**

1.2.3.1 **Molecular pathogenesis of HCC**

Hepatocarcinogenesis is a complex and multistep process that involves accumulation of epigenetic and genetic events within chronically altered hepatic microenvironment, ultimately driving transformation of normal into malignant cells.[61] Many HCCs develop through a sequential evolution from premalignant nodular lesions, i.e. dysplastic nodules (DN), to HCC.[62] DNs are divided into two subtypes – low-grade dysplastic nodules (LGDN) and high-grade dysplastic nodules (HGDN). In general, DNs are defined as dysplastic lesions at least 1 mm in diameter, with dysplasia but without histological criteria of malignancy. Furthermore, hepatocarcinogenesis is directed from DNs toward development of early carcinoma (eHCC) that eventually progresses to HCC (pHCC).[63] During early stages of hepatocarcinogenesis, changes in DNA methylation patterns are believed to be early events preceding allelic imbalances and ultimately leading to cancer progression.[64] Certain cancer-related genes show global hypomethylation as well as promoter hypermethylation, thus, influencing tumor biology and affecting prognosis.[65] Existing evidence show that hypermethylation of CpG islands occur in the premalignant lesions, and tends to accumulate during multistep carcinogenesis.[66] These data further confirm importance of epigenetic events in the initial stages of HCC development. On the genetic level, loss of heterozygosity was described in a subset of dysplastic nodules, whereas classical genetic alterations (such as β-catenin or *TP53* mutations) have not been identified in preneoplastic liver lesions.[67] Moreover, in the group of patients with chronic HBV infection molecular profiles of dysplastic and early lesions are relatively homogeneous, while at the time

of advancement into progressed HCC, tumor lesions show a sharp increase in heterogeneity at both the genetic and genomic level.[68]

As a consequence of epigenetic and genetic alterations, significant number of key oncogenes and tumor-suppressor genes have been affected and dysregulated. Many of them are key players in maintaining cellular balance, such as cell cycle regulators (*TP53, CDKN2A*), proliferation regulators, immune response, β-catenin, ErbB receptor family members, MET and its ligand - HGF, telomerase reverse transcriptase (TERT), E-cadherin etc. (Figure 7).[53]

As hepatocarcinogenesis is considered to be a complex process dependent and influenced by many factors, it should be pointed out that identifying altered signaling pathways involved in HCC initiation and progression, rather than individual mutated genes, may be a key factor in understanding genetic mechanisms underlying hepatocarcinogenesis.[69]

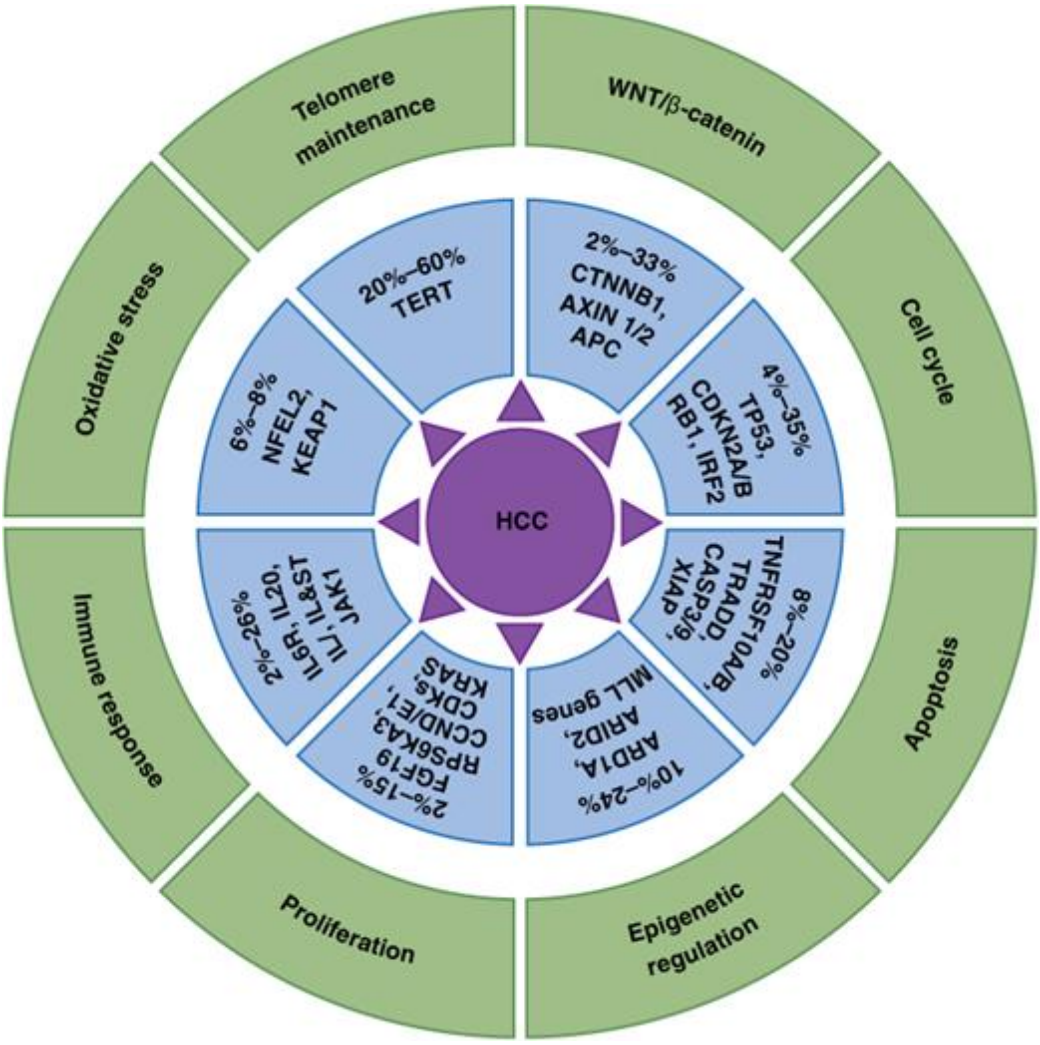

Figure 7 Oncogenic signaling pathways and genetic landscape in HCC.
Shown are major signaling pathways in HCC and corresponding frequencies of genetic alterations contributing to hepatocarcinogenesis (Marquardt *et al.* 2015 in DeVita *et al.* 2015[47]).

1.2.3.2 Molecular pathogenesis of iCCA

iCCAs are rare hepatic malignancies with a complex molecular pathobiology.[70] Malignant transformation of iCCA arises from a chronic biliary inflammation and biliary damage (cholestasis) triggered by external factors. Obstruction of the bile flow can result in aberrant bile acid signaling, further promoting proliferation of cholangiocytes.[56] Release of cytokines and pro-inflammatory mediators, such as interleukin-6 (IL-6) and transforming growth factor beta (TGF-ß) also promotes growth of cholangiocytes.[56, 70] Such increase in the cell proliferation is usually followed by accumulation of molecular aberrations in the cells, leading to the malignant transformation. Besides activation and impairment of proliferative and pro-inflammatory signaling, key role in carcinogenesis plays impairment of DNA damage and repair systems in the tumor suppressor genes as well as activation of proto-oncogenes. In addition, similar to HCC many key signaling pathways and mediators are dysregulated, such as cyclooxygenase-2 (COX2), phosphatidylinositol-3-kinase/Protein Kinase B and the mammalian target of rapamycin (PI3K/Akt/mTOR), epidermal growth factor receptor (EGFR), ERBB2, Ras/MAPK, HGF/MET, IL-6/JAK/STAT, and vascular endothelial growth factor (VEGF). These mechanisms, alongside with interaction between the epithelial and stromal compartments, contribute to uncontrolled proliferation, survival, angiogenesis, invasion and metastasis in iCCA.[70]

In iCCA several major activating mutations in *KRAS* (19%), low frequency mutations in *BRAF* (5%), *FGF* (10-15%), *EGFR* (3%), as well as loss of function mutations in the tumor suppressor *TP53* (approximately 16%) have been described.[71] Moreover, epigenetic alterations are also known to play important role in the development of iCCA. Frequent events that can lead to malignant transformation can occur through promoter hypermethylation in some genes (e.g. *p16INK4A/CDKN2, p14ARF, RASSF1A, APC, GSTP* and *SOCS-3*), but also through the impaired activity of different epigenetic modulators, like DNA methyl-transferases (DNMT). Inflammation-related signaling pathways, such as JAK/STAT3, and proliferation-related pathways, like EGFR and HGF/MET signaling, show profound dysregulation in iCCA. In addition, recent findings imply that Notch and Wnt signaling might play role in iCCA pathogenesis.[70, 71]

1.2.4 Signaling pathways and regulators in molecular pathogenesis of PLC

1.2.4.1 Cell cycle regulation - P53

P53 is a key cell-cycle regulator at the G1/S regulation checkpoint, also involved in control of DNA repair and apoptosis. The signaling pathway is activated in response to a variety of stress signals and coordinates transcriptional programs that ultimately guide tumor suppression. Loss of p53 function is a common feature in the majority of human cancers including HCC.[72, 73] Frequency of *TP53* mutations in HCC vary in the different regions of the world.[67] Asian and African countries show higher frequency of *TP53* mutations due to exposure to aflatoxin B1 and HBV infections. In western countries, aflatoxin B1 exposure is very low and HCC-related to HBV infection is rare. The rate of *TP53* mutations in HCC is therefore lower (10–20%)

than in Asian countries (40–60%).[67] Hot spot mutations at codon 249 (Arg249Ser G:C to T:A transversion) are associated with exposure to aflatoxin B1 and could be identified in more than 50% of HCC in African and Asian patient. Therefore, it was suggested that codon Arg249Ser mutation in *TP53* of HCC may be utilized as a biomarker for exposure to aflatoxin B1 and for detection of early HCC.[74] Furthermore, HBV infection can affect the activity of p53 by inducing DNA damage. Prognostically, *TP53* alterations are generally associated with larger, less differentiated tumors and poor survival.[75]

Frequency of *TP53* mutations in iCCA varies greatly between investigated cohorts of iCCA patients, ranging from 9–38%.[76] Higher frequency of *TP53* mutation is typically observed in the patients with *Opisthorchis viverrini* infection, whereas patient without fluke infection show significantly lower mutations in *TP53* gene.[77] Moreover, there is a positive association between iCCA patients positive for hepatitis B surface antigen (HBsAg) and the presence of mutations in *TP53,* which might further imply that those patients share a common p53-mediated pathway with HBsAg positive HCC.[76]

1.2.4.2 **Wnt/β-Catenin signaling**

CTNNB1 gene encodes β-catenin, a protein involved in multiple processes including organ formation, stem cell renewal and cell survival. β-catenin is found in the adherens junctions and plays a key role in intercellular adhesion and communication. Within the liver, Wnt/β-catenin pathway is highly active in liver development, zonation, amino acid metabolism, regeneration and oxidative stress.[78] It is a well-known oncogene mutated in many types of cancer, such as medulloblastoma, colon, thyroid and breast cancer.[67] Further, impaired activity of Wnt/β-catenin signaling has been described in many HCC studies.[79-83] Deletions or missense mutations in exon 3 of *CTNNB1* gene in the liver are the most common activating mutations associated with the development of HCC.[79, 84] Besides mutations in *CTNNB1* gene, dysregulation of Wnt/β-catenin pathway could be driven by different mechanisms, such as mutations in the genes coding components of this signaling pathway (e.g. Axin-1, GSK3-β) as well as epigenetic changes.[85] Many findings suggest that Wnt/β-catenin mutation and overexpression have an important role in early-stages of tumorigenesis and in transformation of benign liver tumors to HCC.[53, 67]

Only very limited data demonstrated implication of Wnt signaling pathway in development of iCCA.[86] It is known that progressive activation of Wnt pathway mediated by Wnt7B ligand, frequently overexpressed in tumor stroma, promotes cholangiocarcinogenesis and directly correlates with the tumor growth.[86]

1.2.4.3 **PI3K/Akt/mTOR signaling**

The PI3K/Akt/mTOR signaling pathway is essential for cell growth and survival.[87, 88] Somatic mutations and/or gains and losses of key genes in this pathway are detected in a number of different solid and hematological tumors.[89, 90] Activation of the PI3K/Akt/mTOR pathway results in an impaired cell growth and survival, which

leads to competitive growth advantage, metastatic dissemination, angiogenesis, and therapy resistance.[87] PI3K/Akt/mTOR signaling pathway can be induced by binding of variety of different growth factors (e.g. insulin-like growth factor (IGF), epidermal growth factor (EGF)) to corresponding receptors. PI3K subsequently produces the second messenger PIP_3 (phosphoinositoltriphosphate), which in turn activates the serine/threonine kinase Akt. In normal tissue, this pathway is negatively regulated by the phosphatase and tumor suppressor on chromosome 10 (phosphatase and tensin homolog (PTEN)), which targets the lipid products of PI3K for dephosphorylation (Figure 8).[91] In HCC, activity of the PI3K/Akt/mTOR pathway has close association with tumor cell survival and early recurrence.[92] Impaired activity of mTOR signaling pathway is more frequently induced by activation of either the IGF and/or EGF cascade, than direct activation by somatic mutations of the different components.[93] Emerging evidences also suggest that PI3K/Akt/mTOR signaling may be activated by somatic mutations in the PI3K catalytic A gene (*PIK3CA*), which encodes the p110a catalytic subunit of PI3K.[91] Further, decreased expression of *PTEN* gene due to mutation or methylation, as well as changes in PTEN function, can also lead to increased activity of the PI3K/Akt/mTOR pathway in HCC.[94] Reduced activity or expression of the PTEN phosphatase can result in constitutive activation of the PI3K/Akt/mTOR pathway. In addition, *PTEN* expression can be downregulated directly by the hepatitis B virus protein (HBx) protein in HBV-infected patients, or by HCV core protein at transcriptional level.[93, 95]

This signaling pathway also plays a critical role in iCCA and it is involved in drug resistance, autophagy, as well as in programmed cell death regulation.[96] Constitutive activation of PI3K/Akt/mTOR pathway is predominantly caused by PTEN inactivation, or by increased expression in its pathway components, such as EGF and HER-2 growth factors, as well as by IL-6 pathway activation in chronically inflamed biliary epithelium.[97] Activation of the pathway can also be achieved through bile acid intake by apical sodium bile acid cotransporter (ASBT), or by induction of EGFR phosphorylation.[98, 99] Overall, above mentioned factors contribute to the tumor progression and poor prognosis in iCCA patients.[96]

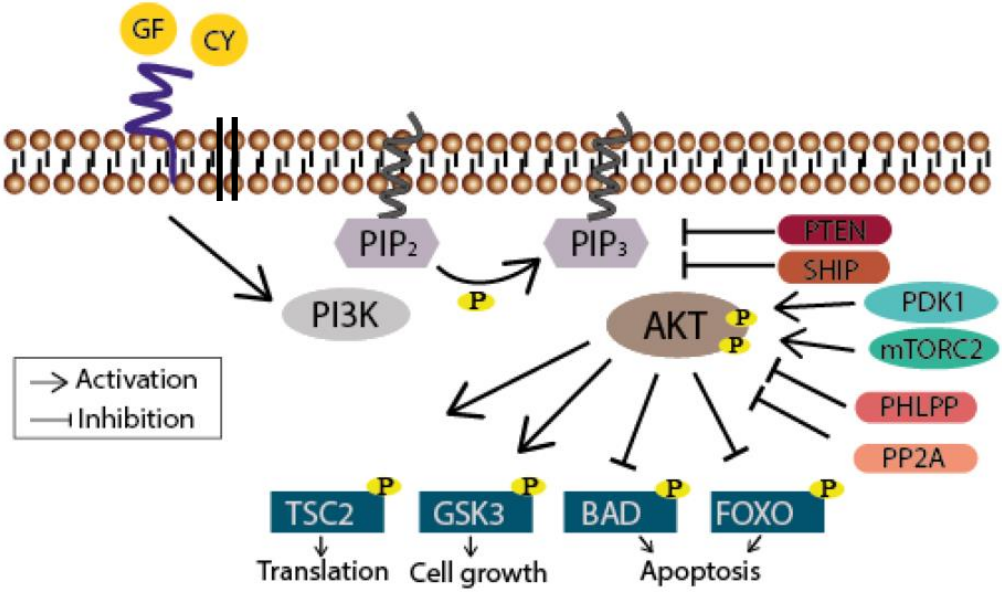

Figure 8 Schematic overview of the PI3K/Akt/mTOR signaling pathway.
PI3K is activated through growth factors (GF) or cytokines (CY) binding to a receptor resulting in the conversion of PIP2 into PIP3 by phosphorylation. PKB/Akt further binds to PIP3 at the plasma membrane and latter undergoes conformational changes leading to its phosphorylation and activation by PDK1 and mTORC2. Akt finally participates in the regulation of cellular processes. Termination of the signaling cascade occurs through the dephosphorylation of PIP3 by the phosphatase PTEN or SHIP, or further downstream through the dephosphorylation of Akt by PHLPP or PP2A (modified from Diehl *et al.* 2013[100])

1.2.4.4 **IL-6/JAK/STAT signaling**

JAK/STAT (Janus kinase/signal transducers and activators of transcription) pathway is activated by more than 40 cytokines and regulates many processes in the cells, mainly immune response, development, proliferation, differentiation and apoptosis.[101, 102] Herein, the signaling pathway is involved in transmitting information from extracellular signal molecules to target gens. Analyses have shown that many solid tumors exhibit activation of the JAK/STAT signaling pathway, including HCC.[103] Mutations in *JAK1* gene are found in about 1% of the HCCs. This pathway is related to chronic inflammation that could be triggered by pro-inflammatory cytokines such as IL-6. A constitutive activation of JAK/STAT pathway can also result from aberrant hypermethylation of *SSI-1* gene (stress survival islet-1), which has been identified in 53% of HCC patients, according to the study of Nagai *et al.*[104, 105] Furthermore, silencing of suppressor of cytokine signaling 1 (*SOCS1*) due to promoter methylation has been described in 61% of HCC. In addition, between 30-38% of HCC exhibit epigenetic inactivation of *SOCS3* due to promoter methylation.[67] Thus, JAK/STAT signaling pathway is crucial for liver homeostasis and cancer.

In iCCA inflammatory cytokine IL-6 can promote tumor growth in autocrine manner by epigenetic modulation of the genes involved in growth-regulatory signaling pathways, such as those involved EGFR.[106] IL-6 can also act as Akt pathway activator, leading to high expression of antiapoptotic protein myeloid cell leukemia-1 (Mcl-1) and consequently promoting apoptosis resistance.[107]

1.2.4.5 **Ras/MAPK signaling**

The Ras/MAPK pathway plays a fundamental role in the control of major cellular processes, such as cell survival and proliferation. Dysregulation of the pathway is implicated in malignant transformation and progression of many cancers including liver cancer.[108] Although the frequency of mutations in *RAS* gene is low (>1%) in HCC, several studies have shown that aberrant activation and overexpression of the *RAS* gene is associated with shorter overall survival in HCC patients.[108, 109] Additionally, overexpression of downstream member of Ras/MAPK pathway, Raf-1 was proven to carry prognostic value, and it can be used as a biomarker for predicting the early tumors recurrence and poor prognosis in HCC.[109] Also, increased MEK1/2 and ERK phosphorylation and expression was frequently observed in HCC when compared to adjacent normal liver tissue.[110] Finally, Ras/MAPK pathway activation is observed in HBV-mediated HCC, where chronic infection with HBV induces expression of two transcriptional activators, hepatitis B

virus X protein (HBx) and the PreS2-activator large surface protein (LHBs), that can trigger the activity of the pathway.[91]

In iCCA several commonly activating mutations in Ras/MAPK signaling were identified. Activating mutations in kristen rat sarcoma (*KRAS*) gene are frequent, in average 19% iCCAs, particularly in codon 12.[111] Moreover, *BRAF* gene, encoding a downstream component of signaling pathway, is mutated in 7% cases. Activating mutations in the epidermal growth factor receptor (*EGFR*) gene is rare event (2%), however, deregulation of Ras/MAPK pathway downstream of EGFR is one of the hallmarks of iCCA.[70]

1.2.4.6 **Notch signaling**

The Notch signaling pathway is evolutionary conserved and present in most multicellular organisms. It is important for many cellular processes including maintenance of stem cells, specification of cell fate, differentiation, proliferation and apoptosis.[112] Activation and regulation of the pathway is finely tuned on multiple levels and highly dependent on the cellular context in which it is activated. In the liver, Notch signaling pathway is activated after injury and mediates interactions between different cell types involved in the repair process. It is important factor in the regulation of liver metabolism, inflammation and cancer.[113] Another important aspect of the pathway is temporal- and dose-dependent coordination of biliary fate and morphogenesis.[114] Earlier studies have shown that overexpression of *NOTCH1* inhibits HCC cell growth by promoting cell cycle arrest and apoptosis.[115, 116] However, in the more recent studies, new evidence demonstrated pro-oncogenic role of Notch during hepatocarcinogenesis. In a study by Villanueva *et al*. authors demonstrated that Notch signaling promotes liver carcinogenesis in a genetically engineered mouse model.[117] This finding was further confirmed in a cohort of HCC patients where activation of the pathway was detected in 30-35% cases. Moreover, they showed that pro-oncogenic function of NOTCH1 depends on molecular context, particularly, upregulation of *IGF2* and *SOX9*.[117] Another study demonstrated that NOTCH3 may function as an important factor contributing to therapy resistance in HCC and that elevated expression of NOTCH3 protein could represent a selective advantage for HCC development, whereas after depletion of NOTCH3 by specific shRNAs, they observed increased *TP53* expression and improved doxorubicin sensitivity by promoting apoptosis.[118] Accordingly, Notch represents a novel candidate in targeted approach and a starting point for new drug development to fight HCC.

As the Notch pathway appears to be a key regulator in normal cholangiocytes for differentiation and bile duct ontogenesis, it is rationale to expect that in a chronically diseased liver this pathway becomes dysregulated and further implicated in malignant processes.[119] Recent studies have demonstrated that dysregulation of Notch pathway can have implications in development and progression of iCCA.[120, 121] Significant number of patients with iCCA demonstrated upregulation in Notch receptors, namely Notch1 in 83%, Notch2 in 56%, Notch3 in 39% and Notch4 in 34% cases. Further, in this study it was revealed that aberrant expression of Notch

receptors 1 and 4 play more important role during iCCA progression than other receptors.[122] In another study exploring differentially expressed genes in HCC and iCCA, Notch pathway was identified as one of the top pathways based on the overexpressed genes, when compared to HCC.[123] Overall, considering the importance of Notch pathway activation in the pathogenesis of iCCA, it is important to target these pathways by using available inhibitors as well as to proceed with development of novel treatments.[71]

1.2.4.7 **Growth factor signaling and other regulators**

Several growth factors and their receptors mediate tumorigenic activity through a variety of signaling pathways.[124] After liver injury or damage, when activation of regenerative processes is required, adult hepatocytes as well as other non-parenchymal cells are able to produce different growth factors, such as EGF, transforming growth factor alpha (TGF-α), IGF and VEGF. In chronically injured liver production of these growth factors as well as activation of corresponding receptors and downstream signaling is dysregulated. Such impaired growth factor production and signaling can lead in the direction of hepatocarcinogenesis.[124]

1.2.4.7.1 **HGF/MET signaling**

c-Met is a receptor tyrosine kinase activated by binding of only one known ligand, i.e. HGF. After binding to MET receptor, HGF can induce cytoprotective role in the liver, by providing protection from damage and suppression of FAS-induced apoptosis in hepatocytes.[125] Accordingly, expression of HGF is increased in response to liver injuries, while depletion of HGF enhances liver damage.[126] Despite having beneficial role in liver regeneration and different liver diseases, increased c-Met activity plays an important role in initiation and progression of HCC.[127] Dysregulation of c-Met has been noted in approximately 50% HCC patients. Further, aberrant c-Met activation is in close connection with enhanced tumor growth, aggressive behavior and poor prognosis.[128] Mechanisms of aberrant activity are heterogeneous and range from gene mutation, gene amplification, receptor overexpression to increased mRNA expression.[126] Tumors with overexpressed c-Met can show reduced dependence on HGF due to constant receptor dimerization and activation. In this context, c-Met inhibition represents an active area of research in HCC, and several selective c-Met inhibitors are under clinical evaluation in patients with advanced HCC.[126]

It has been reported that c-Met overexpression is present in more than half of iCCA cases and that it correlates with degree of tumor differentiation, being highest in well-differentiated and low in poorly differentiated tumors.[129] Moreover, overexpression of the *MET* gene in cholangiocarcinoma can lead to increased cell migration and invasion, angiogenesis and tumor differentiation/proliferation.[130-132]

1.2.4.7.2 **Angiogenesis**

Angiogenesis significantly contributes to the growth of many cancers, including PLC.[91, 133] VEGF is a main regulator of angiogenesis in cancerous tissue known to

be upregulated in both PLCs. Several other angiogenic growth factors, including angiopoietin-2 and platelet-derived growth factor (PDGF) were also shown to be upregulated in HCC.[134] In iCCA several other factors that influence angiogenesis are found to be upregulated, such as angiopoietin 1 and 2, thrombospondin, EGF, EGFR and fibroblast growth factor (FGF).[133] These factors play important roles in proliferation of endothelial cells, which activates neovascularization around and within the tumor tissues leading to tumor expansion and progression. Angiogenic signaling is further mediated through a variety of mechanisms, including activation of the Ras/MAPK, PI3K/Akt/mTOR and Janus kinase.[91, 134]

1.2.4.7.3 **TGF-β signaling**

Transforming growth factor beta TGF-β is an important signaling pathway in the liver affecting and regulating many important processes and cell types.[135] During cancer initiation, TGF-β signaling exerts tumor suppressor effects at pre-neoplastic and early tumor stages, while cytostatic effects of TGF-β are often disrupted in progressed stages due to genetic dysregulation of different members of the signaling pathway.[136] This progressed stage is characterized by a late TGF-β signature which promotes the phenotypic switch from tumor suppressor to tumor promoter. In advanced stage, cancer cells undergo an epithelial-mesenchymal-transition (EMT) where they acquire invasive and pro-metastatic properties.[137] Thus, targeting TGF-β pathway could be a promising therapeutic tool in advanced stages of PLC.

1.2.4.7.4 **c-MYC regulation**

c-MYC is a transcription factor involved in many diverse cellular processes, such as control of cell cycle progression, proliferation, growth, adhesion, differentiation, apoptosis and metabolism.[138] In the context of the liver, it has been strongly associated with hepatocyte proliferation occurring during liver damage and regeneration.[139] Emerging data suggests that dysregulation of c-MYC function might be associated with chronic liver disease and hepatocarcinogenesis.[139] Studies have reported that dysregulation of *MYC* expression is a very early event in liver carcinogenesis, and that *MYC* oncogene amplification is an indicator of malignant potential and poor prognosis in HCC patients.[140, 141] According to Kawate *et al*. dysregulation of c-MYC is closely associated with proliferative activity and *TP53* overexpression, and it has close association to progression of HCC.[140]

Studies have also revealed important roles of c-MYC in different stages of liver disease, including iCCA.[142] It is shown that c-MYC induction promotes cholestatic liver injury and iCCA progression.[142] Moreover, c-MYC is capable of abolishing contact inhibition in human iCCA that is mediated by mTOR pathway and Yes-associated protein (YAP). Loss of contact inhibition is a hallmark of a wide range of human cancer cells, and therefore it represents an important aspect of cholangiocarcinogenesis.[143]

1.2.4.7.5 **Telomere maintenance**

Telomerases are nucleoprotein complexes with the main function to maintain chromosomal integrity and genome stability during cell division, primarily by lengthening terminal regions of telomeric DNA.[144] Human telomerase is composed of two main core subunits, TERT that forms the catalytic subunit and RNA component (TERC) that provides a template for telomerase elongation. A positive correlation between *TERT* mRNA expression and telomerase activity has been observed, thus implying that telomerase is regulated by *TERT* gene expression.[145] Accordingly, reactivation or re-expression of telomerase is frequently observed in many human cancers, including HCC.[146] Molecular alterations in *TERT* are the most frequent somatic genetic alterations in human HCC detected in 20-60% of all cases. They are also observed in cirrhosis as well as in the normal liver tissue.[147] TERT promotor mutations are early major events in carcinogenesis occurring first at preneoplastic stages in cirrhosis and further in malignant transformation, often in association with Wnt/β-catenin pathway activation.[148] Mutations in TERT promotor are rare events in iCCA, contrary to high frequency observed in HCC.[111]

1.2.4.8 **Epigenetic changes in PLC**

Epigenetic changes can be defined as heritable changes in a cellular phenotype that were independent of alterations of the DNA sequence, such as methylation, acetylation, histone modification etc. The information carried by epigenetic modifications play a critical role in the regulation of all DNA-based processes, such as transcription, DNA repair and replication.[149] As a consequence, impaired expression or genomic alterations in chromatin regulators can have critical implication in the induction and maintenance of various cancers including HCC and iCCA.[70, 150] Epigenetic changes such as DNA hypermethylation or hypomethylation, dysregulation of histone modification patterns, chromatin remodeling and aberrant expression of micro-RNAs (miRNAs) and long noncoding RNAs (lncRNAs) are associated with PLC.[70, 151]

1.2.5 **Systemic therapies for advanced HCC and iCCA**

Both primary liver cancers, HCC and iCCA, are asymptomatic at early stage and lack biomarkers of early detection.[152] As a consequence, only one-third of HCC and small number of iCCA patients are diagnosed at early stages, when potentially curative treatments, such as resection, transplantation or local ablation are still available. Majority of primary liver cancers are still diagnosed at late stages when curative treatment options are limited and mortality rates are very high.[153] For patients with advanced stage disease, systemic chemotherapy is the most widely used treatment approach.[154]

1.2.5.1 **First-line therapy in HCC**

Sorafenib was the first systemic therapy to show a significant survival benefit, and consequently, it has become a standard of care for patients with advanced HCC.[154] It is a multikinase inhibitor that affects tumor cell proliferation and tumor angiogenesis. Sorafenib actively affects key signaling pathways by targeting

numerous serine/threonine and tyrosine kinases, such as RAF1, BRAF, vascular endothelial growth factor receptor (VEGFR)1,2,3, platelet-derived growth factor receptor (PDGFR), KIT, FLT3, fibroblast growth factor receptor one (FGFR1) and RET.[155] Treatment with sorafenib in Western patients demonstrated improved median overall survival in comparison with placebo (10,7 vs. 7,9 months) and longer median time to progression (5,5 vs. 2,8 months).[156] Lenvatinib is a multiple-receptor tyrosine kinase (RTK) inhibitor that inhibits the kinase activities of VEGFR1,2,3, FGFR1,2,3,4, PDGFRα, KIT and RET.[157] Lenvatinib was approved by FDA (US Food and Drug Administration) for the first-line HCC treatment in 2018 based on the data from a phase III clinical trial comparing with sorafenib in the patients with unresectable HCC in a non-inferior setting. The median overall survival in the treatment group was increased in comparison with placebo (13,6 vs 12,3 months), as well as progression-free survival (7,4 vs. 3,7 months) and median time to progression (8,9 vs. 3,7 months).[158] In addition, lenvatinib is used in other solid cancers as an antineoplastic agent (in treatment of advanced, metastatic medullary thyroid cancer and refractory renal cell carcinoma).[159]

1.2.5.2 **Second-line therapy in HCC**

One phase III clinical trial demonstrated that regorafenib can result in survival benefit for HCC patients who show progression but tolerated sorafenib. This particular finding led to FDA approval of regorafenib as a second-line treatment for HCC after sorafenib administration.[160] Similar to sorafenib, it inhibits multiple protein kinases, including those involved in tumor angiogenesis (VEGFR1,2,3, TIE2, PDGFR-β, FGFR1) and oncogenesis (KIT, RET, c-RAF/RAF-1, BRAF). It also affects proteins involved in MAPK signaling pathway (P-ERK1/2, P-JNK, P-c-Jun), apoptosis (Bax, Bcl-2, Bcl-X, survivin, cleaved caspase 3,7,8 and 9) and autophagy (Beclin-1, LC3-II).[161]

Additionally, new treatment possibilities are emerging from clinical trials using antibodies targeting the immune checkpoint inhibitors - programmed cell death 1 (PD-1), programmed cell death ligand 1 (PD-L1), or cytotoxic T-lymphocyte-associated protein 4 (CTLA-4).[162] For instance, FDA has approved the use of nivolumab for advanced HCC patients who failed to respond to first-line treatment with sorafenib. In general, nivolumab is a fully human immunoglobulin G4 (IgG4) PD-1 immune checkpoint inhibitor antibody that disturbs interaction between PD-1 and its ligands (PD-L1/2). Positive effects occur due to the restoration of T-cell antitumor immunity directed against tumor cells.[163] Several other inhibitors are showing positive results in phase III clinical trials for sorafenib treated patients with advanced HCC. Treatment with cabozantinib, a tyrosine kinase inhibitor that inhibits VEGFR 1,2,3, MET, and AXL, demonstrated longer overall survival and progression-free survival than placebo. Furthermore, ramucirumab, a fully humanized monoclonal antibody targeting VEGFR2, improved overall survival as well as progression-free survival of the patients in a phase III clinical study.[156]

1.2.5.3 **Systemic chemotherapy in iCCA**

For the patients with advanced stage iCCA, standard treatment options include combination of gemcitabine and cisplatin.[162] Gemcitabine is a nucleoside analog and it has been used as a chemotherapeutic agent for almost two decades. Gemcitabine has several modes of action, and the most important is inhibition of DNA synthesis. Additionally, it can act through self-potentiation by inhibition of enzymes related to deoxynucleotide metabolism, and by induction of apoptosis through caspase signaling.[164] Moreover, cisplatin is capable to crosslink with the purine bases on the DNA. It interferes with DNA repair mechanisms, causing DNA damage, and subsequently induces apoptosis in cancer cells.[165] For the patients who show progression on gemcitabine and platinum based therapy, there is no standard 2nd line option. Several trials that are evaluating regimens for iCCA in the second-line setting show promising activity.[166]

1.2.6 **Models to study PLC**

Recent developments in precision medicine approaches have produced effective molecularly targeted therapies in many solid cancers, however, outcome in PLC remains low due to a pronounced phenotypic and molecular diversity. Development of representative models is urgently needed as a necessity to provide effective translation from descriptive genomic studies into clinical practice.[61, 153] In the liver cancer field, there is a lack of models that accurately represent morphological and molecular heterogeneity of the original tumors. Ideally, models to be used in cancer research should reflect human disease on several levels, from anatomical and physiological to (epi-)genetic and transcriptomic. Importantly, tumor models should reflect the background setting of the disease that it is arising from (etiology), since it can influence molecular basis of the disease evolution and progression.[167]

1.2.6.1 **Animal models**

Animal models play an important role in cancer research, particularly for studying and better understanding mechanisms of human (hepato-)carcinogenesis. The goal of animal research is to mediate a transition from *in vitro* studies to clinical practice and ultimately bring the benefits to patients.[168] Since rodents entered into laboratory studies, particularly mice, a variety of different models have been developed to study liver diseases including hepatocarcinogenesis.[169] In general, they can be divided into distinct categories based on the mechanism of inducing desired phenotype: 1) chemically induced models, 2) transplantation models (syngeneic and xenograft models), 3) viral models, and 4) genetically engineered mouse models. Availability and reproducibility of mice made them one of the most exploited organisms in human cancer research. They carry very important features for liver research, such as small size, short life span, high breeding capabilities, genetic engineering options and similarities to human hepatic diseases.[167] Apart from rodents, many other animal models have been developed over the years, e.g. rabbit, swine, primate etc. Nevertheless, these models show only limited overlap to human liver cancers in terms of physiology, etiology and clinical setting.[170]

1.2.6.1.1 **PDX models**

A novel model potentially closely reflecting and preserving human PLC features is generated by xenotransplantations. Xenograft mouse model (patient-derived xenograft – PDX) is created by transplanting small pieces of primary tumors directly into immunocompromised mice.[171] Propagation of the PDX models includes direct passaging of the cells from a mouse to a mouse, as the tumor burden increases in an animal. There are two main methods to create PDX models - orthotopic and heterotopic. Orthotopic model includes direct implantation to the mouse organ of choice, while heterotopic PDX model includes implantation into the subcutaneous flank of a mouse.[171, 172] PDX models have shown some advantages over classical commercially available cell lines. Examination of PDX indicated that histology and gene expression profiles as well as genomic alterations were retained when compared to their original tumors. In several studies, authors have further shown that PDXs were able to predict patient's response to chemotherapy.[173, 174] Nevertheless, wider application of this model in the medical studies is limited due to existing disadvantages. PDX lack to show tumor progression or metastasis and do not reproduce all the stages of the disease usually observed in the patients. Lack of representative tumor microenvironment, as well as severely compromised immune system limits exploitation of PDXs to the full scale. Additionally, low success rate of implantation hampers global application of the model. Large scale drug testing to identify potential new therapeutics still remains challenging as high amount of resource, time, and animals are required.[175, 176]

1.2.6.2 **Organoids**

In the last years, new 3D models of human cancers emerged as an alternative to classic 2D cell line and PDX models.[177, 178] High expansion rate of 3D organoid models for variety of different cancers has been demonstrated. Establishment and extensive morphological and molecular characterization of early 3D models in prostate, pancreatic, colorectal, bladder etc. cancers had served as a basis for development of equivalent models for liver cancer.[179-183] Organoids are generated from the primary cancerous tissue by enzymatic/mechanic dissociation or from single cells and propagated by using a matrix and a media that promotes cell proliferation. New cultivation system that allows multidimensional growth of the tumor cells is largely comprised of a matrigel as growth matrix and a cocktail of different growth factors that promote expansion of cancer cells.[184] Several studies have reported successful establishment of organoids derived from primary liver cancers, HCC, iCCA and combined hepatocellular cholangiocarcinoma (CHC).[177, 178] Authors of the studies showed that derived organoid models recapitulated histological, transcriptomic and genomic traits of original tumors, and demonstrated that potential drug screening applications are feasible with organoids. [177, 178]

Yet, organoids appear to be very reliable and easy to establish *in vitro* models, but there are several limitations to this. Firstly, success rate of derived organoids remains low and it is highly dependent on properties of each individual tumor (e.g. tumor grading).[177] Furthermore, when compared with cancer cell lines, organoid cultures require significantly higher amount of resources, making them more difficult

to produce for large-scale applications. Intrinsic limitations of organoid culture are the lack of stroma, blood vessels and immune cells. The requirement for extracellular matrix substitutes, such as matrigel, and need for the fetal bovine serum, leaves the possibility that undefined extrinsic factors influence the outcome of the experiments, such as drug sensitivity.[177] Some organoids derived from advanced cancers often display lower proliferation rate than organoids derived from normal epithelial cells. This leaves a space for epithelial-derived organoids to overgrow and become dominant entity in the culture.[177, 178, 185]

1.2.6.3 **Cell lines**

Cancer cell lines have been used for several decades to study biology and molecular processes of the cancers, and they are widely used model in pharmacogenomics studies.[186] Overall, great potential of the cell lines was exploited to dissect general mechanisms of human carcinogenesis, to identify novel molecular targets for therapy, and to discover novel biomarkers for drug sensitivity.[187] Cell lines derived from human tumors provide an unlimited, self-replicating and easily propagating source of cancerous cells. Since cancer cells in the culture harbor high proliferative capacity, they are widely used for mechanistic and high-throughput analyses in many laboratories across the world.[188] Through the history, cell lines have played a significant role in the development of anti-cancer drugs. New idea of large-scale screens of cancer cell line panels, such as NCI-60, is being further explored in order to characterize genomic profiles to mimic genetic heterogeneity of the original tumors and predict sensitivity to many compounds.[189] This approach is already influencing standardized pipelines of drug development, and, thus, cancer cell lines are an important tool for pharmaceutical industries with the main focus on development of molecularly targeted cancer therapies.[189] These investigations clearly demonstrated that cell lines can be used to identify drugs that are active in the specific genetic contexts.

However, due to clonal origin and possible selection during long-term cultivation, several important questions have been raised among the scientific community, questioning whether the cell lines closely represent, both on genomic and transcriptomic level, original tumors which they were derived from.[190] Several decades of propagation under artificial culture conditions, exchange among different laboratories, might have further induced phenotypic, functional and molecular changes that make the cells no longer suitable to accurately represent the primary tumor characteristics. Therefore, detailed comparison of the original tumors and their cell lines is essential, but since many of the cell lines were established several decades ago, a direct comparison to the original tumors cannot be performed anymore.[191] Thus, the establishment of well-characterized novel patient-derived cell lines (PDCL) for PLC that closely resemble phenotypic and molecular features of the original tumor is highly desirable.

In vitro PDCL can be derived from the cancer tissue by mechanical and enzymatic dissociation, followed by cultivation in various conditions and, dependent on cell requirements, medium containing combination of specific growth factors and/or

serum. Limitation to this system is lower success rate to establish stabile growth, of about 10–15% of samples, and the fact that cultures can take weeks to several months to reach significant growth.[192] Several studies successfully established and propagate PDCL in culture, and compare them with their original tumor. One study showed that isolated glioblastoma cells retained mutation in a specific tumor suppressor gene that was originally detected in a corresponding tumor tissue.[193] Furthermore, it was found that human non-small cell lung carcinoma (NSCLC) cell line after long cultivation period in great extent preserved properties of their parental tumors and could be used as a suitable model system for biomedical studies.[188] Recently, a study generated several PDCL from the same tumors, where they tried to dissected intrahepatic tumor heterogeneity in HCC.[194] They demonstrated that PDCL model derived from multiregional cancer samples in early passage could be useful platform to determine how intratumoral heterogeneity affects sensitivity to different therapeutic agents. Additionally, one study successfully utilized lung cancer PDCL to predict therapy response and to select effective drug combinations for a potential patient application.[195]

Overall, results of these studies confirm the similarity in key morphological and molecular features in PDCL and matched primary cancers and support their usefulness as a patient-specific model for treatment evaluation and drug response testing. However, to date the usefulness of PDCL from different cellular origins of human liver cancer has not been fully explored.

Short comparison between different preclinical models can be seen in the Table 1 below. All important aspects of models utilized in cancer research are briefly summarized.

Table 1 Comparison between different cancer models.

In the table are summarized and compared important aspects of preclinical cancer research models. Number of stars represents the importance of a given feature, where three stars stand for the best feature, while one star stands for the modest feature.

	Cell lines		Organoids	Animal models	
	Established	Patient-derived		PDX	Chemical/Genetic
Success rate of establishment	*	*	**	**	***
Time to establish	*	*	**	**	*
Handling	***	***	*	*	**
Long term propagation	***	***	**	**	***
3D growth	-	-	**	***	***
Representation of cancer spectrum	*	**	**	**	**
Matched tumor controls	-	**	**	**	***
Phenotypic stability	*	**	**	***	***
Genetic stability	*	***	***	***	***
Microenvironment (tumor-stroma)	-	-	-	**	***
Immune context	-	-	-	-	**
Genetic modification	***	***	**	-	*
High-throughput drug screening	***	***	*	-	-
Costs of maintenance	***	***	*	*	**

*** best ** very good * modest - N/A

2. Aim

Primary liver cancers rank among the deadliest cancers world-wide with high mortality and poor life expectancy. Lack of clinical symptoms and biomarkers for early detection are the main causes of late diagnosis, when curative options are limited. Despite identification of several potentially drugable targets and subsequent development of next-generation targeted therapies, translation of these findings into clinical practice remains challenging in liver cancer due to a pronounced phenotypic and molecular diversity. Therefore, it is essential to develop representative models of the primary liver cancers that would lead transition from laboratory research into clinical practice. To overcome the existing obstacle in the translational cancer research, it is necessary to establish well-characterized novel PDCL for liver cancers that closely resemble phenotypic and molecular features of the original tumor. While the usefulness of PDCL for individualized, patient-specific modeling of treatment effects and drug response has been shown in different solid tumors, their potential in human liver cancer is largely unknown. Based on these observations, the research project presented in this thesis has aimed to address following aspects of PDCL biology:

- ***To establish long-term cultures of patient-derived cancer cell lines from major primary liver cancers – hepatocellular carcinoma and intrahepatic cholangiocarcinoma***
  With the implementation of standard cell isolation procedure, our goal was to establish stable long-term culture of PLC-PDCL and propagate in *in vitro* 2D conditions to subsequently perform phenotypic, molecular and translational analyses.

- ***To test whether PDCL recapitulate phenotypic and molecular diversity of the primary cancers, and the effects of long-term cultivation on phenotypic and molecular profiles***
  By using state-of-the-art technologies, such as next generation sequencing, we were aiming to deeply characterize and generate molecular profiles of newly derived PDCL and investigate how accurately they represent original cancer tissue. Further, we wanted to test how long-term cultivation conditions affect morphologic, transcriptomic and genomic profiles in newly established PDCL models.

- ***To investigate whether PDCL reflect genomic and prognostic features of authentic primary liver cancers***
  We wanted to implement obtained genomic and transcriptomic results together with authentic human HCC and CCA data to confirm molecular similarities and to test if the PDCL can be used as a representative model for different established prognostic subgroups of PLC patients.

- ***To evaluate if PDCLs could be used as a useful model for personalized treatment approaches***
  We wanted to detect key oncogenic alterations that are potentially amenable to specific inhibition and to predict a response to the therapy. Overall, goal was to determine potential utility of PDCL for individualized treatments strategies.

3. Materials and methods

3.1 Materials

3.1.1 Electronic devices and laboratory equipment

Table 2 Applied instruments.

Name	Manufacturer
Agilent 2100 Bioanalyzer	Agilent, Santa Clara, California, USA
Autoclave Systec V150	Systec, Osnabrück, Germany
Balance Adventurer Pro OHAUS	OHAUS, Greifensee, Switzerland
Biofuge fresco	Heraeus, Hanau, Germany
Cell Counter Biorad TC20	Biorad, Hercules, California, USA
Centrifuge Hettich Universal 320R	Andreas Hettich GmbH & Co.KG, Tuttlingen, Germany
CO_2 Incubator Steri-Cycle i160	Thermo Fischer Scientific, Braunschweig, Germany
Eppendorf centrifuge 5415R	Eppendorf, Hamburg, Germany
Eppendorf Research Plus Pipette 1000 µl	Eppendorf, Hamburg, Germany
Eppendorf Research Plus Pipette 200 µl	Eppendorf, Hamburg, Germany
Eppendorf Research Plus Pipette 20 µl	Eppendorf, Hamburg, Germany
Eppendorf Research Plus Pipette 10 µl	Eppendorf, Hamburg, Germany
Eppendorf Research Plus 12 channel Pipette 100 µl	Eppendorf, Hamburg, Germany
Hera Freeze deep freezer	Thermo Fischer Scientific, Braunschweig, Germany
Herasafe Biological Safety Cabinet	Thermo Fischer Scientific, Braunschweig, Germany
HiSeq 4000 System	Illumina, San Diego, California, USA
Hot plate Leica HI1220	Leica, Wetzlar, Germany
Illumina HiSeq 4000	Illumina, San Diego, California, USA
IKA MS3 Vortexer	IKA, Staufen, Germany
IKA Vortex MS1 Minishaker	IKA, Staufen, Germany
iScan System	Illumina, San Diego, California, USA
Leica CM1850 UV Cryostat	Leica, Wetzlar, Germany
Leica EG1150 C	Leica, Wetzlar, Germany
Leica HI1210	Leica, Wetzlar, Germany

Name	Manufacturer
Leica TP1020	Leica, Wetzlar, Germany
Liebherr Premium Freezer	Liebherr, Bulle, Switzerland
Liebherr MediLine Refrigerator	Liebherr, Bulle, Switzerland
LSM 710 NLO Confocal microscope	Carl Zeiss AG, Oberkochen, Germany
Microtome blade MX 35 premier 34/80 mm	Thermo Fischer Scientific, Braunschweig, Germany
Microtome Leica RM2255	Leica, Wetzlar, Germany
Microscope Axio Zeiss Vert.A1	Carl Zeiss AG, Oberkochen, Germany
Ministar Silverline Minicentrifuge	VWR International, Darmstadt, Germany
MiSeq System	Illumina, San Diego, California, USA
MultiGourment Steamer	Braun, Frankfurt, Germany
NanoDrop 1000 Spectrophotometer	Peqlab, VWR International, Darmstadt, Germany
pH meter inoLab Ph7110	WTW, Weilheim, Germany
Pipetboy Acu 2 Pipette Controller	INTEGRA Biosciences AG, Zizers, Switzerland
Qubit 4 Fluorometer	Invitrogen, San Diego, USA
TECAN infinite M 200Pro	Tecan, Männedorf, Germany
Vacuubrand BVC Control Vacuum pump	Vacuubrand, Wertheim, Germany
Water Bath GFL 1083	GFL Gesellschaft für Labortechnik, Burgwedel, Germany

3.1.2 Consumables

Table 3 Applied consumables.

Name	Manufacturer
1000 µl Tips	Starlab GmbH, Ahrensburg, Germany
200 µl Tips	Starlab GmbH, Ahrensburg, Germany
0,1-20 µl Graduated Tips	Starlab GmbH, Ahrensburg, Germany
96 well-plates flat bottomed	Greiner Bio-One, Frickenhausen, Germany
Cell culture flasks (75 cm^2)	Thermo Fischer Scientific, Braunschweig, Germany
Cell culture TC Dish 100	SARSTEDT AG & Co. KG, Nümbrecht, Germany
Counting slides for cell counter	Biorad, Hercules, California, USA

Name	Manufacturer
Conical centrifuge tubes (15 ml and 50 ml)	SARSTEDT AG & Co. KG, Nümbrecht, Germany
Cell strainer (30 µm and 70 µm)	Miltenyi Biotec, Bergisch Gladbach, Germany
Cryo tubes	Greiner Bio-One, Frickenhausen, Germany
DAKO Pen	Dako Deutschland GmbH, Hamburg, Germany
Inject-F (single use injection) 1 ml	B.Braun, Melsungen, Germany
Knittel glass cover slips 24*50 mm	Iss, Bradford, United Kingdom
Microscope coverslips	LifeTechnologies GmbH, Darmstadt, Germany
One-time reagent reservoir	Carl Roth GmbH, Karlsruhe, Germany
Parafilm M	Bemis Company, Neenah, Wisconsin, USA
Pasteur Pipettes	Carl Roth GmbH, Karlsruhe, Germany
Poly-L-lysine slides	Thermo Fischer Scientific, Braunschweig, Germany
Rotilabo syringe filters	Carl Roth GmbH, Karlsruhe, Germany
Superfrost ultra plus slides	Thermo Fischer Scientific, Braunschweig, Germany
Safe-lock tubes 2,0 ml	Eppendorf, Hamburg, Germany
Safe-lock tubes 1,5 ml	Eppendorf, Hamburg, Germany
Serological pipette, sterile (5, 10, 25 ml)	Greiner Bio-One, Frickenhausen, Germany

3.1.3 Chemicals and kits

Table 4 Applied reagents and kits.

Name	Manufacturer
β-mercapthoethanol	Sigma Aldrich, Steinheim, Germany
4′,6-diamidino-2-phenylindole (DAPI)	Carl Roth GmbH, Karlsruhe, Germany
Acetone	AppliChem GmbH, Darmstadt, Germany
Bovine Serum Albumin (BSA)	Carl Roth GmbH, Karlsruhe, Germany
Collagenase type IV	Gibco Life Technologies, Karlsruhe, Germany
Dimethyl sulfoxide (DMSO)	Carl Roth GmbH, Karlsruhe, Germany
DEPC treated water	Life technologies GmbH, Darmstadt, Germany

Name	Manufacturer
Dulbecco's modified eagle medium (DMEM)	Gibco Life Technologies, Karlsruhe, Germany
DNase I	Sigma Aldrich, Steinheim, Germany
Eosin	Thermo Fischer Scientific, Braunschweig, Germany
Ethanol Technical grade	Thermo Fischer Scientific, Braunschweig, Germany
Ethylendiamintetraacetat (EDTA)	Merck KGaA, Darmstadt, Germany
Eukitt	O. Kindler GmbH & Co, Freiburg, Germany
Fetal bovine serum (FBS)	Pan-Biotech, Aidenbach, Germany
FluorSave Reagent	Merck KGaA, Darmstadt, Germany
Hematoxylin	Merck KGaA, Darmstadt, Germany
Hydrogen peroxide 30%	Carl Roth GmbH, Karlsruhe, Germany
Isoflurane	AbbVie Inc. North Chicago, Illinois, United States
Isopropyl alcohol	Aug. Hedinger GmbH & Co. KG, Stuttgart, Germany
Matrigel BD	Becton Dickinson, Franklin Lakes, New Jersey, USA
Methanol Technical grade	Thermo Fischer Scientific, Braunschweig, Germany
Paraffin	Carl Roth GmbH, Karlsruhe, Germany
Paraformaldehyde (PFA)	Carl Roth GmbH, Karlsruhe, Germany
Penicillin/Streptomycin	Sigma Aldrich, Steinheim, Germany
peqGOLD Tissue DNA Mini Kit	Qiagen GMBH, Hilden, Germany
Phosphat-buffered saline solution (PBS)	Gibco Life Technologies, Karlsruhe, Germany
Proteinase K	Qiagen GMBH, Hilden, Germany
Qiagen RNEasy mini Kit	Qiagen GMBH, Hilden, Germany
Sodium chloride (NaCl)	Carl Roth GmbH, Karlsruhe, Germany
Sodium chloride 0,9% solution	B. Braun Melsungen, Melsungen, Germany
Tissue Tek OCT	Sakura, Torrance, USA
Triton X – 100	Carl Roth GmbH, Karlsruhe, Germany
Trypan Blue	Sigma Aldrich, Steinheim, Germany

Name	Manufacturer
Trypsin/EDTA	Pan-Biotech, Aidenbach, Germany
Tween 20	Carl Roth GmbH, Karlsruhe, Germany
WST-1	Roche Holding AG, Basel, Switzerland
Xylene	Applichem, Darmstadt, Germany

3.1.4 Antibodies

Table 5 Applied primary and secondary antibodies.

Name	Manufacturer
Primary antibody (dilution and host)	
α-Fetoprotein (1:400, rabbit)	Dako Deutschland GmbH, Hamburg, Germany
Albumin (1:100, mouse)	Dako Deutschland GmbH, Hamburg, Germany
Cytokeratin 19 (1:80, mouse)	Dako Deutschland GmbH, Hamburg, Germany
Epithelial cell adhesion molecule (1:80, mouse)	Cell Signaling Technology, Danvers, Massachusetts, United States
Secondary antibody (dilution)	
anti-mouse Alexa 488 (1:500)	Cell Signaling Technology, Danvers, Massachusetts, United States
anti-rabbit Alexa 555 (1:500)	Cell Signaling Technology, Danvers, Massachusetts, United States

3.1.5 Inhibitors

Table 6 Applied inhibitors.

Name	Manufacturer (location, country)
BGJ398	Selleckchem, Huston, Texas, USA
Doxorubicin	Selleckchem, Huston, Texas, USA
Gemcitabine	Selleckchem, Huston, Texas, USA
Imatinib	Selleckchem, Huston, Texas, USA
KU-55933	Selleckchem, Huston, Texas, USA
Refametinib	Selleckchem, Huston, Texas, USA
Sorafenib	Selleckchem, Huston, Texas, USA
Tivantinib	Selleckchem, Huston, Texas, USA
Tofacitinib	Selleckchem, Huston, Texas, USA
Vandetanib	Selleckchem, Huston, Texas, USA

3.2 Establishment of patient-derived cell lines

3.2.1 Patient data and sample processing

Tissues from patients that underwent resection between 2013 and 2015 at the Department of Surgery, University of Mainz, Germany were included in the study following patient informed consent and approval of local ethics committee. Isolation and establishment of PDCL was performed in a total of 38 HCC, 28 iCCA. Clinico-pathological details for successful PDCL are provided in Table 7 and Table 8.

3.2.2 Primary cancer cell isolation

Tissue samples from patients with histologically or radiologically confirmed HCC or iCCA undergoing resection at the Department of Surgery, University of Mainz, Germany were collected. Tumor samples infected with HIV, hepatitis B or C virus were excluded from the experiments in accordance with local requirements. Collected tumor samples were immediately cut into smaller pieces. Tumor cells were isolated by using mechanic and enzymatic dissection: tissue sample was first cut to small pieces (~1 mm^3) and incubated for 30 min. in 8 ml of 1 mg/ml collagenase type IV (Gibco) in Dulbecco's modified eagle medium (DMEM) (Gibco) without Fetal bovine serum (FBS) (Pan-Biotech) at 37°C with gently shaking. After 30 min 4 ml of 1 mg/ml fresh collagenase was added and further incubated for another 30 min at 37°C. After incubation, solution containing cells and undigested pieces was filtered through 70 µm Nylon strainer (Miltenyi Biotec). Undigested pieces from the top of the strainer were collected and plated in 10 cm dish and grown in complete DMEM medium supplemented with 5% FBS. Flow through was centrifuged at 300-400x g, for 5 min at room temperature (RT) and pellet was re-suspended in complete DMEM medium supplemented with 5% FBS and plated in separate 10 cm dish. Isolated tumor cells and the remaining undigested pieces were kept in CO_2 incubator at 37°C and 5% CO_2 atmosphere.

3.2.3 Cell culture

Patient-derived cancer cell lines were cultured in DMEM supplemented with 5% FBS, 1% penicillin and 1% streptomycin (Sigma Aldrich) in humidified 5% CO_2 incubator at 37°C (Thermo Fischer). The medium was routinely changed every 2-3 days and the cells were split after reaching 80% confluence, approximately once in one to two weeks, depending on cell proliferation ratio. For passaging, cells were dissociated by adding 1,5 ml 1x Trypsin/EDTA (Pan-Biotech) and shortly incubated at room temperature. After cells were detached, reaction was inhibited by adding cold DMEM containing 10% FBS. Cells were further centrifuged at 400x g for 5 min at RT and re-suspended in 2 ml of fresh DMEM. Cell number was determined by BioRad cell counter (Biorad TC20), using Trypan Blue vital dye (Sigma Aldrich) staining. In total, $1x10^6$ cells were transferred into new 10 cm petri dish and incubated under conditions mentioned above. At defined passage (P5, P10, P15, P20, P30, P50 and P100), part of the cells was collected in 1,5 ml Eppendorf tubes, centrifuged at 400x g for 5 min at RT, and obtained pellets were stored at -80°C for further analyses. One portion of the cells was frozen in 10% DMSO (Carl Roth), 40%

FBS, 50% DMEM and stored, first in deep freezer at -80°C, then transferred into liquid nitrogen at -196°C. For re-cultivation of the frozen cell lines, they were thawed in water bath at 37°C, transferred into cold medium and centrifuged (400x g, 5 min, 4°C). Cell pellet was re-suspended in a complete medium and transferred into a 10 cm cell culture dish. Next day medium was changed and when cells were reaching confluence, they were passaged.

3.2.4 Paraffin fixation and hematoxylin-eosin staining

Besides establishing primary tumor cell lines, a part of tissue samples obtained from surgery were either fixed in 4% paraformaldehyde (PFA) (Carl Roth) or preserved for cryosections at -80°C. PFA fixed tissue was further embedded in paraffin by Leica TP 1020 automated embedder, following standard protocol. Briefly, tissue was dehydrated through series of alcohol (70-100%) and xylene (Applichem), and then incubated two times 2 hours in paraffin wax (Roth) at 60°C. Next, tissue samples were embedded in paraffin blocks and cut into 3,5 µm sections on LEICA RM2255 microtome. Hematoxylin-eosin (HE) staining was performed by standard techniques using Mayer's Hemalum Solution (Merck) and Eosin-y Alcoholic solution (Thermo Fisher). Before staining, tissue slides were placed in xylene and decreasing alcohol series for rehydration (100-70%). After staining, samples were dehydrated through increasing alcohol series (70-100%) and xylene, and then closed with cover slips and mounting medium (Sigma Aldrich).

3.2.5 Immunoflourescence staining of primary tumor cells and frozen tumor tissue

Staining of isolated primary tumor cells was performed by the following procedure: cells were grown in ibidi 8 well chamber slides (Ibidi) or on standard microscope slides placed in a 10 cm dish (Sarstedt) and cultivated in complete DMEM containing 10% FBS. After reaching confluency of approximately 80%, cells were fixed in 4% PFA or Aceton/MetOH at -20°C. Cells were rehydrated in distilled water and washed with phosphate buffered saline supplemented with 0.1% Tween20 (PBS-T) (Gibco), and permeabilized with triton-x (0,1% in PBS) (Carl Roth). Next, cells were washed with PBS-T and incubated one hour with 10% bovine serum albumin (BSA) (Carl Roth) to inhibit unspecific binding. The primary antibodies against Albumin (1:100), EpCAM (1:80), AFP (1:400) and CK19 (1:80) were added and the slides were placed in a humidified chamber overnight. Antibodies were diluted in PBS-T containing 0,1% BSA. On the following day, slides were washed with PBS-T and the fluorophore-coupled corresponding secondary antibodies were added (anti-mouse alexa488 and anti-rabbit alexa555, 1:500, in PBS-T) for one hour in darkness. Counter staining was performed with DAPI for 20 min (1:1000) (Carl Roth). Lastly, slides were closed with cover slips and FluoroSave embedding medium (Merck). Frozen tissue samples were embedded in OCT gel (Sakura) and cut into 5 µm slices on Leica CM1850 UV Cryostat at -24°C. After fixation with 4% PFA, samples were stained using same procedure as described for primary tumor cells.

3.2.6 **Microscopy**

Hematoxylin-eosin samples were visualized by a Zeiss Axioskop microscope with 10x magnification objective and further processed in cellSens Dimension software (Olympus). Living primary tumor cells were viewed by Zeiss Axioplan microscope with phase-contrast setup. All images were obtained with 10x magnification objective and analyzed in AxioVision 3.1 software.

All immunofluorescent stainings were visualized and recorded by Laser Scanning Microscope LSM-710 Zeiss with 25x magnification oil objective. During scanning "tile" option was enabled, where images were organized together in 4x4 format. Obtained images were further processed in Zen 2.3 software.

3.3 **Functional assays**

3.3.1 **Dose-response analyses**

Stock solutions of inhibitors were prepared by dissolving in dimethyl sulfoxide (DMSO) (Carl Roth) according to manufacturer's recommendations. For the following inhibitors 100 mM stock solutions were prepared: tofacitinib, KU55933, refametinib, imatinib, tepotinib, sorafenib, gemcitabine and doxorubicin. Due to lower solubility in DMSO, vandetanib was prepared as 10 mM and BGJ398 as 1 mM stock solution (inhibitors are listed in the Table 6). Working concentrations were further prepared by diluting stock solution in complete DMEM (10% FBS). Dilutions of specific inhibitors, except tepotinib, were prepared as follows: 0,016; 0,08; 0,4; 2; 10; 20; 30; 40; 80 and 160 µM; Concentrations of tepotinib, sorafenib and gemcitabine were prepared as 2; 4; 8; 12; 16; 32; 64 µM; doxorubicin was prepared as: 0,016; 0,08; 0,4; 2; 4; 10 µM. Totally, 5×10^3 cells were plated in 96 well-plates. After overnight incubation in complete DMEM medium (10% FBS), medium was replaced with fresh medium containing respective inhibitors for 72 hours. Selection of inhibitors was based on predicted specificity to the target alterations determined by panel NGS. HCC derived primary cell lines were treated with imatinib, tepotinib, BGJ398, KU55933, sorafenib and doxorubicin while iCCA derived primary cell lines were treated with tofacitinib, refametinib, vandetanib, sorafenib, gemcitabine and doxorubicine. Results were calculated as viability of treated cells compared to non-treated controls. Viability was measured by WST-1 assay (Sigma Aldrich) according to the manufacturer's protocol and as described in the section 3.3.2. Cell viability defined as the absorbance in the treatment group compared to controls expressed as viability percent ± SD (n = 3). DMSO was used as vehicle control whenever suitable. IC50 values were calculated by non-linear regression using GraphPad Prism 6 software (GraphPad Software, La Jolla, CA).

3.3.2 **Viability assay**

Viability was measured by WST-1 assay according to the manufacturer's protocol (Roche Applied Sciences). This spectrophotometric assay is designed to assess cell proliferation and viability in 96 well-plate format. Moreover, high sensitivity of the assay allows cytotoxic and cytostatic effects of anti-cancer drugs to be investigated. Assay is based on the cleavage of tetrazolium salts to formazan by enzymes present

in viable cells, particularly by mitochondrial dehydrogenases. Accumulation of formazan and accompanying color change directly correlates with number of living cells. Maximum absorption is at 440 nm wavelength, while absorbance could be measured in the range from 420–480 nm. To assess cell viability, WST-1 reagent was first mixed with DMEM (10% FBS) in ratio 1:10. Next, medium was removed from the wells with seeded cells, and then 100 µl of WST-1 working reagent was applied in each well of 96 well-plates. Absorbance at 450 nm was measured every 30 min for next two hours on a microplate spectrophotometer (TECAN infinite M 200Pro). Wells containing only WST-1 working reagent were used as a blank. Reference wavelength was measured at 660 nm.

3.4 Next generation sequencing

3.4.1 RNA isolation

Total RNA from the tissue and cells was extracted using the Qiagen RNEasy mini Kit (Qiagen) following the manufacturer's instructions. In brief, approximately 20-40 mg of tissue or $5x10^5$–$1x10^6$ of cells were mechanically dissociated, lysed and homogenized in 600 µl lysis buffer. Lysate was filtered with Shredder-filter columns to ensure homogenization of the starting material. To provide ideal binding conditions, lysate was mixed with 600 µl ethanol and loaded on a RNeasy Mini spin column allowing RNA to bind to the membrane. Remaining DNA was removed by adding DNase (Qiagen). Column was further washed three times with washing buffer, and total RNA was eluted in 50 µl of RNase-free water. RNA quantity and purity were estimated using a Nanodrop ND-1000 Spectrophotometer (NanoDrop Technologies), and integrity was assessed by Agilent 2100 Bioanalyzer (Agilent). For RNA sequencing only samples reaching integrity number equal or higher than 6 (RIN≥7) was used.

3.4.2 DNA isolation

DNA was extracted using peqGOLD Tissue DNA Mini Kit (Qiagen) following the manufacturer's instructions. Approximately 20-40 mg of tissue or $5x10^5$–$1x10^6$ of the cells was used for genomic DNA isolation. Samples were first homogenized, lysed under denaturing conditions with Proteinase K and RNase A (Qiagen) at 50°C for at least 1 hour and then applied to the PerfectBind DNA columns, where the DNA was effectively bound to the silica membrane. Cellular debris, proteins and other contaminants were washed away by specific buffers. The high-quality DNA was finally eluted in 200 µl of elution buffer. DNA quantity and purity were estimated by using a Nanodrop ND-1000 Spectrophotometer or Qubit Fluorometer (Thermo Fisher). Fluorescence-based method, such as Qubit, employs a double-stranded DNA (dsDNA) specific dye, allowing accurate quantification of dsDNA even in the presence of many common contaminants, which is required for high precision analyses such as DNA sequencing.

3.4.3 **RNA Sequencing**

RNA sequencing (RNA-seq) services were provided by BGI TECH SOLUTIONS (HONGKONG) CO. In total, 27 human RNA samples, obtained from the tissue and cell pellets, were provided for sequencing. Total RNA was extracted from surrounding liver, primary tumor, early passage (P5) and late passage (P30) of corresponding PDCL. All the samples fulfilled quality requirements requested by service provider: (i) RNA samples were treated by DNase and provided without protein contamination; (ii) sample quantity of total RNA was ≥ 200 ng; (iii) sample concentration was ≥ 20 ng/µl; (iv) Sample purity: RNA 28S:18S ≥ 1.0, RIN ≥ 7.0. Before sequencing, library preparation was performed according to manufacturer's instructions (Illumina® TruSeq® RNA Sample Preparation Kit v2). By this process, mRNA was converted into a library of template molecules suitable for subsequent cluster generation and DNA sequencing. The first step of library preparation was purifying the poly-A containing mRNA molecules using oligo-dT attached magnetic beads. After purification, the mRNA was fragmented into small pieces using divalent cations under elevated temperature. The cleaved RNA fragments were copied into first strand cDNA using reverse transcriptase and random primers, followed by second strand cDNA. The cDNA fragments then went through an end repair process, the addition of a single 'A' base, and ligation of the adapters. The products were in the end purified and enriched with PCR to create the final cDNA library. Samples were further sequenced in 3 lanes with 100PE reads by Illumina's HiSeq4000 technology. At the end, 3 lanes of clean data were generated (data after removing adaptor pollution and low quality sequence) and transferred clean data (*.fq files). Raw reads were filtered by removing adapter sequences, contamination and low-quality reads. The reads were then mapped with human genome reference sequence (GRCh37.82) using HISAT2 (hisat2-2.0.2-beta) followed by read summarization with featureCounts (subread-1.5.0-p1). Data analysis was performed using R programming language and related packages. The output matrix from featureCounts was input into the Bioconductor package DESeq2 for differential expression analysis. Significance testing was performed using Wald Test statistics. To visualize the data Principal Components Analysis (PCA) and clustering was performed. All plots were generated using the MADE4 package. Gene Set Enrichment analysis (GSEA) was performed using GSEA software provided by Broad Institutes (http://www.broad.mit.edu/gsea/). Human gene sets from the MSigDB database were tested and gene sets with a NOM P-value <0.05 and FDR <0.25 were considered significantly enriched in a priori defined set of genes.

3.4.4 **Target DNA Sequencing and data analysis**

DNA sequencing services were provided by Institute of Pathology, University Medical Center Mainz. Targeted sequencing was performed using Illumina TruSeq Amplicon - Cancer Panel including 48 important cancer-related genes according to manufacturer's instructions (Figure 9 and Figure 10). Genomic DNA was extracted from surrounding liver, primary tumor and different passages (P3, P5, P8, P10 and P30) of corresponding PDCL. Total amount of genomic DNA provided for the analysis was 250 ng. TruSeq Amplicon cancer panel is a highly multiplexed targeted

resequencing assay for detecting somatic mutations within important cancer-related genes. In the panel, predesigned and optimized oligonucleotide probes for sequencing mutational hotspots in > 35 kilobases (kb) of target genomic sequence were provided. 48 genes were targeted with 212 amplicons in a highly multiplexed, single-tube reaction. One pair of oligos was designed for each amplicon. Hybridization of oligos to unfragmented genomic DNA occurred in a 96well-plate, followed by extension and ligation to form DNA templates consisting of the regions of interest flanked by universal primer sequences. Using index adapters, libraries were indexed, PCR amplified, and then pooled into a single tube before sequencing. After sequencing, further analyses were performed using automated variant calling integrated in the Illumina analyses pipeline.

Figure 9 TruSeq Amplicon - Cancer Panel Workflow.
The following diagram illustrates the workflow using the TruSeq Amplicon - Cancer Panel Kit (modified from Ilumina TruSeq® Amplicon - Cancer Panel Reference Guide).

ABL1	*EGFR*	*GNAS*	*MLH1*	*RET*
AKT1	*ERBB2*	*HNF1A*	*MPL*	*SMAD4*
ALK	*ERBB4*	*HRAS*	*NOTCH1*	*SMARCB1*
APC	*FBXW7*	*IDH1*	*NPM1*	*SMO*
ATM	*FGFR1*	*JAK2*	*NRAS*	*SRC*
BRAF	*FGFR2*	*JAK3*	*PDGFRA*	*STK11*
CDH1	*FGFR3*	*KDR*	*PIK3CA*	*TP53*
CDKN2A	*FLT3*	*KIT*	*PTEN*	*VHL*
CSF1R	*GNA11*	*KRAS*	*PTPN11*	
CTNNB1	*GNAQ*	*MET*	*RB1*	

Figure 10 TruSeq Amplicon – Cancer-Related Genes.
Figure displays cancer-related genes represented in TruSeq Amplicon - Cancer Panel Kit (modified from Ilumina TruSeq® Amplicon - Cancer Panel Reference Guide).

3.4.5 Single nucleotide variations and copy number analysis

Single nucleotide variations (SNV) and Copy number analyses were provided by Institute of Human Genetics, Department of Genomics, Life & Brain Center, University of Bonn. The Infinium Omni2.5Exome-8 v1.3 BeadChip was used to deliver comprehensive coverage of common, rare and exonic SNP content from the 1000 Genomes Project (1 kGP) and provided maximum genomic information. These 8-sample BeadChips allowed high throughput, optimized tag single nucleotide polymorphisms (SNPs) and copy-number variation (CNV) analysis. Genomic DNA was extracted from surrounding liver, primary tumor, and different passages (P5 and P30) of corresponding PDCL. Total amount of genomic DNA provided for the analysis was 200 ng. Calling of genotypes was performed using the Illumina SNP assay software GenomeStudio version 2011.1. All SNVs with call Frequencies>0.95 and Gen TrainScore>0.7 were included. The log R ratio (LRR) and B allele frequency (BAF) were then exported from the normalized Illumina data. Segmentation analyses were performed using CBS algorithm (DNAcopy) and significant copy number changes were determined by GISTIC2.0.

3.5 *In vivo* experiments (xenograft studies)

All procedures were performed in accordance with the guidelines of the National Institutes of Health animal care committee following approval from local authorities. All xenograft experiments were performed in non-obese diabetic/severe combined immunodeficient (NOD/SCID) mice. To investigate tumorigenicity of freshly isolated primary cell lines, in total 1-5x10^6 viable cells were harvested from the 10 cm dishes when reached 80% confluency, re-suspended in 100 µl DMEM and 100 µl matrigel (BD Bioscience) and injected into both flanks of NOD/SCID mice. Tumor formation

was monitored weekly by palpation for 8-10 weeks. After reaching tumor volume of approximately 500 mm^3, mice were sacrificed, and tumors were collected. Part of the obtained xenograft tumors was used for tumor cell isolation (2^{nd} generation), while remaining tissue was either fixed in 4% PFA or preserved at -80°C. *In vivo* experiments addressing the effects of specific inhibitor targeting detected oncogenic mutation were conducted in the following manner: first, inhibitors were dissolved in DMSO in the concentrations of 100 mM as a stock solution. Prior the treatments, inhibitors were further diluted to respective IC50 concentrations in complete DMEM supplemented with 10% FBS. Primary cholangiocarcinoma cells (CCA16) were plated in 10 cm dishes with $1x10^6$ cell density. After 24h medium was removed and replaced by fresh medium containing IC50 concentrations of inhibitors. After 72h of treatment cells were harvested and counted. Prior the injection, animals were divided into three groups (control, refametinib and tofacitinib). In total, three animals per each group were injected in both flanks with $1x10^6$ viable cells mixed with 100 µl DMEM and 100 µl matrigel. Untreated cells were used as a control. Tumor formation was monitored weekly by palpation for 10 weeks, and tumor incidence was reported. After reaching 10 weeks, animals were sacrificed, tumors were collected and either frozen at -80°C or fixed in 4% PFA.

3.6 Statistics, databases and patient integration

Statistical analysis was performed using Student's t-test or Mann–Whitney *U* test as indicated. *P*-values ≤0.05 were considered statistically significant. Results are presented as means ± SD from 3 independent experiments. Survival analyses were performed using log rank (Mantel-Cox) tests. For integration of patients, expression data from HCC and iCCA tumor specimens generated by Illumina beadchips was used.[196, 197]

4. Results

4.1 Generation of PDCL from primary human liver cancer

4.1.1 Clinicopathological information of the patients

We collected fresh tumor tissues from 38 patients with HCC and 28 patients with iCCA (Table 7 and Table 8). The majority of HCC patients were male (79%).[43] In our iCCA cohort, gender distribution was equal (50% male, 50% female), similarly to distribution that was reported in a study of 11296 iCCA cases, where 53% of the patients were male and 47% female.[42] Majority of the HCC patients developed NASH as a dominant etiological factor (32%) followed by alcoholic liver disease (16%). Liver cirrhosis as only predisposing factor without presence of other factors was reported in 8% patients. Etiological factors were not available for 40% of the patients. Importantly, majority of iCCA patients in our cohort showed liver inflammation (75%) (Table 8). Moreover, most of HCC tumors were well to moderately differentiated and it accounted 64% of all cases (well – 8%; well to moderate – 11%; moderate – 45%), while 33% were moderately to poorly differentiated (moderate to poor – 11%; poor – 22%). Differentiation was not determined for 3% HCCs. Similar to HCC, our iCCA samples were mostly well to moderately differentiated with total percentage of 71% (well to moderate – 3%; moderate – 68%), while small number showed poor differentiation (21%). Remaining 8% was not determined. Tumor grading showed that 65% of HCC were low graded (G1, G1-2, G2), while the rest (35%) showed higher grading (G2-3, G3). For iCCA, tendency was even higher for low grading tumors with 71% cases (G1, G1-2, G2), while 21% were high graded (G2-3, G3). Tumor sizes were very heterogeneous, from 0,5 cm to 14,5 cm in diameter (Table 7, Table 8). After surgical resection, tissue samples were processed by mechanical and enzymatic digestion to establish the PDCL. A total of 7 PDCL from PLC (4 HCC and 3 iCCA) were successfully established and cultured over 30 passages (Figure 13). Overall, tumors with derived PDCL were poorly differentiated, mainly with high grading of G2-G3 and G3, whereas only one tumor showed low grading of G1 and higher differentiation status. Pathological reports revealed different tumor sizes, from relatively small (2,6 cm for HCC31) to big in size (13 cm for HCC9) (Table 7, Table 8). Efficacy of establishing the PDCL was 11% for both tumor types, HCC-PDCL and CCA-PDCL. Rapid overgrowth by tumor-associated spindle cells and fibroblasts was the predominant reason for failure of culturing in unsuccessful attempts.

Table 7 Clinicopathological information of HCC tumors.

Tumorigenicity of the primary cell lines and serial transplantation were assessed in NOD/SCID mice. A total of 5 mio cells were transplanted subcutaneously in both flanks of the mice. Green color indicates tumors that PDCLs were successfully derived from.

Tumor sample	Gender	Size (cm)	TNM	Grading	Differentiation	Etiology	*In vivo* tumorigenicity / serial transplantation
HCC2	F	8	pT2, pNx, M0, R0	G3	Poor	NASH	N/A
HCC3	M	11	pT3b, pNx, M1, R2	G3	Poor	NASH	N/A
HCC4	F	3	pT1, pNx, M0, R0	G2	Moderate	N/A	N/A
HCC6	F	12	pT1, pN0, M0, RX	G3	Poor	N/A	N/A
HCC9	F	13	pT2, pNx, M0, R0	G2-G3	Moderate to poor	NASH	Yes / No
HCC10	M	4,5	pT1, pNx, M0, R0	G2	Moderate	NASH	N/A
HCC11	M	9	pT1, pNx, M0; R0	G1-G2	Moderate	NASH	N/A
HCC12	M	10,9	pT1, pNx, M0, pR0	G2	Moderate	NASH	N/A
HCC13	M	11	pT3b, pNx, M0	G2	Moderate	EtOH	N/A
HCC14	M	2	pT1, N0, M0, R0	G2	Moderate	N/A	N/A
HCC15	M	4,7	pT1, pNx, M0, R0	G1	Well	No cirrhosis	N/A
HCC16	M	5,2	pT3b, pNx, M0, R1	G2-G3	Moderate to poor	NASH	No / N/A
HCC17	M	14	pT1, pN0, M0, R0	G1	Well	NASH	N/A
HCC18	F	10	pT0, pNx, M0, R0	N/A	N/A	NASH	N/A
HCC26	M	3,5	pT3a, pN0, M0, R0	G2	Moderate	NASH	N/A
HCC27	M	5	pT1, pNx, M0, R0	G2	Moderate	EtOH	N/A
HCC28	F	4	pT1, pNx, M0, R0	G3	Poor	N/A	N/A
HCC31	M	2,6	pT2, pN0, M0,R0	G1	Well	EtOH	Yes / Yes
HCC33	M	6,3	pT3, pNx, M0, R0	G2	Moderate	NASH	N/A
HCC36	M	3,6	pT1, pNx, M0, R0	G2	Moderate	Cirrhosis	N/A
HCC37	M	11,5	pT1, pNX, M0, R0	G1-G2	Well to moderate	N/A	N/A
HCC39	F	5,8	pT1, pNx, M0, R0	G1-G2	Well to moderate	N/A	N/A
HCC46	M	9	pT3b, pN1, M0, R0	G3	Poor	N/A	N/A
HCC48	M	4,7	pT1, Nx, Mx, R0	G2	Moderate	N/A	N/A
HCC52	M	7	pT1, pN0, M0, R0	G3	Poor	N/A	N/A
HCC53	M	1,7	pT1, rNx, Mx, R0	G2	Moderate	NASH	N/A
HCC54	M	1,3	pT3, Nx, Mx, R1	G2	Moderate	N/A	N/A
HCC55	M	5,5	pT1, Nx, M0, R0	G2-G3	Moderate to poor	EtOH	N/A
HCC57	M	10	pT1, pN0, M0, R0	G1-G2	Moderate	N/A	N/A
HCC58	M	4,8	pT1, pNx, M0, R0	G2-G3	N/A	EtOH	N/A
HCC59	M	6,6	pT1, pN0, M0, R0	G2	Moderate	N/A	N/A
HCC60	M	3,5	pT3b, pN0, M0, R0	G1-G2	Well to moderate	EtOH	N/A
HCC61	M	9	pT1, pN0, Mx, R0	G2-G3	Moderate to poor	No cirrhosis	N/A
HCC62	F	3,5	pT3, pN0, R0	G1-G2	Well to moderate	N/A	N/A
HCC63	M	14,5	pT3a, pN0, M0, R0	G2	Moderate	N/A	N/A
HCC64	M	8,5	pT3b, pN0, M0, R1	G3	Poor	N/A	N/A
HCC65	M	1,8	pT1, Nx, M0; R0	G2	Moderate	Cirrhosis	N/A
HCC68	M	11	pT2, pNx, M0, R0	G3	Poor	No disease	Yes / Yes

Table 8 Clinicopathological information of iCCA tumors.
Tumorigenicity of the primary cell lines and serial transplantation were assessed in NOD/SCID mice. A total of 1 mio cells were transplanted subcutaneously in both flanks of the mice. Green color indicates tumors that PDCLs were successfully derived from.

Tumor sample	Gender	Size (cm)	TNM	Grading	Differentiation	Inflammation	*In vivo* tumorigenicity / serial transplantation
CCA1	M	1,4	N/A	G2	Moderate	Yes	N/A
CCA2	F	13	pT1, pN0, M0, R0	G2	Moderate	Yes	N/A
CCA3	F	6	pT2b, pN0, M0, R0	G1-G2	Well to moderate	Yes	N/A
CCA4	F	6,5	pT2b, pN0, M0, R1	G2	Moderate	No	N/A
CCA5	F	10,3	pT1, pN0, M0, R0	G2	Moderate	Yes	N/A
CCA6	M	3,5	pT1, pN0, M0, R0	G2	Moderate	Yes	N/A
CCA7	M	12	pT2a, pN0, M0, R0	G2	Moderate	No	N/A
CCA8	F	5	pT1, pN0, M0, R0	G2	Moderate	No	N/A
CCA9	F	6,4	pT3, pN0, R0	G2	Moderate	Yes	N/A
CCA10	F	5,9	pT3, pN1, M0, R0	G2	Moderate	Yes	Yes / Yes
CCA13	M	4,3	pT3, pN1, M0, R0	G2	Moderate	Yes	N/A
CCA14	M	3,5	N/A	G2	Moderate	Yes	N/A
CCA15	F	12	pT2b, pN0, M0, R0	G2	Moderate	Yes	N/A
CCA16	M	10	pT3, pN1, M0, R0	G3	Poor	No	Yes / Yes
CCA17	M	14,5	pT3, pN1, M0, R1	G2-G3	Poor	Yes	N/A
CCA18	F	10,2	pT2a, pN1, M0, R0	G3	Poor	Yes	N/A
CCA19	M	7,3	pT3, pN1, M0, R0	G2	Moderate	No	N/A
CCA22	M	9	pT2a, pN0, M0, R0	G3	Poor	Yes	N/A
CCA23	F	N/A	pT1, Nx, M0, R0	G2	Moderate	Yes	N/A
CCA24	M	3	pT1, pNX, M0, R0	G2	Moderate	Yes	N/A
CCA25	M	0,5	ypT1, pN0, Mx, R0	N/A	N/A	Yes	N/A
CCA26	F	6,2	pT3, pN0, pM1, R0	G2	Moderate	No	N/A
CCA27	F	5,5	pT1, pNx, M0, R0	G2	Moderate	Yes	N/A
CCA28	M	2,6	N/A	N/A	N/A	No	N/A
CCA29	F	0,6	pT2b, pN0, Mx, R0	G2	Moderate	Yes	N/A
CCA30	F	14	pT2b, pN0, M0, R0	G2	Moderate	Yes	N/A
CCA31	M	7,5	pT2a, N0, M0, R0	G3	Poor	Yes	N/A
CCA33	M	8,5	pT2a, pN1, M0, R0	G3	Poor	Yes	Yes / Yes

4.1.2 Examining tumor grading and genomic alterations as a background setting for successful PDCL generation

As the success rate of establishing new PDCL was relatively low, we wanted to assess basic characteristics that might contribute to successful cell isolation and PDCL propagation. After analyzing tumor grading for both tumor entities, HCC and iCCA, we observed a trend for a higher tumor grading in tumors with successful generation of PDCL. In HCC group almost 80% of the successful tumors were G2-G3 and G3, and about 80% iCCA tumors were comprised of G3 (Figure 11a). To further investigate underlying mechanisms of successful PDCL generation, we performed genomic analyses and compared the spectrum of genetic alterations in tumor specimens of HCC and iCCA patients with and without successful establishment of PDCL. We observed a significant number of increased genomic gains and losses in the tumors with successful PDCL establishment (Figure 11b,c). Furthermore, recurrent copy number alterations (CNAs) were observed in several

chromosomal locations, including 4q, 5q, 8p, 9p and 13q. These CNAs affected amplifications in 4q13.1 (*LPHN3*), 5q22.1 (*TSLP*), 8p21.1 (*CCDC25, PBK, ESCO2*), 9p22.2 (*CNTLN*) and 13q14.3 (*MIR1297*) previously associated with the proliferative capacity and cancer (Figure 11b).[198-200 201, 202] Additionally, by using Ingenuity Pathway Analysis (IPA), we identified molecular and cellular functions of significant genomic alterations present in HCC and iCCA with successful PDCL establishment. Overall, major molecular and cellular functions centered on pro-oncogenic properties such as cellular growth and proliferation, movement as well as cell death and survival (Figure 11d). These investigations indicate that a poor differentiation status, as well as increased genomic alterations, favor successful PDCL establishment.

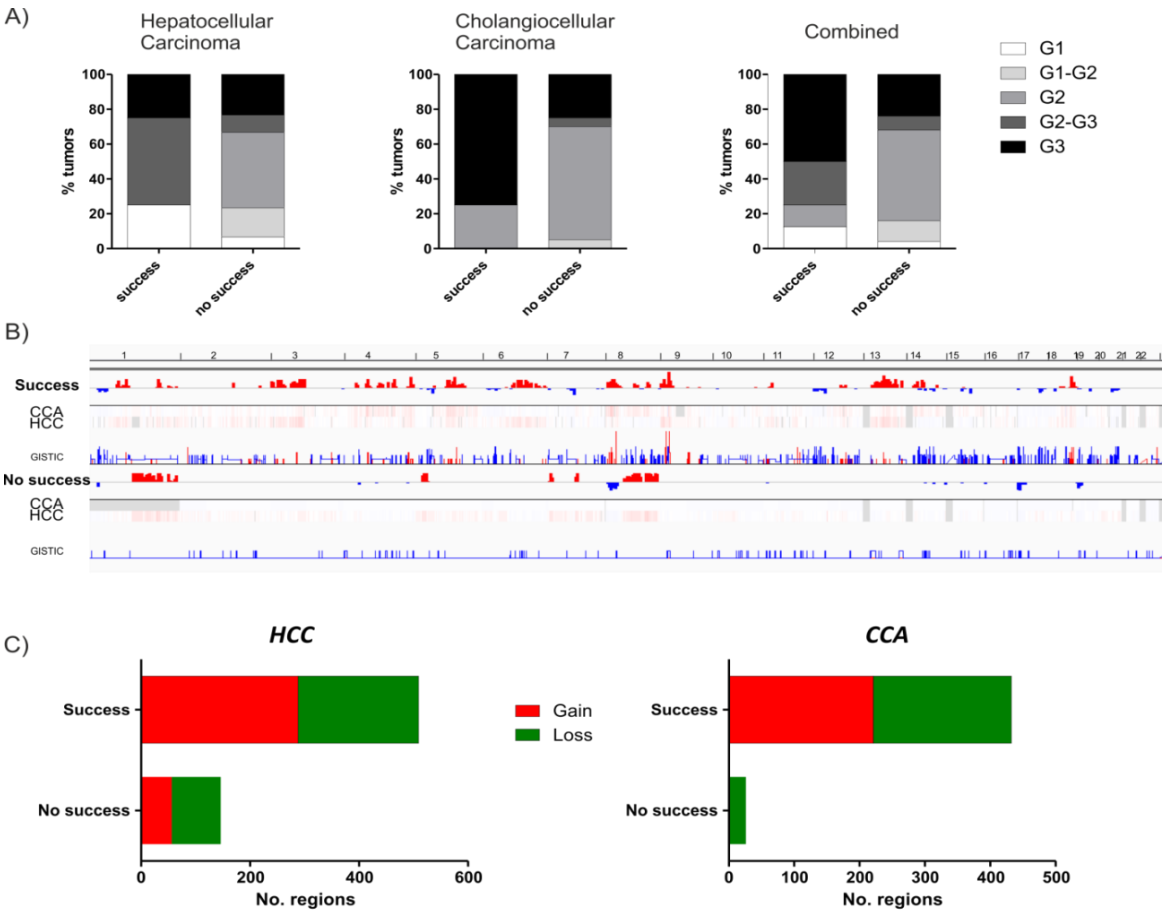

Molecular and Cellular Functions _ HCC

Name	p-Value	#Molecules
Cell Morphology	7,63E-04 - 9,87E-09	888
Cellular Development	7,64E-04 - 1,08E-07	955
Cellular Growth and Proliferation	7,64E-04 - 1,08E-07	849
Cell Movement	6,28E-04 - 6,95E-07	765
Cell Death and Survival	6,29E-04 - 1,02E-06	1085

Molecular and Cellular Functions _ CCA

Name	p-Value	#Molecules
Cellular Development	3,82E-03 - 8,46E-07	303
Cellular Growth and Proliferation	3,92E-03 - 8,46E-07	329
Cellular Movement	4,15E-03 - 1,59E-06	397
Cell Morphology	4,39E-03 - 6,18E-06	491
Cellular Assembly and Organization	3,82E-03 - 6,18E-06	294

Figure 11 Tumor grading and genomic alterations underlying successful and non-successful PDCL establishment.

A) Percentage of differently graded tumors in successful and unsuccessful PDCL establishment. Left is shown grading of HCCs, middle iCCAs and right combined both entities B) Significant genomic alterations for primary tumors with successful vs non-successful PDCL establishment. Lower rows show CNAs analyses for each entity as well as the corresponding GISTIC analyses. Red and blue colors represent level of gain and loss, respectively C) Number of significant copy number alterations. D) Molecular and cellular functions of significant genomic alterations present in HCC and iCCA with successful PDCL establishment.

4.2 Morphological and molecular characterization of the PDCL

4.2.1 Morphology of the PDCL during long-term cultivation

Using slightly modified, established culture conditions (see “3.2.3 Cell culture”), clean epithelial cultures, free of fibroblast and macrophages, were progressively established and confirmed within 1-3 passages in the newly derived PDCL (Figure 13). Initial culturing of the cells (passage 0) was continued until sufficient number of epithelial cells were detected (>100000 cells). Cells were then split into a new passage (passage P1), and further propagated until fibroblasts and macrophages were exhausted and clean cultures could be obtained. Time from isolation to stable growth and clean cultures ranged between four and eight weeks. For each newly established PDCL average doubling time across different passages was calculated (Figure 12). The fastest growth was observed in CCA10 with an average doubling time of 31 hours, while other PDCL showed slower doubling, in average between 50 and 54 hours. Proliferation rate influenced time necessary to reach passage 30, and it was between 34 and 52 weeks. Once stable growth of PDCLs was achieved, morphological characteristics of the cells over the course of time were assessed by phase-contrast microscopy. Cells were analyzed after defined number of passages, at P3, P5, P8, P10, P15 and P30. We observed that morphology of established cultures remained relatively stable over the complete observation time and comparable to early passages (e.g. P3, P5). However, one of the PDCL (HCC16) acquired additional morphological changes reflected in increased cellular size and appearance of vacuole-like structures. They further showed a decline in proliferation rate, which led to complete cessation of cell growth after 10 passages. Inability to further proliferate and no vital cultures could be re-established for this cell line after initial freezing which prevented us from further characterization of this PDCL.

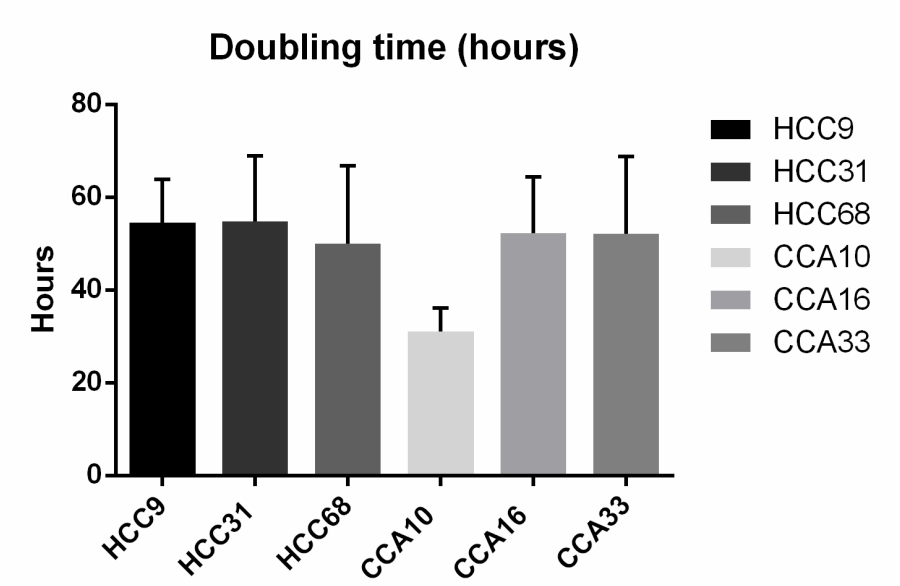

Figure 12 Population doubling time of PDCL.
Doubling time for each PDCL (except HCC16) was calculated as an average value across different passages. Bars represent number of hours required for each cell lines to double cell population. n=3

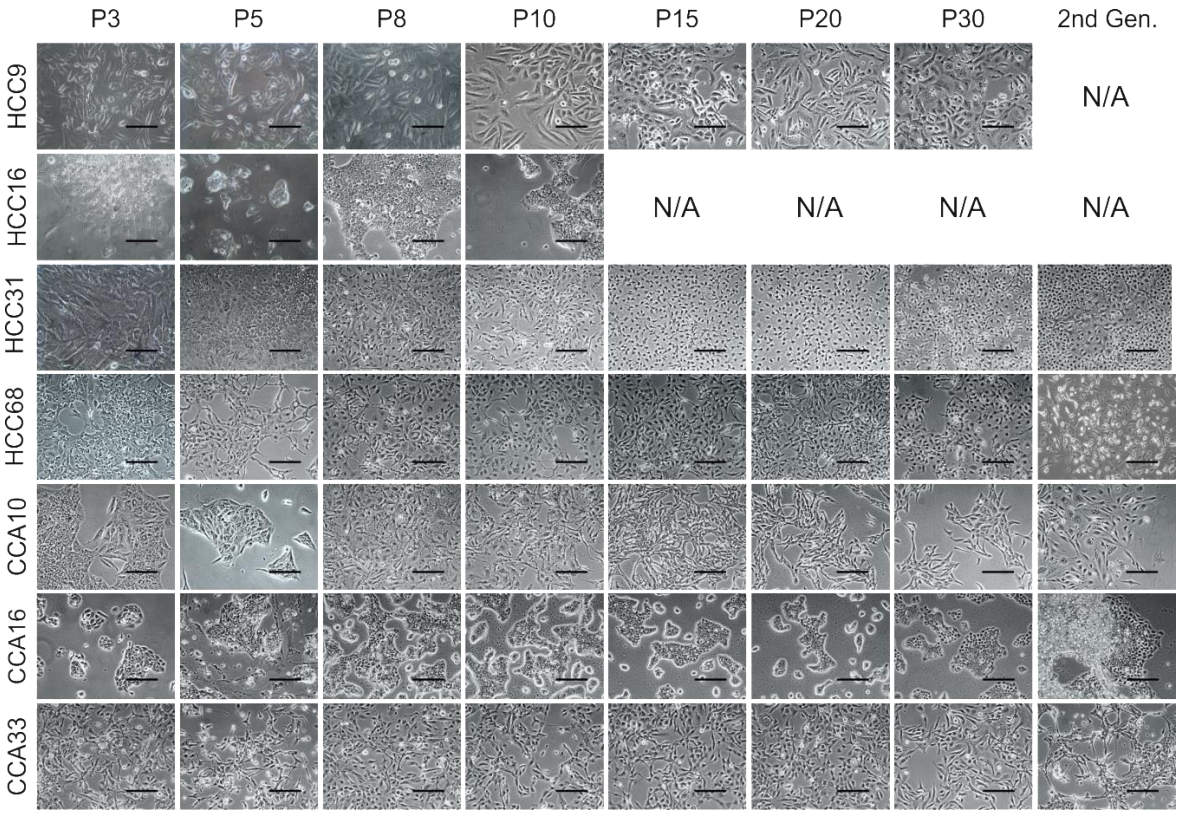

Figure 13 Morphology of PDCLs at different passages and the second generation obtained from xenograft tumors.
Bright field images demonstrating morphology of newly-derived PDCL over 30 passages. Last pictures on the right side represent cells isolated from patient-derived xenograft tumors. Representative PDCLs for HCC and iCCA are shown. Scale bars indicating 100 µm.

4.2.2 Examining malignant status of the PDCL by xenotransplantation

To confirm malignant potential of PDCL, we performed subcutaneous xenotransplantations as well as serial transplantations into immune-compromised NOD/SCID mice (Table 7, Table 8, Figure 13, Figure 14). For HCC-PDCL we transplanted 5 million cells in each flank of the animals, while for CCA-PDCL a total of 1 million cells were used. Successful tumor growth was achieved for all 6 PDCL, confirming their tumorigenic properties. As mentioned before, one cell line (HCC16) stopped to proliferate, and its malignant status could not be confirmed thereafter by this method. After the first generation of xenograft tumors had grown, we isolated second generation of PDCL and successfully performed serial transplantation of 1 million cells (Table 7, Table 8). Importantly, tumor cells that were re-isolated from xenograft tumors, except from HCC9 (did not grow second generation of tumors), showed similar morphological features to the parental cells that were initially transplanted into immune-compromised NOD/SCID mice (Figure 13). Next, we compared histological features of the xenograft tumors to the matched primary tumor tissues (Figure 14). Overall, PDCL closely recapitulated morphological patterns of the original tumor. Both HCC primaries and HCC-PDLC showed trabecular growth with large hepatocytic tumor cells with minimal stromal desmoplasia, whereas iCCA as well as corresponding PDCL showed glandular differentiation with stromal desmoplasia indicating that the newly derived PDCL could serve as a valid patient-specific *in vitro* model.

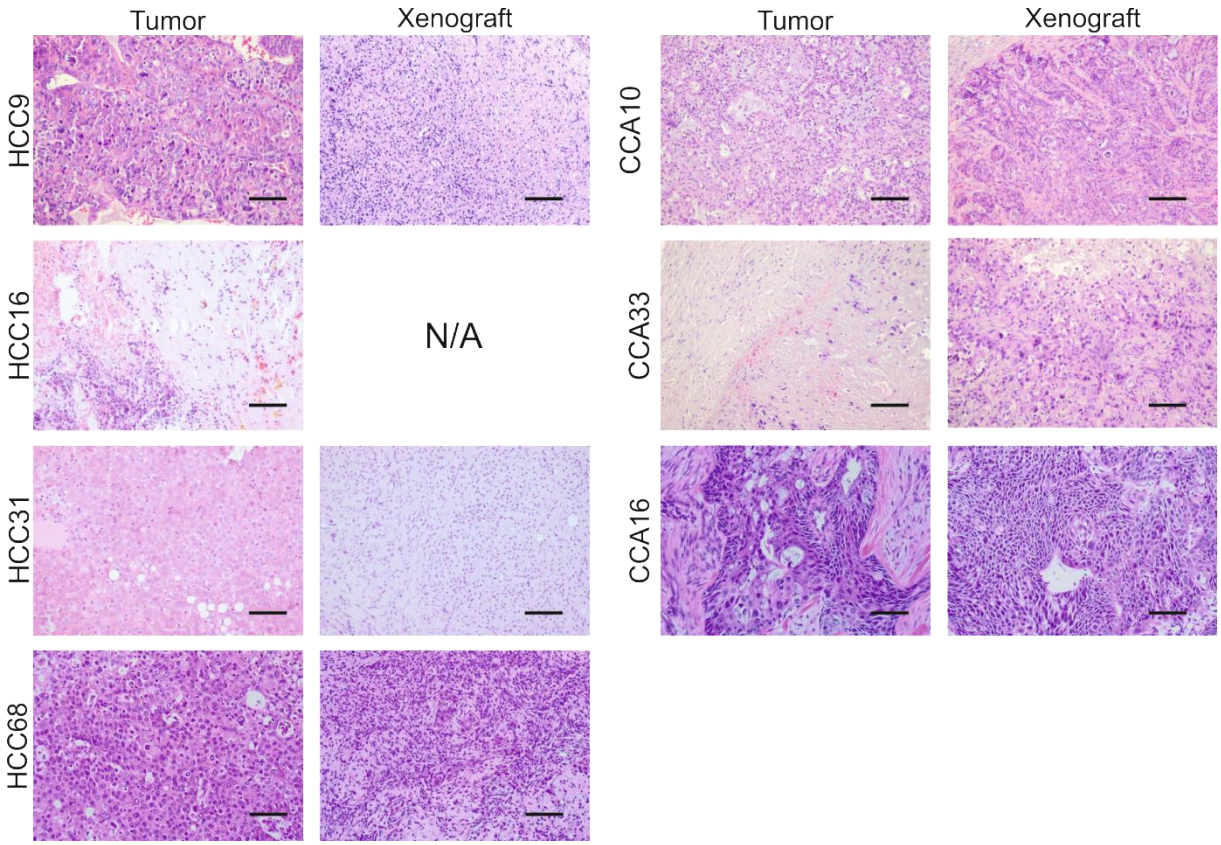

Figure 14 Histology of the xenograft and matched primary tumors.
Hematoxylin and eosin staining of primary tumors and xenograft transplantations. Scale bars indicating 100 µm.

4.2.3 **Expression of specific markers to validate cellular origin of PDCL**

Immunofluorescence staining and confocal microscopy analyses of the classic hepatocellular (AFP, Albumin), biliary (CK19) and epithelial progenitor (EpCAM) markers gave us more insight into cellular origin of our freshly derived cell lines. We compared our PDCL with corresponding primary cancers. Expression of albumin was observed in all HCC-derived cell lines as well as the original tumors, while EpCAM and AFP were only stained in HCC68. High expression of CK19 and EpCAM was noticed in iCCA tumors and corresponding PDCL, while albumin staining remained completely negative. Overall, expression patterns between original tumor tissue and PDCL were similar which confirmed the cellular origin of the newly established HCC and iCCA cell lines (Figure 15).

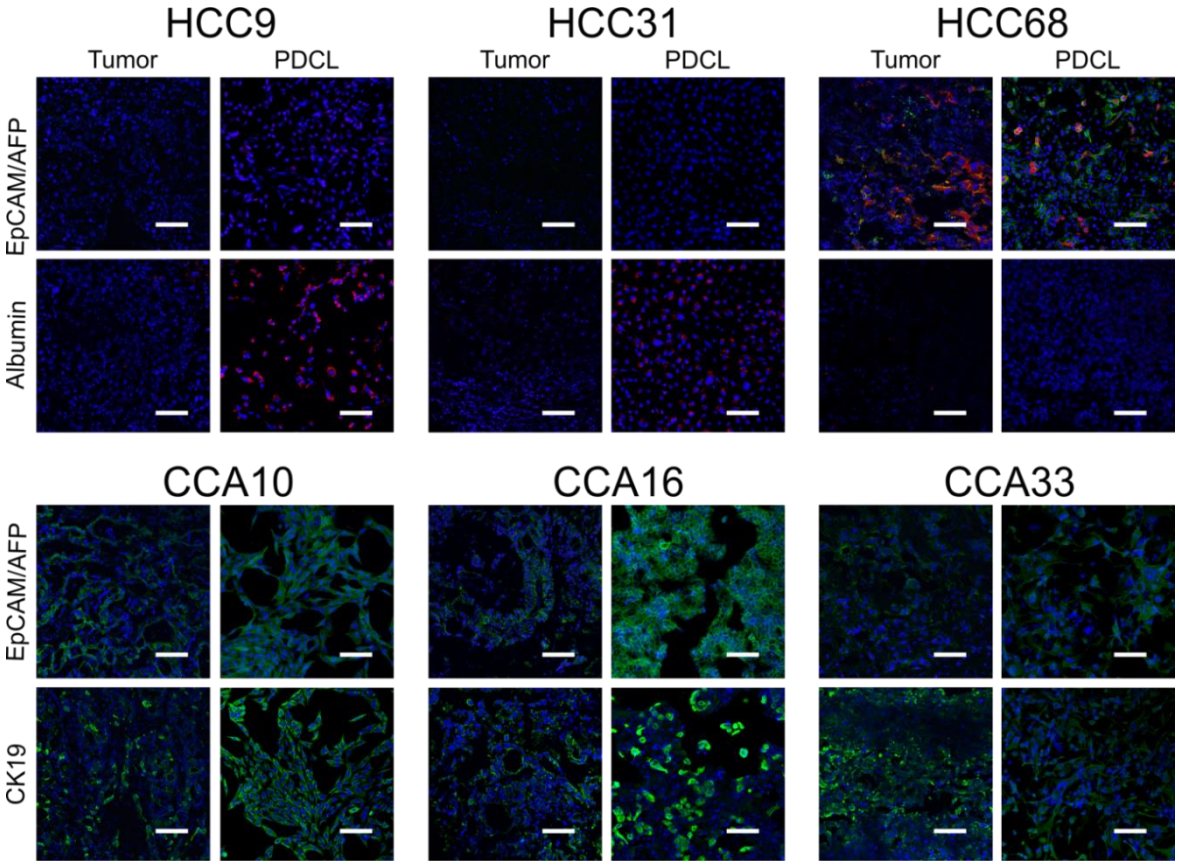

Figure 15 Expression of selected markers in tumors and PDCL by immunofluorescence.

Immunofluorescence staining of selected hepatocellular (Albumin, AFP), biliary (CK19) and epithelial progenitor (EpCAM) markers by confocal microscopy. Shown are representative images from matched tumors and PDCL. Scale bars indicating 100 µm.

4.2.4 **Transcriptome profiling of PDCL and original tumor**

As we observed that morphological and molecular features of PDCL remained similar to primary tumors, we further assessed the landscape of molecular alterations in order to confirm the utility of the PDCL as patient-specific models. First, RNA sequencing was performed to assess the transcriptomic profile of the tumor surrounding liver tissue, PDCL and the original tumor. By performing multiple comparison analysis between different groups (tumor (T), passage 5 and passage

30), we identified a total of 5014 differentially expressed genes. Unsupervised hierarchical cluster analyses based on these significantly differentially expressed genes demonstrated that both early stage (passage 5) and later stage (passage 30) PDCL formed dense sub-clusters with the corresponding primary tumor, confirming that the gene expression profiles are similar between the newly derived PDCL and the tumors and remain stable during transient expansion of the cells. Analysis further revealed clear separation between HCC and iCCA entities, with exception of HCC31. Interestingly, this PDCL and original tumor formed a cluster together with iCCA indicating presence of similar expressional profile between those entities, particularly with CCA10. Similar transcriptional profile between HCC31 and other CCAs could also be observed in a PCA (principal component analyses) plot (Figure 16a,b). A similar observation was noted in several studies examining expressional profiles of PLCs.[203-205] For instance, Woo *et al.* defined a novel HCC subtype that expressed CCA-like traits and defined it as CCA-like HCC.[204] Transcriptome correlation further confirmed that the molecular characteristics of the tumors are retained in the PDCL. As expected, tumor-surrounding liver tissue (SL) from all different primary tumors formed a distinct sub-cluster overall validating that PDCL resemble malignant tumor properties (Figure 16c).

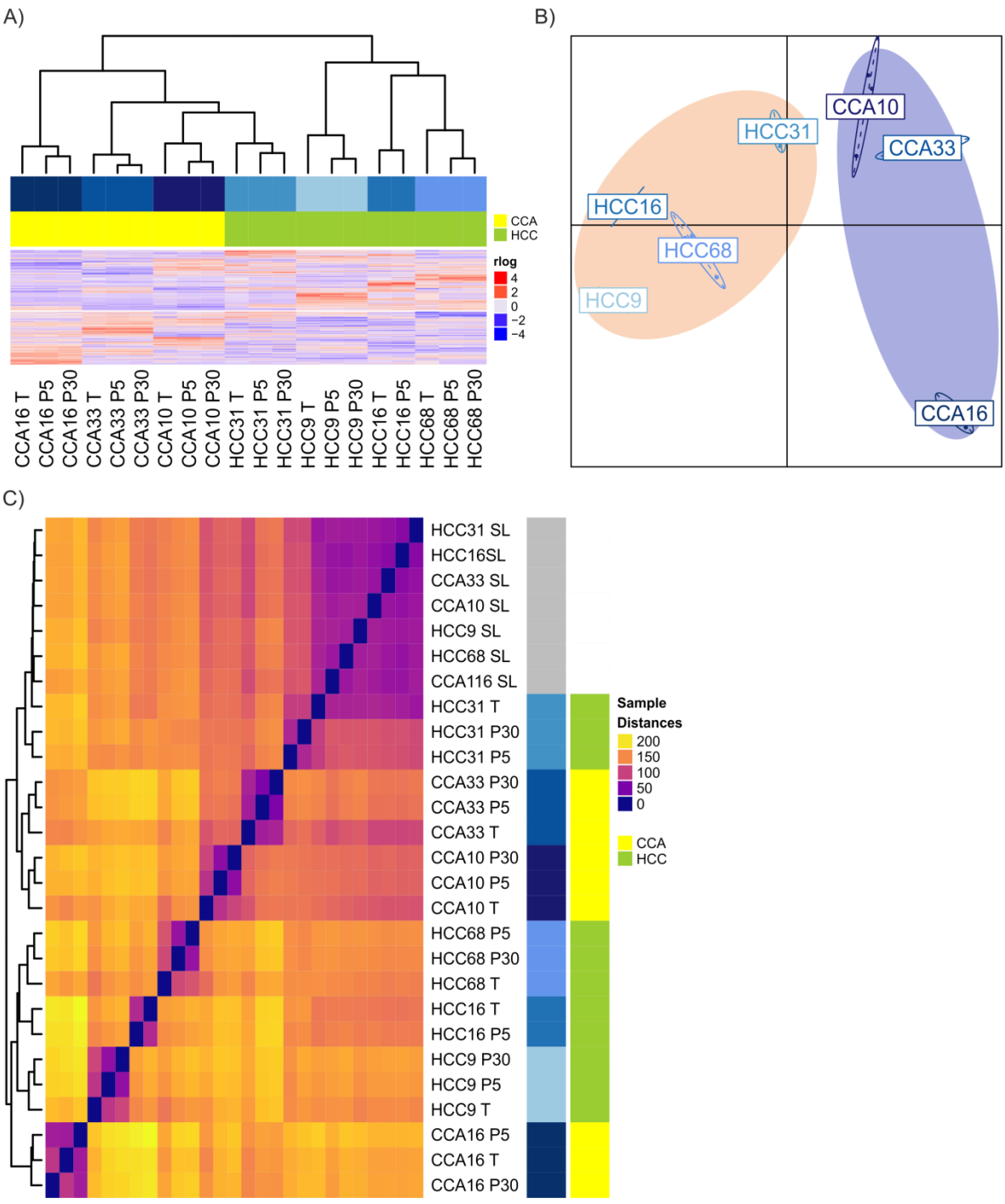

Figure 16 Concordance in transcriptome profiles of PDCLs and matched primary tumors and separation of surrounding liver tissue.

Whole RNA-seq was performed on surrounding liver (SL), primary tumors (T) and PDCLs at passage 5 and 30. A total of 5014 genes significantly differed across the different PDCLs. A) Unsupervised clustering analyses and B) principal component analyses (PCA) of the PDCLs and matched tumors (T). C) Transcriptome correlation confirms a clear separation of tumor-surrounding livers from transformed tumors and PDCL. Result shows that different PDCL form tight sub-clusters with the primary tumors.

Comparative functional network and pathway analyses for commonly disrupted genes in each PDCL were performed. Several key oncogenic pathways associated with the different primary cancers could be revealed (Figure 17). For HCC-PDCL this included activation of MYC, p14/p19ARF, Sirtuin, p53 as well as Notch signaling.[53, 206] Genes centering on MAPK, ubiquitination, autophagy and pluripotency were also enriched. In CCA-PDCL we observed activation and enrichment of Wnt/β-Catenin, Pi3K, insulin receptor, VEGF signaling as well as pathways mediating p53 and pro-inflammatory related pathways.[207] Interestingly, some of the affected pathways were only detected in a single PDCL, such as cyclin dependent cell cycle regulation and mitotic regulation through polo-like kinase in HCC68, also reported to be dysregulated in some HCC.[208, 209] Moreover, our CCA-PDCL showed a higher number of uniquely activated pathways in each primary cell line than observed in HCC-PDCL (Figure 17). Accordingly, CCA10 showed the highest diversity of unique pathways, predominantly involved in different aspects of immunity, such as modulation of immune response, induction of inflammation, as well as role in cell proliferation and apoptosis.[210, 211] These pathways include CD40, TLR, Lymphotoxin β receptor, B-cell activating factor, TWEAK and TNFR2 signaling. Other CCA-PDCL showed lower number of unique pathways, where CCA16 was characterized by activation of VEGF and MAPK signaling through Erk5, and CCA33 by PI3/Akt/mTOR.[212] However, several signaling pathways were commonly activated in two or more of the respective PDCL from the same cellular origin (Figure 17). For instance, majority of HCC-PDCL exhibit frequently enriched pathways that are related to p53 signaling, pluripotency and stemness features (Nanog and Human embryonic stem cell pluripotency signaling), cell cycle regulation (p53 and cell cycle G2/M damage checkpoint regulation).[213] Furthermore, number of commonly overlapping signaling pathways was highest in HCC9, HCC16 and HCC68, while HCC31 had the most distinct profile. In addition, CCA-PDCL overlapped in the signaling pathways commonly found in this tumor entity, such as MYC, cyclin and cell cycle regulation, p53 and Wnt/β-catenin signaling.[76, 86, 142]

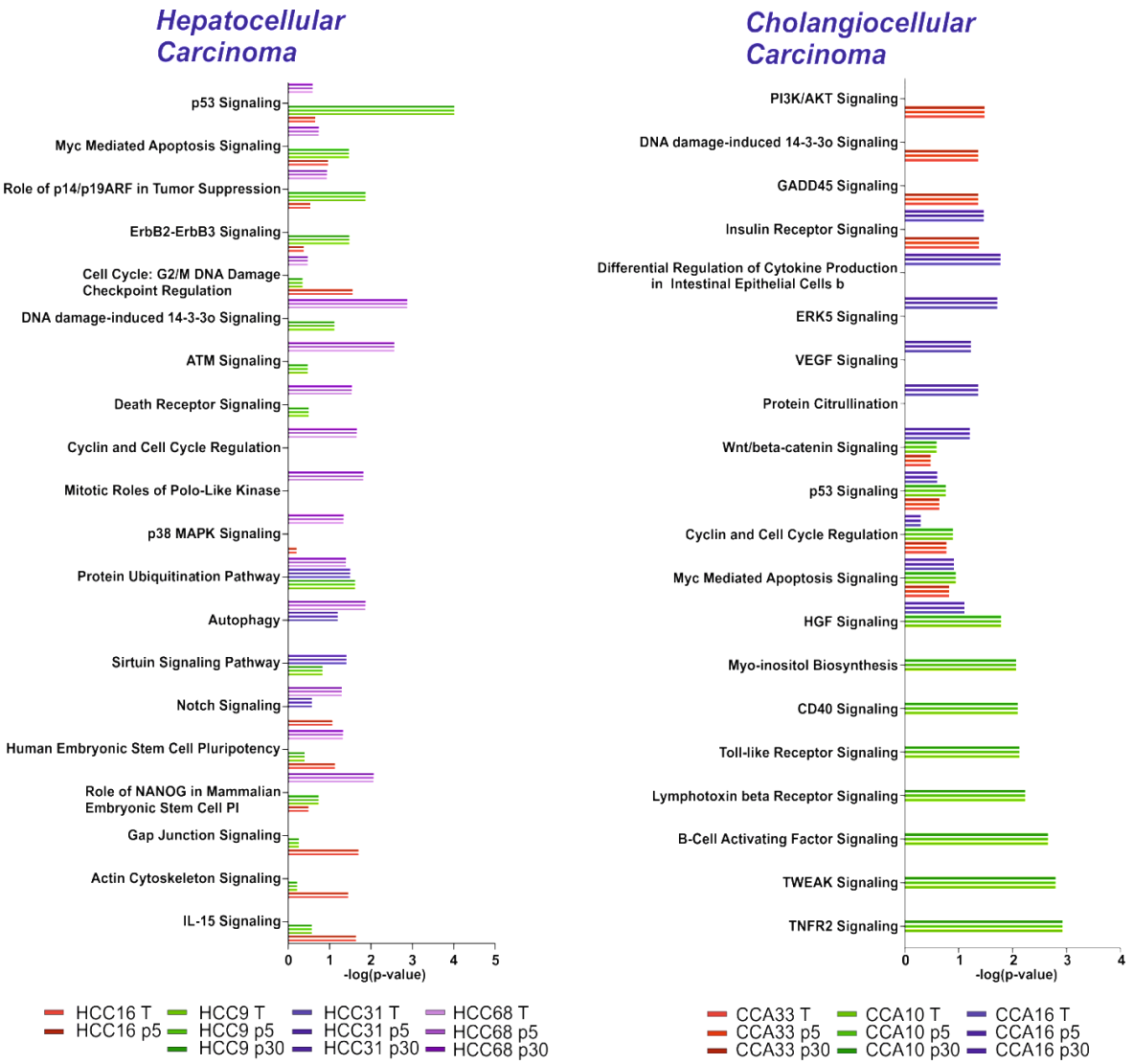

Figure 17 Activated signaling pathways in the different PDCLs.
Comparative ingenuity pathway analyses (IPA) were performed based on the specific transcriptome profiles of the different PDCLs. Each color represents different PDCLs/primary tumors. Pathways were selected based on log p-values for each PDCL and divided according to the cellular origin, i.e. HCC, CCA.

Gene Set Enrichment Analysis (GSEA) further confirmed that distinct gene sets associated with the corresponding tissue of origin are commonly enriched in different PDCL. While MYC and EpCAM signaling could be revealed in the HCC-PDCL, CCA-PDCL were characterized by enrichment of KRAS signaling (Figure 18a). We next explored activated signaling pathways and gene sets in individual HCC- and CCA-PDCL (Figure 18b). Interestingly, the spectrum of the activated gene sets resembled major signaling pathways of PLC, e.g. MYC, IL-6/JAK/STAT3, HGF as well as KRAS. However, activation of the selected pathways was quite heterogeneous and unique for the corresponding PDCL (e.g. E2F targets, cholesterol homeostasis, EGFR). These investigations confirm that the PDCL retain common and individual transcriptomic features and key signaling pathways as well as oncogenic molecules of the primary cancers.

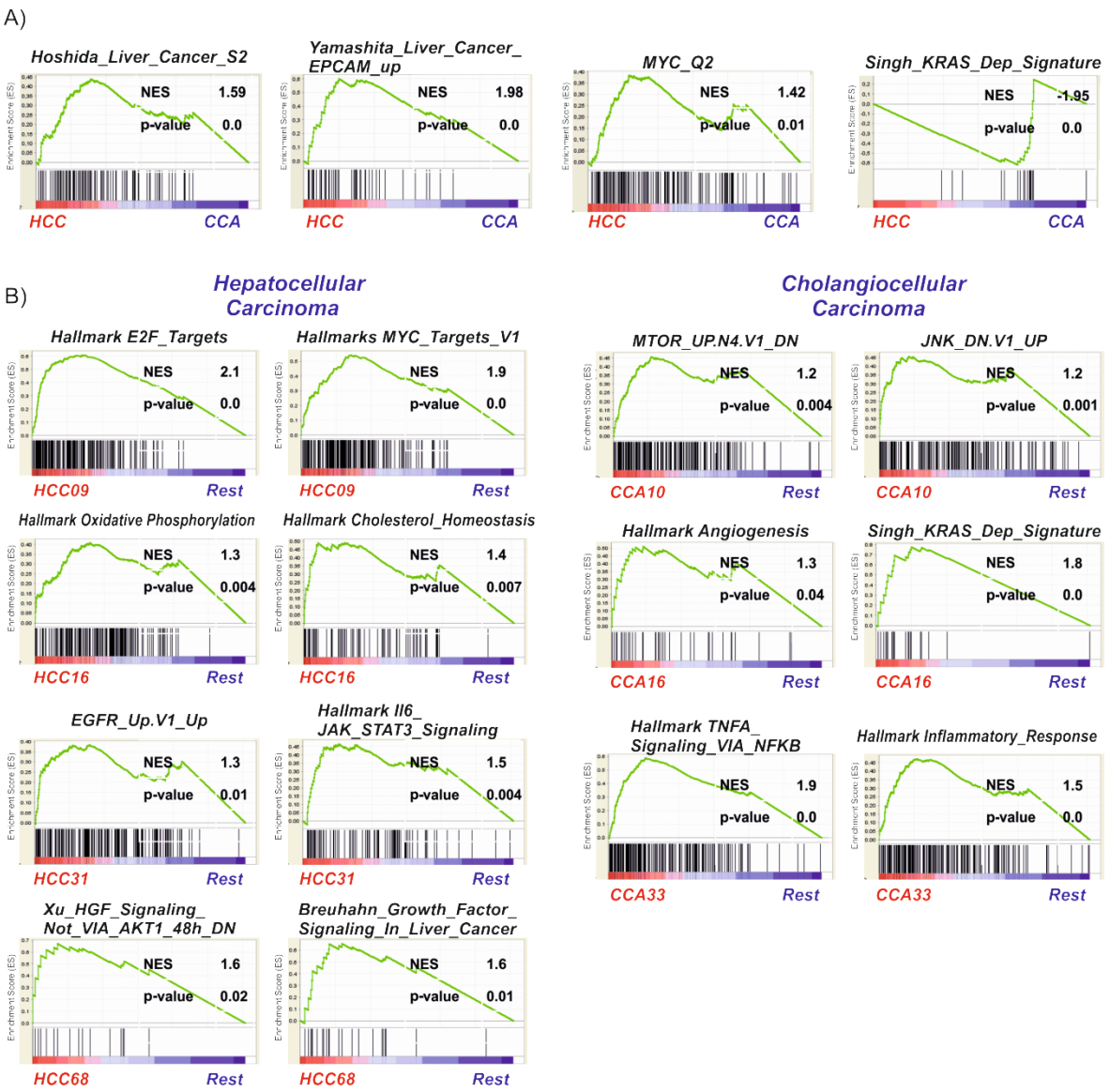

Figure 18 Activated gene sets in HCC- and CCA-PDCLs.
A) Figure B shows GSEA of combined HCC-PDCLs vs CCA-PDCLs. B) Gene set enrichment analysis (GSEA) of each individual HCC- and CCA-PDCL was performed. Normalized enrichment score (NES) reflects degree of overrepresentation for each group at the peak of the entire set. Statistical significance calculated by nominal P value of the ES by using an empirical phenotype-based permutation test.

4.2.5 Genomic landscape of PDCL and original tumors

Genome-wide genetic alterations including SNVs and CNAs were assessed using genotyping arrays. Clustering by PCA was based on 44.329 significant SNVs within the transcriptome signature, where SNVs confirmed that different stage PDCL and matched tumor group together in the same cluster (Figure 19a). Moreover, both PDCL and tumors displayed a similar spectrum of recurrent CNAs (Figure 19b). Among those, typical CNAs associated with the primary cancers could be detected.[214, 215] For example, amplifications of 6p, 8q, 9p and 12p including well known oncogenes *MYC* and *KRAS* as well as losses of 1p, 4q, 8p, 13q, 16q and 17p associated with PLC could be recognized in different PLC-PDCL.[40] Interestingly, the overall genomic alterations were highly similar among PDCL and

matched tumors and, generally, concordance in detected changes from the normal counterpart generally exceeded 70% (Figure 19c). Several of the PDCL (e.g. HCC9, CCA16, CCA33) showed an increasing frequency of alterations from tumor to late passage PDCL. Collectively, these observations confirm that the PDCL closely recapitulate the original tumor and could be a valuable patient-specific tumor model.

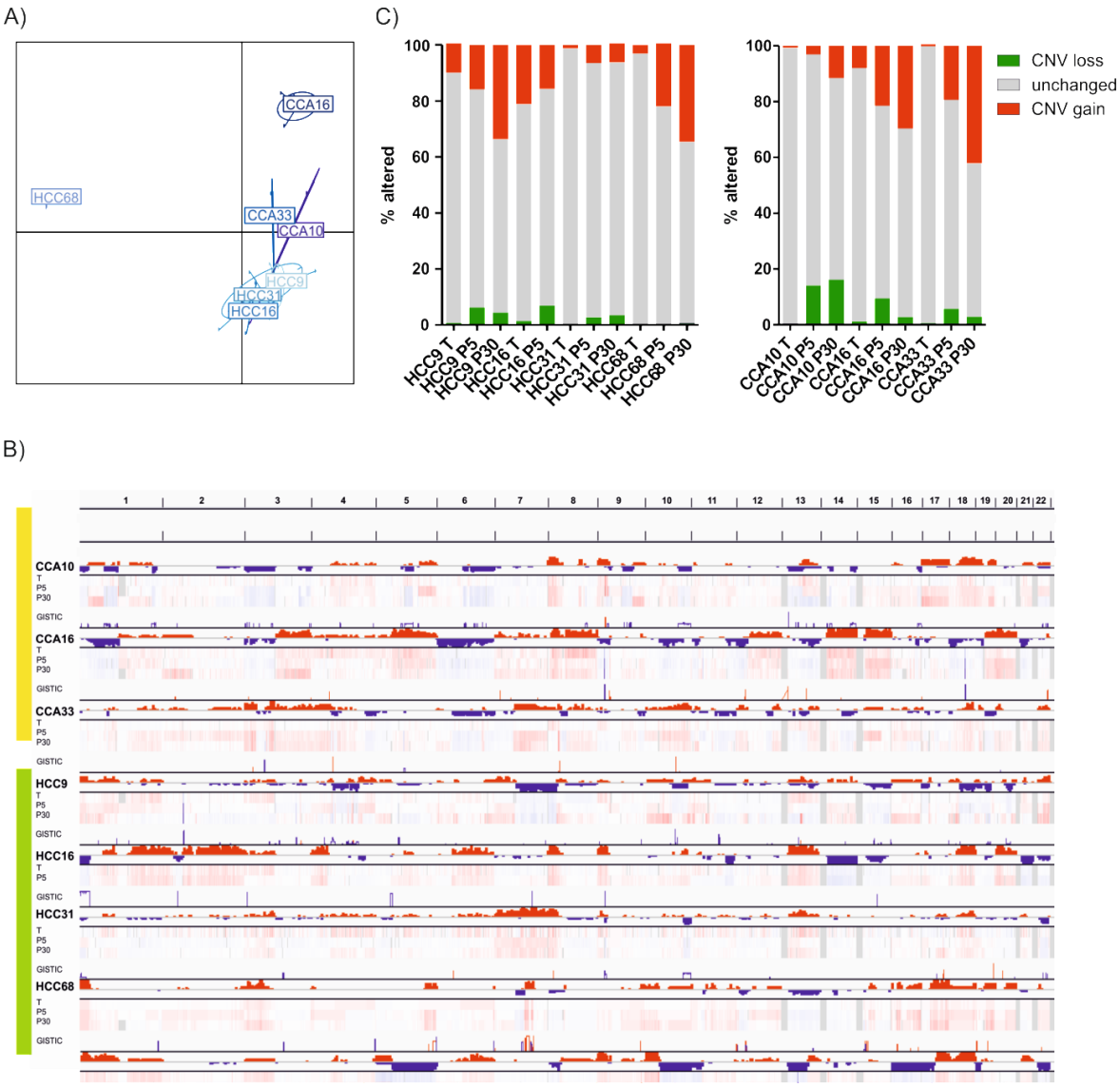

Figure 19 Landscape of genomic alterations in PDCLs and matched primary tumors. A) Principal component analyses (PCA) of the primary tumors and PDCLs at different passages are shown. Analyses were based on genome-wide SNVs assessed by genotyping arrays. Analyses were based on 44.329 significant SNVs within the transcriptome signature. B) Upper rows show the combined significant genomic alterations for the seven PDCL. Lower rows show CNAs analyses for each sample as well as the corresponding GISTIC analyses. Red and blue colors represent level of gain and loss, respectively. C) Paired analyses of genetic alterations in PDCLs from different passages and matched primary cancers in comparison to surrounding liver were performed. Samples were grouped according to the corresponding cellular origins of the tumors, i.e. HCC, iCCA.

4.2.6 **PDCL reflect genomic and prognostic features of primary liver cancer**

To test whether PDCL can be used as a representative model for different established prognostic subgroups of PLC patients, we integrated our transcriptome data with pre-existing data from authentic human HCC and iCCA (53 and 45 patients) representing well defined prognostic subgroups of PLC patients (i.e. good and poor outcome).[196, 197] While HCC9 and HCC16 grouped together with poor prognostic HCC patients, HCC31 and HCC68 recapitulated transcriptome features of good prognostic HCC (Figure 20). Similar, CCA10 and CCA33 formed a cluster with good prognostic iCCA patients. *KRAS*-mutated CCA16 shared adverse gene expression profiles of poor prognostic iCCA patients with enrichment for KRAS mutations (Figure 20). Overall, these results indicate that PDCL resemble a broad spectrum of different prognostic subclasses of PLC patients.

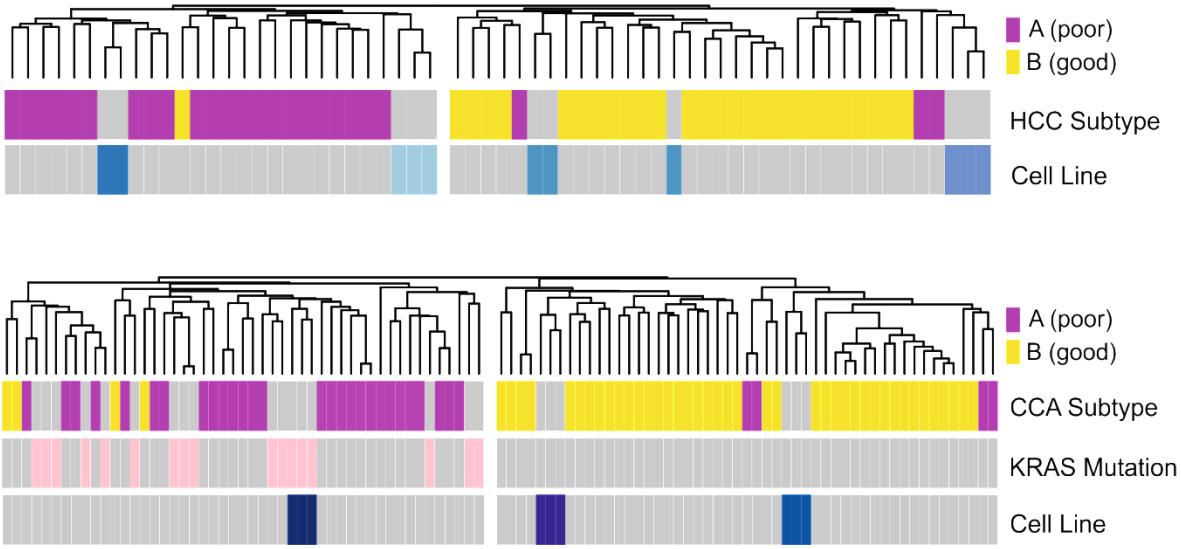

Figure 20 Integration of PLC-PDCLs with prognostic subgroups of the patients.
Upper graph shows integration of HCC-PDCLs with our previously published dataset of 53 HCC patients. In the poor prognostic group (left) are clustered HCC9 and HCC16 PDCL. In the good prognostic group (right) are clustered HCC31 and HCC68 PDCL. Lower graphs show integration of CCA-PDCLs with a previously published dataset of 45 iCCA patients. iCCA patients with *KRAS* mutations are depicted and labeled with pink color. In the poor prognostic group (left) is clustered CCA16 PDCL. In the good prognostic group (right) are clustered CCA10 and CCA33 PDCL.

We further evaluated the genomic similarity between PDCL and established cell lines by integrating SNV data from both PLC-PDCL with 7 established HCC and 8 CCA cell lines. PCA showed that the spectrum of alteration is quite distinct, and a higher concordance within the established cell line than across different PDCLs (Figure 21a,b). Furthermore, we integrated both PLC-PDCL and established cell lines with the cohorts of 48 HCC and 28 iCCA patients based on corresponding SNV profiles.[48] PDCL reliably formed sub-clusters within a broad spectrum of primary HCC and CCA, whereas established lines showed a distinct genomic alterations, reflecting genetic profiles of only few primary cancers (Figure 21c,d, Supplementary Table 1 and 2).

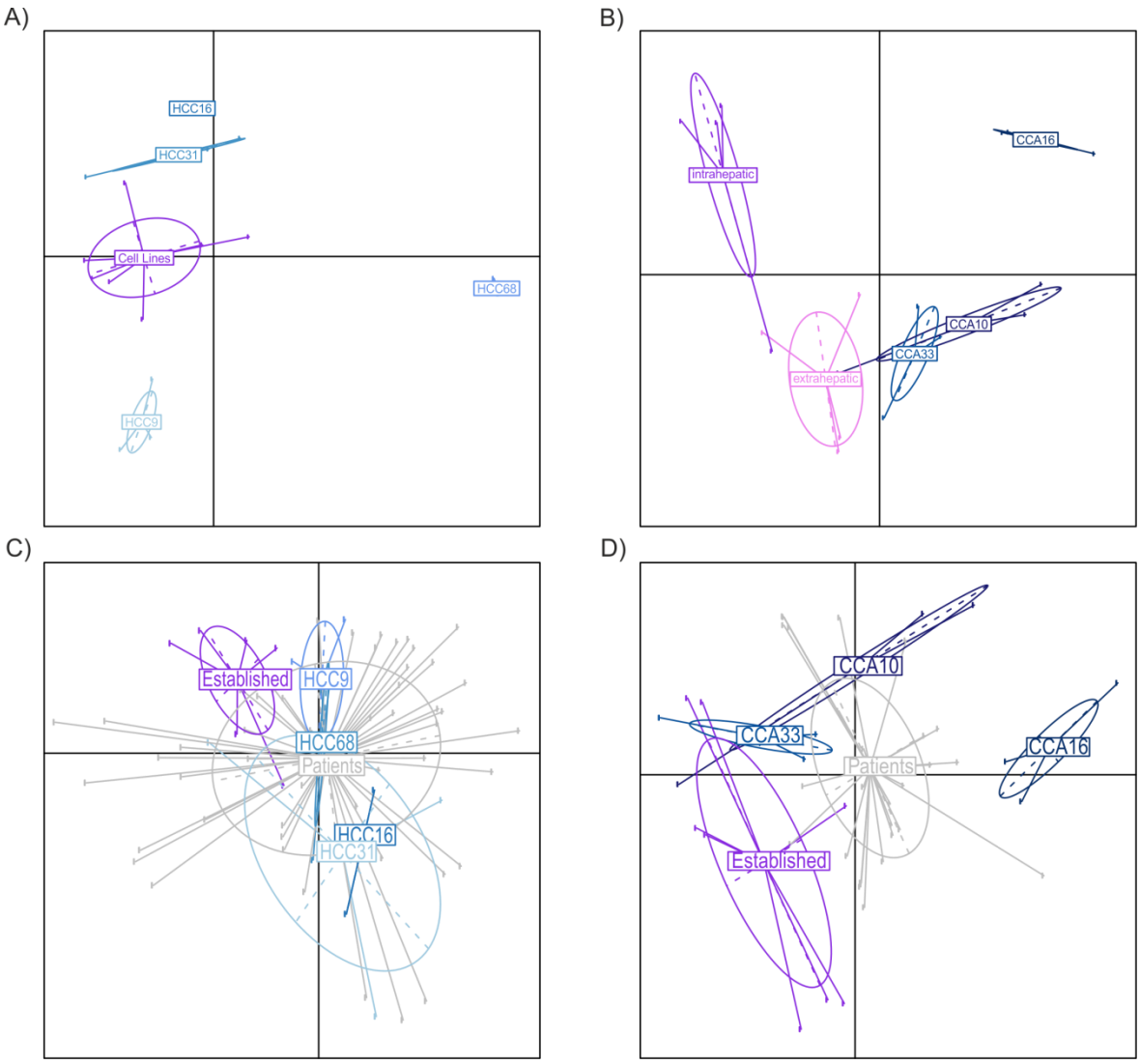

Figure 21 Integration of PLC-PDCLs with established cell lines and human HCC and iCCA based on genomic alterations.

A) PCA of HCC-PDCLs and B) CCA-PDCLs with established cell lines based on corresponding SNVs determined by array-based genotyping. Colors indicate the PDCLs and corresponding cell lines. For CCA, cell lines from extrahepatic and intrahepatic CCA origin were distinguished. C) PCA of HCC-PDCLs, established HCC cell lines and 48 authentic human HCC based on corresponding SNV profiles. D) PCA of CCA-PDCLs, established iCCA cell lines and 28 authentic human iCCA based on corresponding SNV profiles.

In line with this, while genetic losses were quite similar across authentic tumors, PDCL and established cell lines, the number of genetic gains was highly comparable in primary tumors (13% HCC; 17% iCCA) and PDCL at early passages (passage 5 – 17% HCC; 16% iCCA). In addition, number of genetic gains slightly increased over time in culture (passage 30 – 26% HCC; 28% iCCA) and further remained stable during long period of cultivation (passage 50 – 27% HCC; 24% iCCA and passage 100 – 21% HCC; 25% iCCA). Amount of genetic alterations were markedly higher in established cell lines in comparison with PDCL and primary tumors (31% HCC; 41% iCCA) (Figure 22). Together, these results suggest that there is an acquisition of genetic alterations at earlier stages of cell culture propagation, while during further extended *in vitro* culturing level of genetic alterations remains equal without

significant changes. These results clearly demonstrate that PDCL model more closely mimic the genomic landscape of authentic HCC than established cell lines.

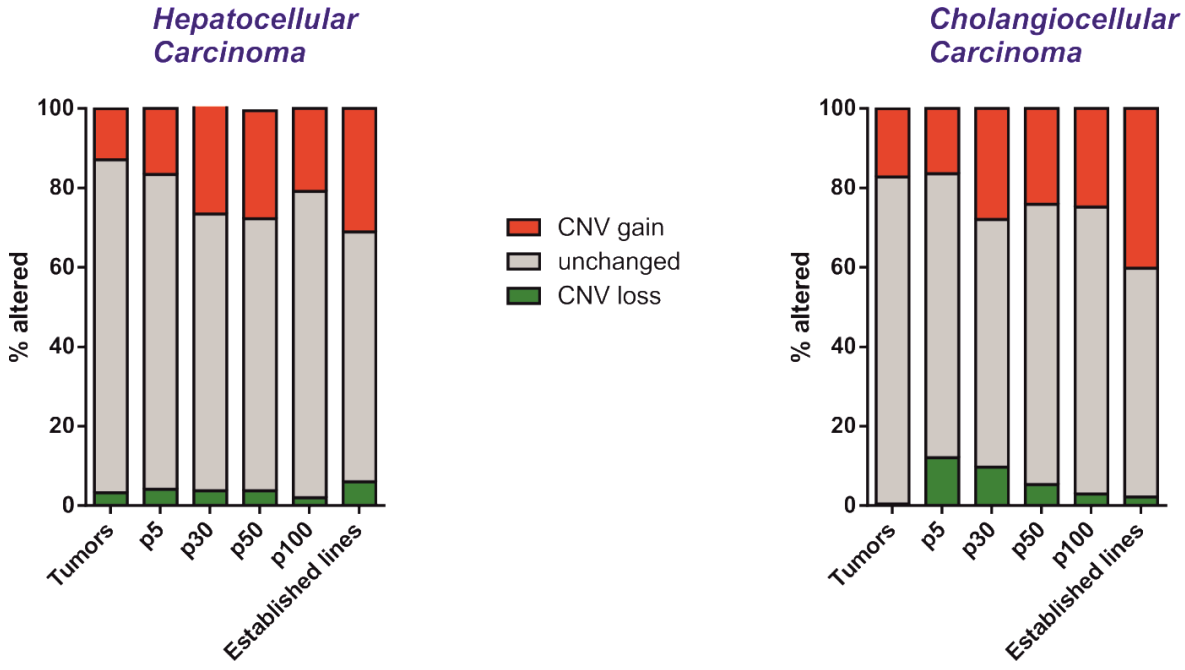

Figure 22 Compared genetic alteration of PLC-PDCLs, established cell lines and authentic human HCCs and iCCAs.

Left are shown paired analyses of genetic alterations in 48 authentic human HCC, HCC-PDCLs and established HCC cell lines and right 28 authentic human iCCA, CCA-PDCLs, established HCC cell lines.

4.3 PDCL for targeted therapy and personalized medicine approach

4.3.1 Mutational profiles of key oncogenes and tumor suppressor genes in PDCL, matched primary tumor and surrounding liver tissue

To explore the potential of the PDCLs as a model for therapeutic approaches and subsequent target evaluation we assessed changes in several key oncogenes or tumor suppressor genes in PDCL, primary tumors and surrounding liver tissue (N) (Figure 10, Figure 23). As expected, DNA sequencing unveiled high frequency of mutations in *TP53,* a hallmark feature of PLC.[40] Several oncogenic mutations and variants were detected in HCC-PDCL, such as *FGFR3, CTNNB1, KIT, MET, ATM,* frequently reported in HCC patients.[40, 215, 216] Similarly, CCA-PDCL mutational profile displayed several alterations distinctive for iCCA, namely *JAK3, KRAS*, *KDR* and *ABL1*. *JAK3* mutation and dysregulation of IL-6/JAK/STAT3 signaling pathway is typically observed in more than 50% iCCA cases, while activating *KRAS* Gly12Asp mutation is detected in 19% iCCA cases and associated with invasiveness and poor outcome.[40, 111, 217] Additionally, presence of several alterations was observed in the surrounding liver tissue, and could be a consequence of tumor cell infiltration, germline or a passenger mutation. Nevertheless, once alteration was detected in the tissue (tumor or N), frequency remained stable in PDCL over continued period of cultivation. These results showed that all the cell lines, except CCA33, poses distinct genetic alterations in known key oncogenes.[218]

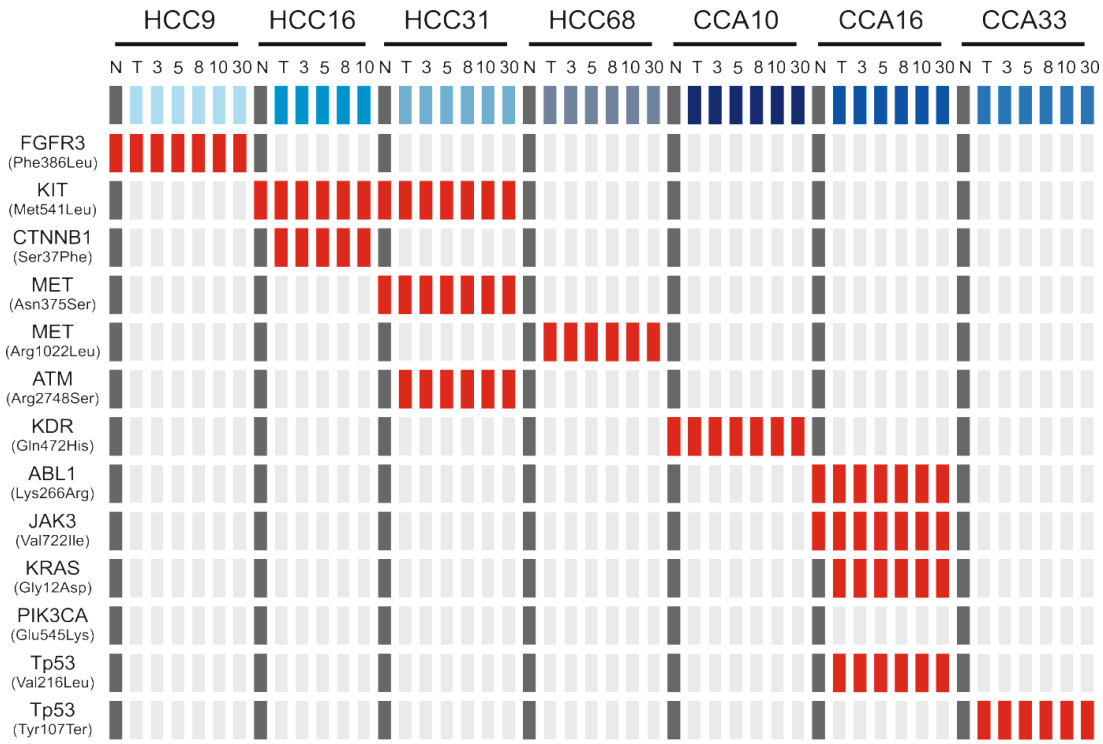

Figure 23 Targeted DNA sequencing of key oncogenes.

DNA sequencing of 48 key genes associated with cancer using Illumina TruSeq Amplicon - Cancer Panel. Results for individual PDCLs including matched primary cancers (T) and tumor surrounding liver (N; dark grey) are shown. Red color indicates mutated samples.

4.3.2 **Targeting key oncogenic alterations as an individualized therapeutic approach**

After obtaining information about mutational profiles of our cell lines, we interrogated different publicly available resources as well as TARGET database (http://archive.broadinstitute.org/cancer/cga/target) to identify whether detected molecular alterations could be used for specific drug targeting. As a result, we identified several commercially available inhibitors that potentially target, with high specificity, the detected genetic alterations or corresponding downstream targets (Table 9). We used specific inhibitors to perform dose-response analyses and to determine IC50 values conforming to detected alterations in a PDCL. Several alterations showed significantly higher sensitivity to corresponding targeted treatment approaches than non-altered counterpart, such as *KIT* Met541Leu (HCC31), *KRAS* Gly12Asp (CCA16) and *MET* Arg1022Leu (HCC68). Altered and non-altered cells demonstrated completely different dynamics of dose-response (Figure 24a-d) as well as IC50 values (imatinib: *KIT*-altered cell line HCC31 = 15,59 µM vs 29,06 µM in non-altered cell line HCC9; tepotinib: *MET*-altered cell line HCC68 = 5,9 µM vs non-altered cell lines HCC9 = 16,5 µM and HCC31 = 15,3 µM; refametinib: *KRAS*-altered cell line CCA16 = 1,30 µM vs 72,26 µM in non-altered CCA10). Interestingly, some of the cell lines did not show treatment benefit or showed more resistant phenotype than non-altered cells. Lack of significant response between specific inhibition and a control was observed in *ATM* and *JAK3* altered cell lines with the alterations in *ATM* Arg748Ser and *JAK3* Val722Ile (KU-55933: *ATM* altered cell line HCC31 = 90,90 µM vs 104,50 µM in non-altered cell line HCC9; tofacitinib: not assessable) (Figure 24e-f). In the cell lines containing *FGFR3* Phe386Leu and *KDR* Gln472His was observed more resistant phenotype when treated with the specific inhibitors BGJ398 and vandetanib (BGJ398:*FGFR3*-altered cell line HCC9 = 10,02 µM vs 5,14 µM in non-altered cell line HCC31; vandetanib: *KDR*-altered cell line CCA10 = 5,30 µM vs 2,33 µM in non-altered cell line CCA16) (Figure 24g-h).

Table 9 List of specific inhibitors used in targeted and long term approach.
In the table are listed single and multi-target inhibitors, target/drug function and manufacturer.

Inhibitors	Target / Drug function	Manufacturer
BGJ398	FGFR3	Selleckchem
Doxorubicin	DNA topoisomerase II inhibitor	Selleckchem
Gemcitabine	Inhibits DNA synthesis	Selleckchem
Imatinib	KIT	Selleckchem
KU-55933	ATM	Selleckchem
Refametinib	MEK	Selleckchem
Sorafenib	VEGFR2, VEGFR3, PDGFRβ, Flt3, c-Kit	Selleckchem
Tepotinib	MET	Selleckchem
Tofacitinib	JAK3	Selleckchem
Vandetanib	KDR	Selleckchem

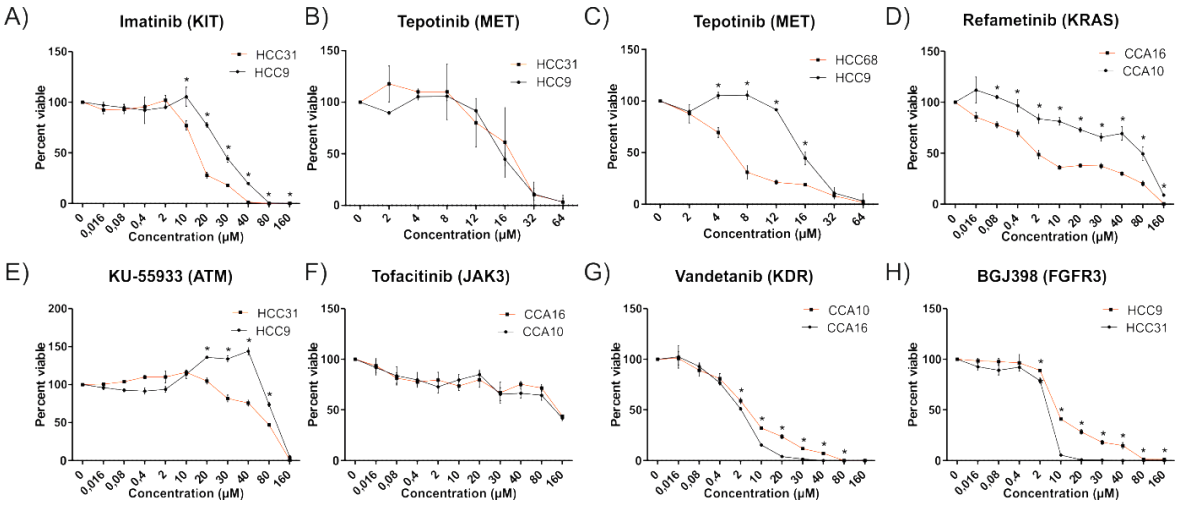

Figure 24 Sensitivity to targeted treatment based on individual oncogenic alterations.
PDCLs containing potential targetable mutations and non-altered controls from the same cellular origin were treated with specific inhibitors to target individual molecular alterations. Dose-response curves for specific inhibitors are shown. Growth was measured in triplicates and viability was assessed 3 days after treatment at the indicated drug concentrations (mean ± SD). * indicating p-value <0.05. A-D) Shows alterations in *KIT*, *MET* and *KRAS* potentially conferring to higher sensitivity to corresponding inhibitors. E-H) Cell lines with alterations in *ATM* and *JAK3* showed a similar viability after administration of the specific inhibitor. Cell lines with alterations in the corresponding genes are plotted in red lines. G-H) Cell lines carrying alterations in *FGFR* and *KDR* displaying a higher resistance to the corresponding inhibitor.

To validate our *in vitro* findings, we tried to recapitulate selective sensitivity to specific inhibitors in *in vivo* setting (Figure 25). Consistent with our *in vitro* findings, results demonstrated that *KRAS*- and *JAK3*-cell line CCA16 had beneficial response to refametinib treatment, reflected in a considerable reduction in both frequency and latency of tumor growth. In addition, treatment with tofacitinib did not show a significant tumor incidence reduction when compared with non-treated control cells (Figure 25). These investigations confirm that individual genetic alterations could be potentially explored for individualized treatment approaches.

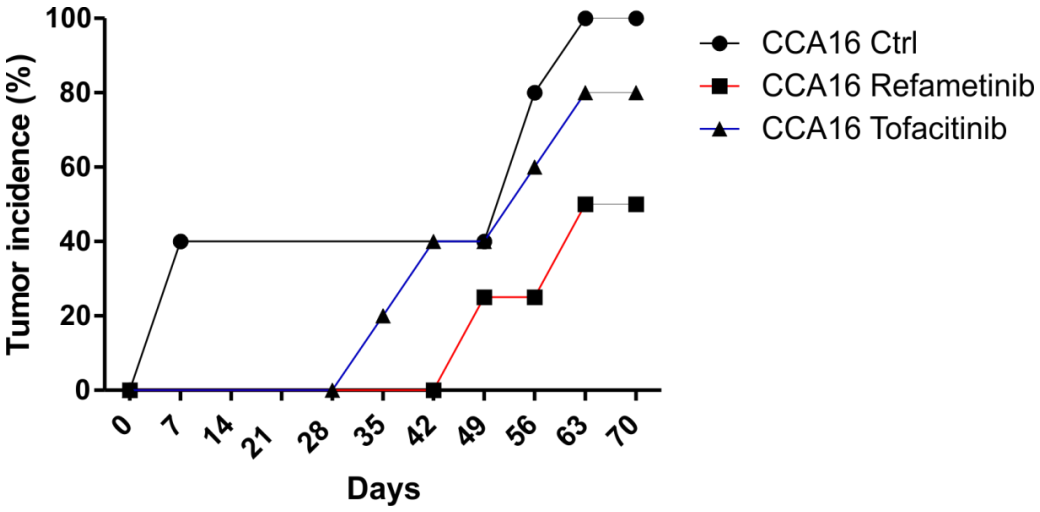

Figure 25 Validation of sensitivity for targeted treatment *in vivo.*
CCA16 cells harboring known *KRAS*- and *JAK3*-alterations showed a predicted high sensitivity to refametinib *in vivo* while remained without mentionable effects after treatment with tofacitinib. 1 mio. cells treated with specific inhibitors for 72h or control cells were transplanted into both flanks of NOD/SCID animals. Tumor growth was monitored for a total of 10 weeks.

4.3.3 Effects of established chemotherapies on PDCL after extended *in vitro* cultivation

To test the utility of the established PDCL for drug evaluation in long term cultures, different passages of PDCLs up to passage 100 (1-2 years in culture) were treated with established chemotherapeutic and targeted compounds for the respective entity. HCC-PDCL were exposed to increasing concentrations of doxorubicin, sorafenib and tepotinib, while CCA-PDCL were exposed to doxorubicin, sorafenib and gemcitabine. Cell viability was reported (Figure 26). Overall, response to the treatment was highly consistent across the different cell lines and passages, confirming the utility of the PDCL for translational approaches during long-term culturing.

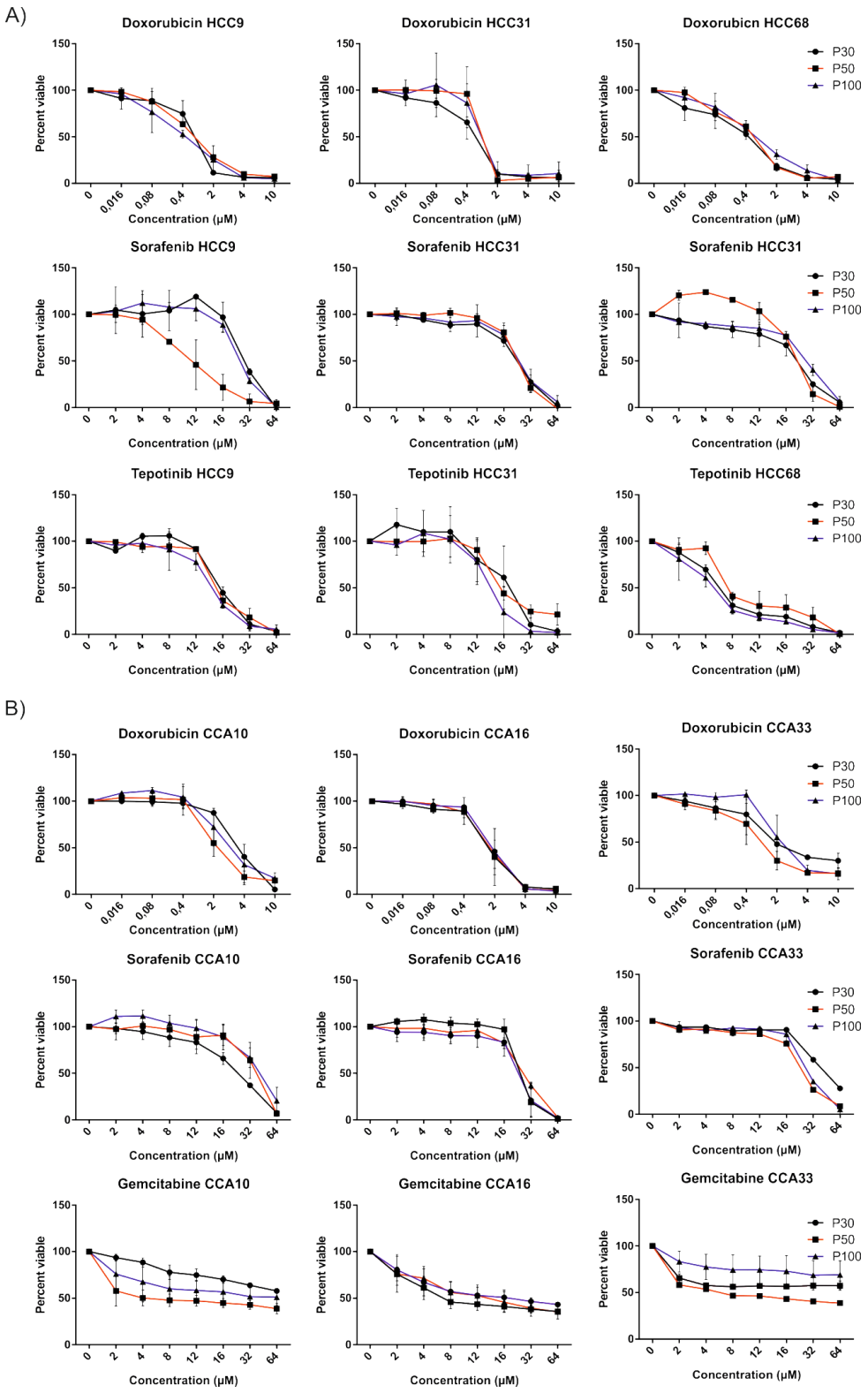

Figure 26 Response to established therapies during extended time in culture.
Different passages of the PDCLs were treated with established chemotherapeutic compounds (i.e. doxorubicin for HCC; doxorubicin and gemcitabine for iCCA) as well as the tyrosine-kinase inhibitor sorafenib. Dose-response curves for the corresponding compounds and cell lines are shown. Growth was measured in triplicates and viability was assessed 3 days after treatment at the indicated drug concentrations (mean ± SD). * indicating p-value <0.05. A) Shown are treatments of HCC-PDCLs and B) CCA-PDCLs

5. Discussion

Over the past two decades, rapid technological advancement and growing expertise led to a tremendous progress in cancer research. Today, changes towards cutting-edge technologies, for instance, from array-based gene profiling to next generation (DNA, RNA) sequencing are emerging by the minute. While DNA sequencing was costly and time-consuming almost two decades ago, when the human genome project was initiated,[219] nowadays next-generation sequencing technologies are rapid, standardized and accessible to the larger scientific community.[220] The relatively low costs of sequencing and fast data acquisition accompanied by advancement in bioinformatics and machine learning algorithms,[221] allow more individualized approach to target specific diseases, such as primary liver cancers.[220] Therefore, it seems promising to utilize these technologies for the benefit of each individual patient, i.e. by implementing them into representative models. Currently, existing models to study primary liver cancers are lacking to accurately represent individual aspects of the diseases, thus, hampering further therapeutic progress.[167, 190] Since dissection of the diseases with much higher resolution than ever before is possible, it is of great importance to generate novel models that would ideally represent patients. This includes the full range of etiological background of the diseases, to the phenotypical and molecular complexity. New models should consider heterogeneity from different perspectives - genetic, epigenetic, transcriptomic, as well as morphologic, and explore potential consequences on the treatment options as well as survival benefits.

Developing a new liver cancer model, which would fulfill these important criteria, could help to better understand complex processes that occur during disease initiation and progression, but most importantly, to help finding adequate treatment strategy for each patient. We successfully generated seven PDCL from a Western cohort of patients as a representative model to study hepatocellular and cholangiocarcinoma. In our study, we comprehensively analyzed the newly generated PDCL and matched primary cancers on several different levels. We perform transcriptomic and genomic analyses to confirm the utility of the newly-derived PDCL as a patient-specific *in vitro* model. A key goal of our study was to explore whether PDCL closely resemble the molecular and phenotypic features as well as key oncogenic alterations present in matched primary tumors. Therefore, we performed long-term cultivation of PDCL and propagated them continuously for more than 30 passages *in vitro*. Finally, we tried to identify potentially actionable genetic and transcriptomic targets for individual PDCL and predict a treatment response in order to determine potential utility of PDCL for individualized treatments strategies.

Except the PDCL model that we are investigating in this study, there are several alternative models that have been developed over the past several years. Two promising and novel, but still very distinct approaches, involve 3D organoid cultures and patient-derived xenografts.[222, 223] Two recent studies exploited the potential of organoids to be utilized as a model of PLC.[177, 178] Authors of the studies derived the organoids directly from resected HCC, CCA and mixed HCC/CCA, or from the tumor

needle biopsies. They were able to show that derived organoids could faithfully recapitulate the molecular profile of the original tumors.[177, 178] Similarly to the organoids, only a few studies exploited the potential of PDX as a model for PLC and demonstrated similar histopathologic and genomic characteristics with the original HCC tumors.[224, 225] Nevertheless, all the available patient-derived models have important common as well as specific limitations. While selective growth expansion in immunocompromised animals is utilized in PDX models, three dimensional growth might be problematic for drug evaluation in organoid cultures.[226] Also, all approaches require significant amount of resources, making it difficult to be used for large-scale applications. Most importantly, all the models including the current PDCL 2D approach lack the tissue context of the hepatic microenvironment. Therefore, detailed comparative analyses are needed to estimate the impact and utility of each approach for translational research.

5.1 Higher tumor grading and increased genomic alterations favor successful PDCL generation

Despite usefulness of PDCL as a reliable model, there are certain limitations that should be considered and further addressed: major obstacles in PDCL, as well as other patient-derived models, are low efficacy of successful generation. In addition, it is unclear whether these models can cover a representative spectrum of human liver cancers. In our study, success rate of generating PLC-PDCL reached 11%, a similar range as observed in other solid malignancies.[227] Success rate of established PDCL reported in our study is in concordance with other approaches such as PDX and organoid cultures derived from tumor needle biopsies (usually ranging from 10-33%).[178, 179, 224, 225] Interestingly, a recent study of Broutier *et al.* reported successful establishment of tumor organoid cultures from PLC (HCC, CCA and mixed HCC/CCA phenotype) with success rate of 100% from tumor samples with high cellular proliferation rate and moderate to poor differentiation.[177] However, it is interesting to observe that well-differentiated tumors completely failed to establish primary culture, remaining at 0% of success rate. Taken together, results in this study show that successful establishment of organoid cultures does not exceed 47% and that is favored in poorly differentiated tumors.[177] Therefore, further validation and identification of factors contributing to successful establishment of PDCL and subsequent optimization of the culture conditions is urgently needed to establish large and representative repositories required for extensive studies in PLC. This should also include establishment of PDCL from more advanced stages of PLC, such as biopsies, and comparative analyses of PDCL from primary and metastatic sites. [177] Of note, Nuciforo *et al.* also reported that successful establishment of organoid cultures from the needle biopsies had strong correlation with the histopathological grading of the HCC. In that study, all the organoids were derived from poorly differentiated tumors (grading III and IV), with cells showing high proliferation rate. Authors were able to establish 26% organoid cultures from a total number of needle biopsies (10 out of 38), while a complete number of established

organoids, based on the number of patients (from some patients multiple biopsies were taken), was 33%. [178]

In our study we can observe similar trend, where 50% of all successful PLCs are graded as G3 and more than 25% as G2-G3, indicating higher grade and low differentiation status. Overall, these analyses confirm the observation that successful establishment of PDCL is favored by less differentiated tumors and high grading (Figure 11). Furthermore, we demonstrate that genetic heterogeneity, as well as pro-tumorigenic genomic amplifications, might be additional factors contributing to a success rate. Our findings show significant number of increased genomic gains and losses in the tumors with successful PDCL establishment (Figure 11), notably in the chromosome regions associated with high proliferation and cancer, such as 4q, 5q, 8p, 9p and 13q (Figure 11). Expression of *LPHN3* and *TSLP* genes, located on 4q and 5q, has been associated with poor prognosis and metastases in several solid tumors.[198, 199] For instance, *TSLP* expression was the most frequently observed in advanced gastric cancer (T2, T3 and T4) as well as in liver metastases from this tumor.[198, 199] Additionally, *CCDC25* (8p) was identified to modulate EGFR signaling and reported that overexpression can significantly enhance cell migration in iCCA.[228] Furthermore, importance of miRNAs (miRs) in tumorigenesis has been shown over the past decade and it is emerging as a potential therapeutic target in many cancers, including PLC.[229] Chengyoung *et al.* showed potential impact of miR-1297, encoded by *MIR1297* gene (13q), on cell death and cell cycle regulation in liver cancer cells. They noticed that tumor cell proliferation was significantly induced by miR-1297 overexpression and proposed a mechanism of carcinogenesis via miR-1297 induced downregulation of the tumor-suppressor gene *RB1.*[200] Overall, our findings support the evidence that miRNAs, particularly miR-1297, might contribute to higher tumor proliferation and consequently to successful establishment of primary cancer cell lines. Additionally, molecular and cellular functions of a significant number of genomic alterations present in PLC with the successful PDCL establishment centered on pro-oncogenic properties, favoring cellular growth and proliferation, as well as cell death and survival (Figure 11c).

5.2 Morphology of the PDCL remains stable during long-term cultivation

Until now, very limited number of investigators tried to characterize and utilize PDCL as a reliable liver cancer model in personalized medicine.[230] Only a few studies reported successful establishment of few HCC primary cell lines, with a limited data output and very narrow translational implications. In one study, authors used an early-stage and moderately differentiated HCC to derive primary cell lines.[231] Despite a fairly high number of primary cancer tissues that were processed, cell line authentication and characterization was conducted in one specimen, thus making further translational implications of this study challenging.[231] Similarly, in another study authors derived nine cell lines from primary HCC tissue and compared early

stage passages with corresponding tumor tissue. Transcriptomic and genomic data of the early passages showed similarities with cancerous tissue and unveiled possible protein-altering mutations. In spite of early-stage characterization, long-term effects of cultivation and functional validation were missing.[230] Overall, limited number of representative cell lines as well as characterization only at the early stage, together with lack of functional validation and translational implications, hinder further utilization of proposed models.

The here presented study is one of the first to demonstrate preserved phenotypic stability of PDCL over an extended period of propagation in 2D culture conditions for the entire spectrum of primary liver cancers. Our results clearly show that cells at early stage of cell propagation are highly comparable with cells in the late stage as well as with xenograft-derived second generation (Figure 13). Serial transplantation and rapid tumor expansion in immunocompromised mice emphasize the ability of PDCL to maintain tumorigenic properties. However, necessity of higher cell number in HCC-PDCL to initiate tumor growth was observed in our study. Difference in tumor-initiating capacity between HCC-PDCL and CCA-PDCL could be a consequence of distinct biology of these tumor entities, where iCCA mainly show more aggressive phenotype than HCC, which is also reflected in shorter long-term survival of iCCA patients.[232-234] In addition, difference in tumor initiating capacity can be explained by differential expression of EpCAM in our cell lines. Studies have shown that EpCAM and genes regulated by this protein are involved in cellular growth, proliferation, cell cycle and cell death.[235] Consequently, overexpression of EpCAM in many solid tumors has been associated with poor prognosis.[235-237] Recently Sulpice *et al.* demonstrated a new potential role of EpCAM on iCCA progression and indicated that EpCAM might represent a promising candidate in personalized medicine.[237] Interestingly, in our study, all CCA-PDCL and matching primary tumors showed strong expression of EpCAM, unlike HCC-PDCL, where only HCC68 exhibited very weak EpCAM expression (Figure 15). Strong expression of EpCAM in CCA-PDCL could potentially confer higher tumorigenicity than HCC-PDCL and, therefore, demonstrate more aggressive phenotype. Histological analyses further provide better insight into xenograft tumors, where morphological and cellular patterns are highly preserved and resemble matched primary tumors (Figure 14). Homology with the original tumor is further confirmed by the expression of well-established hepatocellular, biliary and epithelial progenitor markers (Figure 15).[238-240] Cellular origin of HCC-PDCL is characterized by the strong expression of albumin and AFP, and weak expression of EpCAM in one PDCL, while CCA-PDCL display substantial expression of biliary marker CK19 as well as EpCAM.

5.3 Transcriptome profiles of PDCL closely recapitulate original tumor characteristics

High-throughput technologies, such as RNA-seq, have been decisively instrumental to explore diversity and complexity of the gene expression profiles in PLC over the last two decades. These types of analyses have produced a large amount of

information, utilized to better understand the oncogenic process in PLC.[241] It is generally accepted that altered gene expression patterns in cancer tissues are observed during malignant processes, such as tumor initiation and progression.[242] Many studies have demonstrated the importance of characterizing HCC- and CCA-specific gene expression patterns and crosstalk between different signaling pathways, to provide useful insights for potential drug development and prognosis.[243, 244] Taking this into consideration, it is important to develop a PDCL model which preserves transcriptional profile of the original cancerous tissue and remains stable during the course of time.

Our transcriptome analyses indicate that early and late stages of PDCL retain very similar transcriptional profiles with the primary cancers and remain stable during extended expansion (Figure 16). Importantly, our PDCL and tumor tissue show completely distinct profile from surrounding liver demonstrating malignant tumor properties (Figure 16c). Notably, our detailed molecular characterization confirmed that PDCL recapitulate hallmark features of the primary cancers.[40, 215, 245, 246] Commonly for HCC, our HCC-PDCL demonstrated activation of MYC, p53 and Notch signaling, as well as genes centering on MAPK, pluripotency and several others relevant genes (Figure 17). Similarly, CCA-PDCL clearly showed activation of Wnt/β-Catenin, Pi3K, VEGF signaling as well as pathways mediating p53. We observed enrichment of key cancer-associated common, as well as individual, transcriptomic changes resembling proliferative and invasive properties observed in most of the PDCL. Our HCC-PDCL were enriched for gene sets centering around MYC or mTOR, while CCA-PDCL were characterized by activation of networks involved in KRAS, Notch and Hedgehog signaling (Figure 18).[9, 247] Overall, our transcriptome analyses confirm that the PDCL retain common and individual transcriptomic features and key signaling pathways as well as oncogenic molecules of the primary cancers.

5.4 Stabile genomic landscape of PDCL faithfully reflects genomic and prognostic features of primary liver cancer

As our findings demonstrate that expressional profiles of PDCL remain stable and that PDCL faithfully recapitulate hallmark features of the primary cancers, we additionally provide evidence that spectrum of genomic alterations remain consistent with profiles of primary tumors, thus, confirming the utility of the newly-derived PDCL as a patient-specific and reliable *in vitro* model. By analyzing the spectrum of recurrent CNAs, we can observe that PLC-PDCL, both in the early and late stage, display similar profiles to the corresponding primary tumors (Figure 19). In addition, chromosomal amplifications/losses detected in our model are commonly reported in PLC together with amplification of known oncogenes (*MYC* and *KRAS*) (Figure 19).[40] Despite of relatively stable and representative genomic profile, an interesting aspect of our results is increasing number of genetic alterations over time observed for several PDCL. A similar observation was recently revealed for PDX and organoid cultures during serial passaging. Ben-David *et al.* observed increasing

accumulation of CNAs during PDX propagation in an earlier stage, followed by gradual reduction and reaching stabile level in the late stage of passaging. Authors also observed that pre-existing alterations play a major role in acquiring CNAs in PDXs, especially at early stages, but point out that *de novo* events can severely influence genomic instability. They emphasize that specific selection pressure between physiological conditions in patients and cultivation in animal hosts can cause different evolution paths of PDXs and, consequently, have an impact on therapy response. Overall, such implications should be considered when using PDX as a model for personalized medicine approach.[248] To test whether our PDCL would continue gaining additional alterations, we extended cultivation time up to two years in the culture (up to P100), and in parallel we monitored CNV changes. Similarly, to the findings of Ben-David *et al.*, our PDCL stopped accumulating additional alterations after passage 30 and remained stable during extended time period (P50 and P100) (Figure 22). In concordance with that, response to the commonly used chemotherapeutic agents, including standard therapy for HCC (Sorafenib) and iCCA (Gemcitabine), remained stable over extended time in culture for our PDCLs (P30, P50 and P100) (Figure 26).

Early categorization of the patients into specific prognostic subgroups, based on their molecular profile, could further define course of a therapy and potentially bring survival benefit. Our PLC-PDCL model shows similar molecular profile with the authentic HCC and iCCA patients and integrates into different established prognostic subgroups of PLC (poor and good prognosis).[196, 197] It is known that activating mutations in *KRAS,* particularly mutation in codon 12, has close association with reduced overall survival in comparison with non-mutated iCCA and represents a poor prognostic marker for the patients.[249, 250] Our CCA16 cell line, that carries activating *KRAS* mutation (Gly12Asp), clustered with other *KRAS* mutated tumors into poor-survival subgroup, reflecting adverse characteristics typical for those patients. Overall, our results imply that both PLC-HCC groups resemble a broad spectrum of different prognostic subclasses of PLC patients, and could be used to predict the outcome and course of a treatment (Figure 20).

5.5 PDCL more closely reflect PLC than established cell lines

Since commercial cell lines are widely used as a model for PLC, we wanted to test how closely cell lines can recapitulate molecular features of authentic patients and compare the molecular profiles with our PDCL model. A significant limitation of established cell lines is the fact that direct comparison to the earlier stages of culturing and, most importantly, corresponding original tumors is not feasible due to long time span between culture establishment and today's applications. This further raises concerns to which extent existing functional and molecular properties of cell lines can accurately represent primary tumors. Nevertheless, usefulness of established cell lines should not be undermined, since many important findings in translational cancer research are based on comprehensive investigations on cell lines. However, here presented data confirms results from several reports suggesting that newly-derived cell line might share the highest degree of molecular

similarities with primary cancers regarding key genetic alterations at early stages after isolation.[251]

Our Integrative analyses of SNV in PDCL and established cell lines further show that the spectrum of alterations in established cells is more homogenous and quite distinct from our PDCL (Figure 21a,b). Additionally, we integrated both PLC-PDCL and established cell lines with our HCC and iCCA patient cohorts based on corresponding SNV profiles.[48] Results show that PDCL reliably form sub-clusters within a primary HCCs and iCCAs, while established lines show more distinct genomic profile, similar only to few primary cancers (Figure 21c,d). Overall, integration of PLC-PDCL with authentic human PLC patients demonstrated that newly-derived cell lines faithfully recapitulate both the genomic profile as well different prognostic subclasses of liver cancer.

5.6 Targeting key oncogenic alterations as an individualized therapeutic approach

Development of next-generation sequencing technology has allowed us to evaluate and describe in great details genes and molecular pathways altered in PLC and to effectively distinguish driver from passenger mutations.[252] The most prominent alteration in PLC have been well characterized and include somatic mutations in *CTNNB1, TP53, MYC, MET, TERT* promoter*, KRAS* as well as dysregulation in Notch, PI3K/Akt/mTOR, IL-6/JAK/STAT, Ras/MAPK signaling pathways**.** Detection and characterization of mutated driver genes and affected pathways in HCC, opens an interesting and testable avenue for development of novel targeted therapies.[252] Application of molecular targeted treatments could more effectively prevent disease progression and bring survival benefit to the patients.[253] However, characterization of genomic landscape in HCC to identify potential targets has not been fully explored.[147] Comprehensive whole exome sequencing studies showed that around one third of HCC patients and up to 70% of iCCA patients might harbor genetic alterations potentially targetable by US Food and Drug Administration (FDA)-approved drugs.[215, 254] Therefore, identification and prospective evaluation of potentially drugable targets is a main objective of patient-specific models. PDCL, as a model of PLC, could be exploited for predicting drug sensitivity to both existing therapeutics as well as for identification of new drugable targets. Implementation of PDCL in drug screening could make a crucial link between laboratory and patients, thus, become a mandatory constituent of translational cancer research.

In this study we demonstrate the potential of the PDCL as a representative model for therapeutic target evaluation. Our comprehensive NGS analysis shows that the majority of our PDCL harbor potentially actionable mutations (Figure 23). Although many oncogenes have been identified in HCC and associated with tumor development and progression, such as *TERT*, *TP53* and *CTNNB1*,[252] suitable targeted treatments exploring this genetic diversity have not been developed yet. Although we were able to detect the presence of *TP53* and *CTNNB1* in several PDCL, absence of specific inhibitors currently prevents targeted approaches for

affected patients. In addition, we detected several well-described germline variants such as *KDR*, *KIT* and *FGFR3*. Interestingly, several studies described that these variants have an impact on either the clinical course or response to specific inhibitors in different tumor entities.[255-257] Masago *et al.* reported that *KIT* Met541Leu variant plays a role in recurrence and drug resistance of NSCLC, and points out that suppression of KIT with drugs like imatinib may be a useful therapeutic choice in patients with *KIT* variant tumors.[255] Similarly, one of our PDCL with detected *KIT* Met541Leu variant shows beneficial response to the imatinib treatment (Figure 24a) It is also known that Gly12Asp *KRAS* mutation leads to constitutive activation of this oncogene and such tumors usually harbor more adverse and invasive properties.[258] This potent oncogene is mutated in 10-19% of iCCA, therefore significant number of patients could benefit from a targeted therapy.[71] Notably, inhibition of constitutively active KRAS (Gly12Asp mutation) in one of ours CCA-PDCL by MEK inhibition demonstrates favorable treatment effect. Furthermore, as a result of detailed mutational profiling, we revealed two *MET* variations in our PDCL with apparently differential effect on the kinase activity of the receptor. In accordance with the study of Krishnaswamy *et al.*, identified *MET* Asn375Ser alteration in our HCC31 cell line might lead to suboptimal kinase activity after ligand binding,[259] while the detected *MET* Arg1022Leu in HCC68 is a potentially activating and damaging mutation. So far, the alteration was only identified in biliary tract cancers in the context of PLC, but with limited functional information and number of studies have reported functional consequences of the variant.[260] Importantly, our data provide the first evidence for the relevance of this alteration in HCC. Here, we also demonstrate benefit of specific MET inhibition in the cell line carrying *MET* Arg1022Leu mutation. HCC68 displays significantly higher sensitivity to tepotinib than *MET* Asn375Ser mutated HCC31 and non-mutated HCC9 (Figure 24b,c). Finally, selective sensitivity to specific targeted inhibition is further recapitulated in *in vivo* xenograft setting (Figure 25). Together, our observations clearly underline the potential of individual PDCL for mechanistic studies, therapeutic validation of specific genetic alterations as well as prospective drug screenings as an important tool to improve precision medicine approaches.

Similar to our PDCL, other PLC models could also have significant implications for potential translational therapeutic approaches. It is important to note that in the recent study Broutier *et al.* tested sensitivity of generated PDOs to general anti-cancer compounds. Several of the tested drugs significantly impaired expansion and viability of organoids, allowing authors to identify potential drug-candidates that might results in a benefit for the patients.[177] Moreover, this study showed that some PDOs possess several potentially actionable genetic alterations. However, authors did not perform further validation against respective inhibitors, and despite complexity of the study, potential application in targeted therapy and, consequently, in personalized medicine have not been explored. Lack of critical standardization in the experimental setting, where “cell clumps” and organoids of uncertain and diverse sizes were utilized rather than single cells, despite overall complexity as well as costs of the conditions necessary for organoid propagation, keeps this approach further away from large-scale drug screenings and limits its translational impact.[177]

Nuciforo *et al.* went one step further with development of PDO model, where they were able to create more standardized testing conditions and provide, to the certain extent, insight into intratumoral heterogeneity and its implications in PDOs.[178] In parallel with individually established PDOs, multiple organoid lines from two patients were derived (e.g. HCC5A and HCC5B; HCC12I and HCC12II) and comprehensively analyzed. As anticipated, majority of detected mutations remained stable in PDOs, reflecting mutational profile of the original tissue. However, several mutations were detected only in one of two PDOs (and corresponding tumor tissue) established from the same patient, indicating existence of genetic heterogeneity and clonal expansion within the same tumor. Moreover, investigation of sorafenib response in those PDOs showed shift in treatment sensitivity.[178] As existence of intratumoral heterogeneity has already been documented in HCC, these results imply that heterogeneity within the tumors could have important role in organoid propagation as well as significant implications in treatment response.[261]

Overall, development and optimizations of all *in vitro* models should be vigorously supported, as at the moment, there is no ideal model to cover all the spectrums of the disease, from etiological background and (intra-)tumoral heterogeneity to translational implications and drug screening. Mutual complementation of the models, together with continuous advancements in this challenging field, could bring a bright future to the translational cancer research, and more importantly, to the patients.

6. Summary

Cancer is a complex genetic disease. Despite of many models that were developed to mimic the human, all of them harbor obstacles that limit their applicability for authentic human patients and, thus, translational value. Therefore, development of new more representative models is essential. Established cell lines have been present in the cancer studies for several decades and they have made key contributions to many important discoveries in the cancer field. However, since the lines are conserved for many years in culture, the main concern is how accurately they represent the tumors that they were derived from, and consequently the patients *per se*. Patient-derived xenograft models and organoids were recently introduced as a novel model, but due to specific conditions that are required for isolation, propagation and large-scale analyses, such as drug screening, their advancements for translational applications as well as large scale screenings are questionable.

To address the issue of limited patient-specific models of primary liver cancers, we have successfully generated and comprehensively characterized seven novel PDCL from hepatocellular carcinoma and intrahepatic cholangiocarcinoma. Firstly, we were able to identify potential cellular and molecular characteristics for successful establishment of PDCL. Results of this study provide evidence that less differentiated tumors with higher genomic instability are more prone to successfully establish PDCL. Nevertheless, since there are a significant number of the patients with highly differentiated and low graded tumors, it is important to optimize isolation and cultivation conditions to promote growth of PDCL from these tumor entities.

Our results further confirmed phenotypical stability of the PDCL over an extended period in culture. Preserved cellular morphology and long-term stability of key lineage markers are additionally complemented with results of transcriptomic and genomic profiling. We performed detailed transcriptome analyses of the original tissue and compared with early and late stage of PDCL. Notably, our detailed characterization confirms that PDCL recapitulate hallmark features of the primary cancers and that the PDCL retain common as well as individual transcriptomic characteristics of the primary cancers. Importantly, expression and activation of key signaling pathways and oncogenic molecules remains stable over the long-term cultivation.

Genomic analyses additionally confirm that our cells maintain similar profile to the corresponding primary tumors, both in the early and later stages of cultivation. Integration of PDCL with authentic human PLC patients implies that both PDCL groups resemble a broad spectrum of different prognostic subclasses of PLC patients.

By utilizing next-generation sequencing approach, we are able to shows that key oncogenic alterations such as *TP53, KRAS, CTNNB1* as well as actionable alterations (e.g. *MET, KIT, KDR*) are highly conserved in the PDCL. Detailed analyses of detected alterations and drug evaluation are essential steps in translational approach, since distinct alterations within one particular gene can

cause differential response to a therapy. Respectively, we show here that two MET variants harbor different sensitivity to specific inhibition, which could potentially have clinical implications in the patients carrying the same alterations. Also, we could demonstrate that some alterations display beneficial response to the targeted treatment, while a few show no benefit or reverse effect. Overall, our study indicates importance of precise drug testing for the purpose of personalized treatment approach.

Altogether, our results for the first time provide solid evidence that PDCL can faithfully recapitulate the full spectrum of human liver cancer over extended time in culture. The PDCL represent a sophisticated model for both genomic sub-classification as well as direct exploring of precision medicine approaches for the treatment of this deadly disease.

7. References

1. Malarkey DE, Johnson K, Ryan L, Boorman G, Maronpot RR. New insights into functional aspects of liver morphology. *Toxicol Pathol* 2005;**33**: 27-34.

2. Abdel-Misih SR, Bloomston M. Liver anatomy. *Surg Clin North Am* 2010;**90**: 643-53.

3. Hall JE. *Guyton and Hall textbook of medical physiology*, 13th edition. ed. Philadelphia, PA: Elsevier, 2016. xix, 1145 pages.

4. Muriel P. *Liver pathophysiology : therapies and antioxidants*ed. Boston, MA: Elsevier, 2017. pages cm.

5. Jungermann K, Kietzmann T. Zonation of parenchymal and nonparenchymal metabolism in liver. *Annu Rev Nutr* 1996;**16**: 179-203.

6. Jungermann K, Katz N. Functional specialization of different hepatocyte populations. *Physiol Rev* 1989;**69**: 708-64.

7. Kietzmann T. Metabolic zonation of the liver: The oxygen gradient revisited. *Redox Biol* 2017;**11**: 622-30.

8. Cheng X, Kim SY, Okamoto H, Xin Y, Yancopoulos GD, Murphy AJ, Gromada J. Glucagon contributes to liver zonation. *Proc Natl Acad Sci U S A* 2018;**115**: E4111-E9.

9. Zender L, Villanueva A, Tovar V, Sia D, Chiang DY, Llovet JM. Cancer gene discovery in hepatocellular carcinoma. *J Hepatol* 2010;**52**: 921-9.

10. Duncan AW, Dorrell C, Grompe M. Stem cells and liver regeneration. *Gastroenterology* 2009;**137**: 466-81.

11. Huch M, Dolle L. The plastic cellular states of liver cells: Are EpCAM and Lgr5 fit for purpose? *Hepatology* 2016;**64**: 652-62.

12. Katoonizadeh A, Poustchi H. Adult Hepatic Progenitor Cell Niche: How it affects the Progenitor Cell Fate. *Middle East J Dig Dis* 2014;**6**: 57-64.

13. Zorn AM. Liver development *StemBook*ed. Cambridge (MA), 2008.

14. Treyer A, Musch A. Hepatocyte polarity. *Compr Physiol* 2013;**3**: 243-87.

15. Gissen P, Arias IM. Structural and functional hepatocyte polarity and liver disease. *J Hepatol* 2015;**63**: 1023-37.

16. Fries E, Gustafsson L, Peterson PA. Four secretory proteins synthesized by hepatocytes are transported from endoplasmic reticulum to Golgi complex at different rates. *EMBO J* 1984;**3**: 147-52.

17. Sevior DK, Pelkonen O, Ahokas JT. Hepatocytes: the powerhouse of biotransformation. *Int J Biochem Cell Biol* 2012;**44**: 257-61.

18. Corless JK, Middleton HM, 3rd. Normal liver function. A basis for understanding hepatic disease. *Arch Intern Med* 1983;**143**: 2291-4.

19. Teng M, Pirrie S, Ward DG, Assi LK, Hughes RG, Stocken D, Johnson PJ. Diagnostic and mechanistic implications of serum free light chains, albumin and alpha-fetoprotein in hepatocellular carcinoma. *Br J Cancer* 2014;**110**: 2277-82.

20. Liu YR, Lin BB, Zeng DW, Zhu YY, Chen J, Zheng Q, Dong J, Jiang JJ. Alpha-fetoprotein level as a biomarker of liver fibrosis status: a cross-sectional study of 619 consecutive patients with chronic hepatitis B. *BMC Gastroenterol* 2014;**14**: 145.

21. Arrieta O, Cacho B, Morales-Espinosa D, Ruelas-Villavicencio A, Flores-Estrada D, Hernandez-Pedro N. The progressive elevation of alpha fetoprotein for the diagnosis of hepatocellular carcinoma in patients with liver cirrhosis. *BMC Cancer* 2007;**7**: 28.

22. Tessari P. Protein metabolism in liver cirrhosis: from albumin to muscle myofibrils. *Curr Opin Clin Nutr Metab Care* 2003;**6**: 79-85.

23. Spinella R, Sawhney R, Jalan R. Albumin in chronic liver disease: structure, functions and therapeutic implications. *Hepatol Int* 2016;**10**: 124-32.

24. Ballmer PE, Walshe D, McNurlan MA, Watson H, Brunt PW, Garlick PJ. Albumin synthesis rates in cirrhosis: correlation with Child-Turcotte classification. *Hepatology* 1993;**18**: 292-7.

25. Takikawa Y, Suzuki K. Is AFP a new reliable marker of liver regeneration in acute hepatic failure? *J Gastroenterol* 2002;**37**: 681-2.

26. Jones H, Alpini G, Francis H. Bile acid signaling and biliary functions. *Acta Pharm Sin B* 2015;**5**: 123-8.

27. Raynaud P, Carpentier R, Antoniou A, Lemaigre FP. Biliary differentiation and bile duct morphogenesis in development and disease. *Int J Biochem Cell Biol* 2011;**43**: 245-56.

28. Yoo KS, Lim WT, Choi HS. Biology of Cholangiocytes: From Bench to Bedside. *Gut Liver* 2016;**10**: 687-98.

29. Alpini G, Glaser S, Robertson W, Rodgers RE, Phinizy JL, Lasater J, LeSage GD. Large but not small intrahepatic bile ducts are involved in secretin-regulated ductal bile secretion. *Am J Physiol* 1997;**272**: G1064-74.

30. Alpini G, Roberts S, Kuntz SM, Ueno Y, Gubba S, Podila PV, LeSage G, LaRusso NF. Morphological, molecular, and functional heterogeneity of cholangiocytes from normal rat liver. *Gastroenterology* 1996;**110**: 1636-43.

31. Tabibian JH, Masyuk AI, Masyuk TV, O'Hara SP, LaRusso NF. Physiology of cholangiocytes. *Compr Physiol* 2013;**3**: 541-65.

32. Uenishi T, Kubo S, Hirohashi K, Tanaka H, Shuto T, Yamamoto T, Nishiguchi S. Cytokeratin-19 fragments in serum (CYFRA 21-1) as a marker in primary liver cancer. *Br J Cancer* 2003;**88**: 1894-9.

33. Zhou H, Rogler LE, Teperman L, Morgan G, Rogler CE. Identification of hepatocytic and bile ductular cell lineages and candidate stem cells in bipolar ductular reactions in cirrhotic human liver. *Hepatology* 2007;**45**: 716-24.

34. Zatloukal K, Stumptner C, Fuchsbichler A, Fickert P, Lackner C, Trauner M, Denk H. The keratin cytoskeleton in liver diseases. *J Pathol* 2004;**204**: 367-76.

35. Seo W, Jeong WI. Hepatic non-parenchymal cells: Master regulators of alcoholic liver disease? *World J Gastroenterol* 2016;**22**: 1348-56.

36. Braet F, Wisse E. Structural and functional aspects of liver sinusoidal endothelial cell fenestrae: a review. *Comp Hepatol* 2002;**1**: 1.

37. Racanelli V, Rehermann B. The liver as an immunological organ. *Hepatology* 2006;**43**: S54-62.

38. Gale RP, Sparkes RS, Golde DW. Bone marrow origin of hepatic macrophages (Kupffer cells) in humans. *Science* 1978;**201**: 937-8.

39. Gao B, Jeong WI, Tian Z. Liver: An organ with predominant innate immunity. *Hepatology* 2008;**47**: 729-36.

40. Marquardt JU, Andersen JB, Thorgeirsson SS. Functional and genetic deconstruction of the cellular origin in liver cancer. *Nat Rev Cancer* 2015;**15**: 653-67.

41. Kew MC. Hepatocellular carcinoma: epidemiology and risk factors. *J Hepatocell Carcinoma* 2014;**1**: 115-25.

42. Mosadeghi S, Liu B, Bhuket T, Wong RJ. Sex-specific and race/ethnicity-specific disparities in cholangiocarcinoma incidence and prevalence in the USA: An updated analysis of the 2000-2011 Surveillance, Epidemiology and End Results registry. *Hepatol Res* 2016;**46**: 669-77.

43. Wands J. Hepatocellular carcinoma and sex. *N Engl J Med* 2007;**357**: 1974-6.

44. Wong MC, Jiang JY, Goggins WB, Liang M, Fang Y, Fung FD, Leung C, Wang HH, Wong GL, Wong VW, Chan HL. International incidence and mortality trends of liver cancer: a global profile. *Sci Rep* 2017;**7**: 45846.

45. Lozano R, Naghavi M, Foreman K, Lim S, Shibuya K, Aboyans V, Abraham J, Adair T, Aggarwal R, Ahn SY, Alvarado M, Anderson HR, et al. Global and regional mortality from 235 causes of death for 20 age groups in 1990 and 2010: a systematic analysis for the Global Burden of Disease Study 2010. *Lancet* 2012;**380**: 2095-128.

46. Ghouri YA, Mian I, Rowe JH. Review of hepatocellular carcinoma: Epidemiology, etiology, and carcinogenesis. *J Carcinog* 2017;**16**: 1.

47. DeVita VT, Lawrence TS, Rosenberg SA. *Devita, Hellman, and Rosenberg's cancer : principles & practice of oncology*, 10th edition. ed. Philadelphia: Wolters Kluwer, 2015. xlv, 2234 pages.

48. Castven D, Fischer M, Becker D, Heinrich S, Andersen JB, Strand D, Sprinzl MF, Strand S, Czauderna C, Heilmann-Heimbach S, Roessler S, Weinmann A, et al.

Adverse genomic alterations and stemness features are induced by field cancerization in the microenvironment of hepatocellular carcinomas. *Oncotarget* 2017;**8**: 48688-700.

49. Sherman M. Hepatocellular carcinoma: epidemiology, surveillance, and diagnosis. *Semin Liver Dis* 2010;**30**: 3-16.

50. Ferlay J, Soerjomataram I, Dikshit R, Eser S, Mathers C, Rebelo M, Parkin DM, Forman D, Bray F. Cancer incidence and mortality worldwide: sources, methods and major patterns in GLOBOCAN 2012. *Int J Cancer* 2015;**136**: E359-86.

51. Frenette C, Gish RG. Hepatocellular carcinoma: molecular and genomic guideline for the clinician. *Clin Liver Dis* 2011;**15**: 307-21, vii-x.

52. El-Serag HB, Marrero JA, Rudolph L, Reddy KR. Diagnosis and treatment of hepatocellular carcinoma. *Gastroenterology* 2008;**134**: 1752-63.

53. Farazi PA, DePinho RA. Hepatocellular carcinoma pathogenesis: from genes to environment. *Nat Rev Cancer* 2006;**6**: 674-87.

54. Blechacz B. Cholangiocarcinoma: Current Knowledge and New Developments. *Gut Liver* 2017;**11**: 13-26.

55. Bergquist A, von Seth E. Epidemiology of cholangiocarcinoma. *Best Pract Res Clin Gastroenterol* 2015;**29**: 221-32.

56. Rizvi S, Gores GJ. Pathogenesis, diagnosis, and management of cholangiocarcinoma. *Gastroenterology* 2013;**145**: 1215-29.

57. Prawan A, Kukongviriyapan V, Tassaneeyakul W, Pairojkul C, Bhudhisawasdi V. Association between genetic polymorphisms of CYP1A2, arylamine N-acetyltransferase 1 and 2 and susceptibility to cholangiocarcinoma. *Eur J Cancer Prev* 2005;**14**: 245-50.

58. Wadsworth CA, Dixon PH, Wong JH, Chapman MH, McKay SC, Sharif A, Spalding DR, Pereira SP, Thomas HC, Taylor-Robinson SD, Whittaker J, Williamson C, et al. Genetic factors in the pathogenesis of cholangiocarcinoma. *Dig Dis* 2011;**29**: 93-7.

59. Mabrut JY, Bozio G, Hubert C, Gigot JF. Management of congenital bile duct cysts. *Dig Surg* 2010;**27**: 12-8.

60. Lee JY, Kim JS, Moon JM, Lim SA, Chung W, Lim EH, Lee BJ, Park JJ, Bak YT. Incidence of Cholangiocarcinoma with or without Previous Resection of Liver for Hepatolithiasis. *Gut Liver* 2013;**7**: 475-9.

61. Marquardt JU, Galle PR, Teufel A. Molecular diagnosis and therapy of hepatocellular carcinoma (HCC): an emerging field for advanced technologies. *J Hepatol* 2012;**56**: 267-75.

62. Kojiro M, Roskams T. Early hepatocellular carcinoma and dysplastic nodules. *Semin Liver Dis* 2005;**25**: 133-42.

63. Kudo M. Multistep human hepatocarcinogenesis: correlation of imaging with pathology. *J Gastroenterol* 2009;**44 Suppl 19**: 112-8.

64. Feinberg AP, Ohlsson R, Henikoff S. The epigenetic progenitor origin of human cancer. *Nat Rev Genet* 2006;**7**: 21-33.

65. Calvisi DF, Ladu S, Gorden A, Farina M, Lee JS, Conner EA, Schroeder I, Factor VM, Thorgeirsson SS. Mechanistic and prognostic significance of aberrant methylation in the molecular pathogenesis of human hepatocellular carcinoma. *J Clin Invest* 2007;**117**: 2713-22.

66. Lee S, Lee HJ, Kim JH, Lee HS, Jang JJ, Kang GH. Aberrant CpG island hypermethylation along multistep hepatocarcinogenesis. *Am J Pathol* 2003;**163**: 1371-8.

67. Nault JC, Zucman-Rossi J. Genetics of hepatobiliary carcinogenesis. *Semin Liver Dis* 2011;**31**: 173-87.

68. Marquardt JU, Seo D, Andersen JB, Gillen MC, Kim MS, Conner EA, Galle PR, Factor VM, Park YN, Thorgeirsson SS. Sequential transcriptome analysis of human liver cancer indicates late stage acquisition of malignant traits. *J Hepatol* 2014;**60**: 346-53.

69. Sia D, Villanueva A. Signaling pathways in hepatocellular carcinoma. *Oncology* 2011;**81 Suppl 1**: 18-23.

70. Andersen JB. Molecular pathogenesis of intrahepatic cholangiocarcinoma. *J Hepatobiliary Pancreat Sci* 2015;**22**: 101-13.

71. Moeini A, Sia D, Bardeesy N, Mazzaferro V, Llovet JM. Molecular Pathogenesis and Targeted Therapies for Intrahepatic Cholangiocarcinoma. *Clin Cancer Res* 2016;**22**: 291-300.

72. Muller PA, Vousden KH. p53 mutations in cancer. *Nat Cell Biol* 2013;**15**: 2-8.

73. Puisieux A, Ponchel F, Ozturk M. p53 as a growth suppressor gene in HBV-related hepatocellular carcinoma cells. *Oncogene* 1993;**8**: 487-90.

74. Hussain SP, Schwank J, Staib F, Wang XW, Harris CC. TP53 mutations and hepatocellular carcinoma: insights into the etiology and pathogenesis of liver cancer. *Oncogene* 2007;**26**: 2166-76.

75. Martin J, Dufour JF. Tumor suppressor and hepatocellular carcinoma. *World J Gastroenterol* 2008;**14**: 1720-33.

76. Zou S, Li J, Zhou H, Frech C, Jiang X, Chu JS, Zhao X, Li Y, Li Q, Wang H, Hu J, Kong G, et al. Mutational landscape of intrahepatic cholangiocarcinoma. *Nat Commun* 2014;**5**: 5696.

77. Chan-On W, Nairismagi ML, Ong CK, Lim WK, Dima S, Pairojkul C, Lim KH, McPherson JR, Cutcutache I, Heng HL, Ooi L, Chung A, et al. Exome sequencing identifies distinct mutational patterns in liver fluke-related and non-infection-related bile duct cancers. *Nat Genet* 2013;**45**: 1474-8.

78. Monga SP. beta-Catenin Signaling and Roles in Liver Homeostasis, Injury, and Tumorigenesis. *Gastroenterology* 2015;**148**: 1294-310.

79. Khalaf AM, Fuentes D, Morshid AI, Burke MR, Kaseb AO, Hassan M, Hazle JD, Elsayes KM. Role of Wnt/beta-catenin signaling in hepatocellular carcinoma, pathogenesis, and clinical significance. *J Hepatocell Carcinoma* 2018;**5**: 61-73.

80. Kitao A, Matsui O, Yoneda N, Kozaka K, Kobayashi S, Sanada J, Koda W, Minami T, Inoue D, Yoshida K, Yamashita T, Yamashita T, et al. Hepatocellular Carcinoma with beta-Catenin Mutation: Imaging and Pathologic Characteristics. *Radiology* 2015;**275**: 708-17.

81. Tien LT, Ito M, Nakao M, Niino D, Serik M, Nakashima M, Wen CY, Yatsuhashi H, Ishibashi H. Expression of beta-catenin in hepatocellular carcinoma. *World J Gastroenterol* 2005;**11**: 2398-401.

82. Wang Z, Sheng YY, Gao XM, Wang CQ, Wang XY, Lu XU, Wei JW, Zhang KL, Dong QZ, Qin LX. beta-catenin mutation is correlated with a favorable prognosis in patients with hepatocellular carcinoma. *Mol Clin Oncol* 2015;**3**: 936-40.

83. Wong CM, Fan ST, Ng IO. beta-Catenin mutation and overexpression in hepatocellular carcinoma: clinicopathologic and prognostic significance. *Cancer* 2001;**92**: 136-45.

84. Krishnamurthy N, Kurzrock R. Targeting the Wnt/beta-catenin pathway in cancer: Update on effectors and inhibitors. *Cancer Treat Rev* 2018;**62**: 50-60.

85. Suarez MI, Uribe D, Jaramillo CM, Osorio G, Perez JC, Lopez R, Hoyos S, Hainaut P, Pineau P, Navas MC. Wnt/beta-catenin signaling pathway in hepatocellular carcinomas cases from Colombia. *Ann Hepatol* 2015;**14**: 64-74.

86. Boulter L, Guest RV, Kendall TJ, Wilson DH, Wojtacha D, Robson AJ, Ridgway RA, Samuel K, Van Rooijen N, Barry ST, Wigmore SJ, Sansom OJ, et al. WNT signaling drives cholangiocarcinoma growth and can be pharmacologically inhibited. *J Clin Invest* 2015;**125**: 1269-85.

87. Porta C, Paglino C, Mosca A. Targeting PI3K/Akt/mTOR Signaling in Cancer. *Front Oncol* 2014;**4**: 64.

88. Davis WJ, Lehmann PZ, Li W. Nuclear PI3K signaling in cell growth and tumorigenesis. *Front Cell Dev Biol* 2015;**3**: 24.

89. Barrett D, Brown VI, Grupp SA, Teachey DT. Targeting the PI3K/AKT/mTOR signaling axis in children with hematologic malignancies. *Paediatr Drugs* 2012;**14**: 299-316.

90. LoRusso PM. Inhibition of the PI3K/AKT/mTOR Pathway in Solid Tumors. *J Clin Oncol* 2016;**34**: 3803-15.

91. Whittaker S, Marais R, Zhu AX. The role of signaling pathways in the development and treatment of hepatocellular carcinoma. *Oncogene* 2010;**29**: 4989-5005.

92. Matter MS, Decaens T, Andersen JB, Thorgeirsson SS. Targeting the mTOR pathway in hepatocellular carcinoma: current state and future trends. *J Hepatol* 2014;**60**: 855-65.

93. Villanueva A, Chiang DY, Newell P, Peix J, Thung S, Alsinet C, Tovar V, Roayaie S, Minguez B, Sole M, Battiston C, Van Laarhoven S, et al. Pivotal role of mTOR signaling in hepatocellular carcinoma. *Gastroenterology* 2008;**135**: 1972-83, 83 e1-11.

94. Khalid A, Hussain T, Manzoor S, Saalim M, Khaliq S. PTEN: A potential prognostic marker in virus-induced hepatocellular carcinoma. *Tumour Biol* 2017;**39**: 1010428317705754.

95. Zhang Y, Li RQ, Feng XD, Zhang YH, Wang L. Down-regulation of PTEN by HCV core protein through activating nuclear factor-kappaB. *Int J Clin Exp Pathol* 2014;**7**: 7351-9.

96. Yothaisong S, Dokduang H, Techasen A, Namwat N, Yongvanit P, Bhudhisawasdi V, Puapairoj A, Riggins GJ, Loilome W. Increased activation of PI3K/AKT signaling pathway is associated with cholangiocarcinoma metastasis and PI3K/mTOR inhibition presents a possible therapeutic strategy. *Tumour Biol* 2013;**34**: 3637-48.

97. Schmitz KJ, Lang H, Wohlschlaeger J, Sotiropoulos GC, Reis H, Schmid KW, Baba HA. AKT and ERK1/2 signaling in intrahepatic cholangiocarcinoma. *World J Gastroenterol* 2007;**13**: 6470-7.

98. Xia X, Francis H, Glaser S, Alpini G, LeSage G. Bile acid interactions with cholangiocytes. *World J Gastroenterol* 2006;**12**: 3553-63.

99. Yoon JH, Higuchi H, Werneburg NW, Kaufmann SH, Gores GJ. Bile acids induce cyclooxygenase-2 expression via the epidermal growth factor receptor in a human cholangiocarcinoma cell line. *Gastroenterology* 2002;**122**: 985-93.

100. Diehl N, Schaal H. Make yourself at home: viral hijacking of the PI3K/Akt signaling pathway. *Viruses* 2013;**5**: 3192-212.

101. Yilmaz Y, Gunes A, Topel H, Atabey N. Signaling Pathways as Potential Therapeutic Targets in Hepatocarcinogenesis. *J Gastrointest Cancer* 2017.

102. Calvisi DF, Ladu S, Gorden A, Farina M, Conner EA, Lee JS, Factor VM, Thorgeirsson SS. Ubiquitous activation of Ras and Jak/Stat pathways in human HCC. *Gastroenterology* 2006;**130**: 1117-28.

103. Lamarca A, Mendiola M, Barriuso J. Hepatocellular carcinoma: Exploring the impact of ethnicity on molecular biology. *Crit Rev Oncol Hematol* 2016;**105**: 65-72.

104. Thomas SJ, Snowden JA, Zeidler MP, Danson SJ. The role of JAK/STAT signalling in the pathogenesis, prognosis and treatment of solid tumours. *Br J Cancer* 2015;**113**: 365-71.

105. Nagai H, Kim YS, Konishi N, Baba M, Kubota T, Yoshimura A, Emi M. Combined hypermethylation and chromosome loss associated with inactivation of SSI-1/SOCS-1/JAB gene in human hepatocellular carcinomas. *Cancer Lett* 2002;**186**: 59-65.

106. Wehbe H, Henson R, Meng F, Mize-Berge J, Patel T. Interleukin-6 contributes to growth in cholangiocarcinoma cells by aberrant promoter methylation and gene expression. *Cancer Res* 2006;**66**: 10517-24.

107. Kobayashi S, Werneburg NW, Bronk SF, Kaufmann SH, Gores GJ. Interleukin-6 contributes to Mcl-1 up-regulation and TRAIL resistance via an Akt-signaling pathway in cholangiocarcinoma cells. *Gastroenterology* 2005;**128**: 2054-65.

108. Delire B, Starkel P. The Ras/MAPK pathway and hepatocarcinoma: pathogenesis and therapeutic implications. *Eur J Clin Invest* 2015;**45**: 609-23.

109. Chen L, Shi Y, Jiang CY, Wei LX, Wang YL, Dai GH. Expression and prognostic role of pan-Ras, Raf-1, pMEK1 and pERK1/2 in patients with hepatocellular carcinoma. *Eur J Surg Oncol* 2011;**37**: 513-20.

110. Schmidt CM, McKillop IH, Cahill PA, Sitzmann JV. Increased MAPK expression and activity in primary human hepatocellular carcinoma. *Biochem Biophys Res Commun* 1997;**236**: 54-8.

111. Sia D, Tovar V, Moeini A, Llovet JM. Intrahepatic cholangiocarcinoma: pathogenesis and rationale for molecular therapies. *Oncogene* 2013;**32**: 4861-70.

112. Radtke F, Raj K. The role of Notch in tumorigenesis: oncogene or tumour suppressor? *Nat Rev Cancer* 2003;**3**: 756-67.

113. Geisler F, Strazzabosco M. Emerging roles of Notch signaling in liver disease. *Hepatology* 2015;**61**: 382-92.

114. Zong Y, Panikkar A, Xu J, Antoniou A, Raynaud P, Lemaigre F, Stanger BZ. Notch signaling controls liver development by regulating biliary differentiation. *Development* 2009;**136**: 1727-39.

115. Qi R, An H, Yu Y, Zhang M, Liu S, Xu H, Guo Z, Cheng T, Cao X. Notch1 signaling inhibits growth of human hepatocellular carcinoma through induction of cell cycle arrest and apoptosis. *Cancer Res* 2003;**63**: 8323-9.

116. Wang C, Qi R, Li N, Wang Z, An H, Zhang Q, Yu Y, Cao X. Notch1 signaling sensitizes tumor necrosis factor-related apoptosis-inducing ligand-induced apoptosis in human hepatocellular carcinoma cells by inhibiting Akt/Hdm2-mediated p53 degradation and up-regulating p53-dependent DR5 expression. *J Biol Chem* 2009;**284**: 16183-90.

117. Villanueva A, Alsinet C, Yanger K, Hoshida Y, Zong Y, Toffanin S, Rodriguez-Carunchio L, Sole M, Thung S, Stanger BZ, Llovet JM. Notch signaling is activated in human hepatocellular carcinoma and induces tumor formation in mice. *Gastroenterology* 2012;**143**: 1660-9 e7.

118. Giovannini C, Gramantieri L, Chieco P, Minguzzi M, Lago F, Pianetti S, Ramazzotti E, Marcu KB, Bolondi L. Selective ablation of Notch3 in HCC enhances doxorubicin's death promoting effect by a p53 dependent mechanism. *J Hepatol* 2009;**50**: 969-79.

119. Cigliano A, Wang J, Chen X, Calvisi DF. Role of the Notch signaling in cholangiocarcinoma. *Expert Opin Ther Targets* 2017;**21**: 471-83.

120. El Khatib M, Bozko P, Palagani V, Malek NP, Wilkens L, Plentz RR. Activation of Notch signaling is required for cholangiocarcinoma progression and is enhanced by inactivation of p53 in vivo. *PLoS One* 2013;**8**: e77433.

121. Zender S, Nickeleit I, Wuestefeld T, Sorensen I, Dauch D, Bozko P, El-Khatib M, Geffers R, Bektas H, Manns MP, Gossler A, Wilkens L, et al. A critical role for notch signaling in the formation of cholangiocellular carcinomas. *Cancer Cell* 2013;**23**: 784-95.

122. Wu WR, Shi XD, Zhang R, Zhu MS, Xu LB, Yu XH, Zeng H, Wang J, Liu C. Clinicopathological significance of aberrant Notch receptors in intrahepatic cholangiocarcinoma. *Int J Clin Exp Pathol* 2014;**7**: 3272-9.

123. Xue TC, Zhang BH, Ye SL, Ren ZG. Differentially expressed gene profiles of intrahepatic cholangiocarcinoma, hepatocellular carcinoma, and combined hepatocellular-cholangiocarcinoma by integrated microarray analysis. *Tumour Biol* 2015;**36**: 5891-9.

124. Wang X, Ding J, Feng Y, Weng L, Zhao G, Xiang J, Zhang M, Xing D. Targeting of growth factors in the treatment of hepatocellular carcinoma: The potentials of polysaccharides. *Oncol Lett* 2017;**13**: 1509-17.

125. Wang X, DeFrances MC, Dai Y, Pediaditakis P, Johnson C, Bell A, Michalopoulos GK, Zarnegar R. A mechanism of cell survival: sequestration of Fas by the HGF receptor Met. *Mol Cell* 2002;**9**: 411-21.

126. Bouattour M, Raymond E, Qin S, Cheng AL, Stammberger U, Locatelli G, Faivre S. Recent developments of c-Met as a therapeutic target in hepatocellular carcinoma. *Hepatology* 2018;**67**: 1132-49.

127. Zhang Y, Xia M, Jin K, Wang S, Wei H, Fan C, Wu Y, Li X, Li X, Li G, Zeng Z, Xiong W. Function of the c-Met receptor tyrosine kinase in carcinogenesis and associated therapeutic opportunities. *Mol Cancer* 2018;**17**: 45.

128. Zhan N, Michael AA, Wu K, Zeng G, Bell A, Tao J, Monga SP. The Effect of Selective c-MET Inhibitor on Hepatocellular Carcinoma in the MET-Active, beta-Catenin-Mutated Mouse Model. *Gene Expr* 2018;**18**: 135-47.

129. Terada T, Nakanuma Y, Sirica AE. Immunohistochemical demonstration of MET overexpression in human intrahepatic cholangiocarcinoma and in hepatolithiasis. *Hum Pathol* 1998;**29**: 175-80.

130. Leelawat K, Leelawat S, Tepaksorn P, Rattanasinganchan P, Leungchaweng A, Tohtong R, Sobhon P. Involvement of c-Met/hepatocyte growth factor pathway in cholangiocarcinoma cell invasion and its therapeutic inhibition with small interfering RNA specific for c-Met. *J Surg Res* 2006;**136**: 78-84.

131. Gao CF, Vande Woude GF. HGF/SF-Met signaling in tumor progression. *Cell Res* 2005;**15**: 49-51.

132. Zhang YW, Vande Woude GF. HGF/SF-met signaling in the control of branching morphogenesis and invasion. *J Cell Biochem* 2003;**88**: 408-17.

133. Leyva-Illades D, McMillin M, Quinn M, Demorrow S. Cholangiocarcinoma pathogenesis: Role of the tumor microenvironment. *Transl Gastrointest Cancer* 2012;**1**: 71-80.

134. Cao G, Li X, Qin C, Li J. Prognostic Value of VEGF in Hepatocellular Carcinoma Patients Treated with Sorafenib: A Meta-Analysis. *Med Sci Monit* 2015;**21**: 3144-51.

135. Weiss A, Attisano L. The TGFbeta superfamily signaling pathway. *Wiley Interdiscip Rev Dev Biol* 2013;**2**: 47-63.

136. Katz LH, Likhter M, Jogunoori W, Belkin M, Ohshiro K, Mishra L. TGF-beta signaling in liver and gastrointestinal cancers. *Cancer Lett* 2016;**379**: 166-72.

137. Dooley S, ten Dijke P. TGF-beta in progression of liver disease. *Cell Tissue Res* 2012;**347**: 245-56.

138. Wasylishen AR, Penn LZ. Myc: the beauty and the beast. *Genes Cancer* 2010;**1**: 532-41.

139. Zheng K, Cubero FJ, Nevzorova YA. c-MYC-Making Liver Sick: Role of c-MYC in Hepatic Cell Function, Homeostasis and Disease. *Genes (Basel)* 2017;**8**.

140. Kawate S, Fukusato T, Ohwada S, Watanuki A, Morishita Y. Amplification of c-myc in hepatocellular carcinoma: correlation with clinicopathologic features, proliferative activity and p53 overexpression. *Oncology* 1999;**57**: 157-63.

141. Kaposi-Novak P, Libbrecht L, Woo HG, Lee YH, Sears NC, Coulouarn C, Conner EA, Factor VM, Roskams T, Thorgeirsson SS. Central role of c-Myc during malignant conversion in human hepatocarcinogenesis. *Cancer Res* 2009;**69**: 2775-82.

142. Yang H, Li TW, Ko KS, Xia M, Lu SC. Switch from Mnt-Max to Myc-Max induces p53 and cyclin D1 expression and apoptosis during cholestasis in mouse and human hepatocytes. *Hepatology* 2009;**49**: 860-70.

143. Luo G, Li B, Duan C, Cheng Y, Xiao B, Yao F, Wei M, Tao Q, Feng C, Xia X, Zhou H, Zhao X, et al. cMyc promotes cholangiocarcinoma cells to overcome contact inhibition via the mTOR pathway. *Oncol Rep* 2017;**38**: 2498-506.

144. Blackburn EH. Switching and signaling at the telomere. *Cell* 2001;**106**: 661-73.

145. Pestana A, Vinagre J, Sobrinho-Simoes M, Soares P. TERT biology and function in cancer: beyond immortalisation. *J Mol Endocrinol* 2017;**58**: R129-R46.

146. Nault JC, Zucman-Rossi J. TERT promoter mutations in primary liver tumors. *Clin Res Hepatol Gastroenterol* 2016;**40**: 9-14.

147. Lee JS. The mutational landscape of hepatocellular carcinoma. *Clin Mol Hepatol* 2015;**21**: 220-9.

148. Nault JC, Mallet M, Pilati C, Calderaro J, Bioulac-Sage P, Laurent C, Laurent A, Cherqui D, Balabaud C, Zucman-Rossi J. High frequency of telomerase reverse-transcriptase promoter somatic mutations in hepatocellular carcinoma and preneoplastic lesions. *Nat Commun* 2013;**4**: 2218.

149. Handy DE, Castro R, Loscalzo J. Epigenetic modifications: basic mechanisms and role in cardiovascular disease. *Circulation* 2011;**123**: 2145-56.

150. Dawson MA, Kouzarides T. Cancer epigenetics: from mechanism to therapy. *Cell* 2012;**150**: 12-27.

151. Wahid B, Ali A, Rafique S, Idrees M. New Insights into the Epigenetics of Hepatocellular Carcinoma. *Biomed Res Int* 2017;**2017**: 1609575.

152. Sengupta S, Parikh ND. Biomarker development for hepatocellular carcinoma early detection: current and future perspectives. *Hepat Oncol* 2017;**4**: 111-22.

153. Pinyol R, Nault JC, Quetglas IM, Zucman-Rossi J, Llovet JM. Molecular profiling of liver tumors: classification and clinical translation for decision making. *Semin Liver Dis* 2014;**34**: 363-75.

154. Ikeda M, Mitsunaga S, Ohno I, Hashimoto Y, Takahashi H, Watanabe K, Umemoto K, Okusaka T. Systemic Chemotherapy for Advanced Hepatocellular Carcinoma: Past, Present, and Future. *Diseases* 2015;**3**: 360-81.

155. Keating GM. Sorafenib: A Review in Hepatocellular Carcinoma. *Target Oncol* 2017;**12**: 243-53.

156. Aggarwal M, Arain A, Jin Z. Systemic treatment for hepatocellular carcinoma. *Chronic Dis Transl Med* 2018;**4**: 148-55.

157. Scott LJ. Lenvatinib: first global approval. *Drugs* 2015;**75**: 553-60.

158. Kudo M, Finn RS, Qin S, Han KH, Ikeda K, Piscaglia F, Baron A, Park JW, Han G, Jassem J, Blanc JF, Vogel A, et al. Lenvatinib versus sorafenib in first-line treatment of patients with unresectable hepatocellular carcinoma: a randomised phase 3 non-inferiority trial. *Lancet* 2018;**391**: 1163-73.

159. Killock D. Neuroendocrine cancer: SELECT-lenvatinib in thyroid cancer. *Nat Rev Clin Oncol* 2015;**12**: 189.

160. Bruix J, Qin S, Merle P, Granito A, Huang YH, Bodoky G, Pracht M, Yokosuka O, Rosmorduc O, Breder V, Gerolami R, Masi G, et al. Regorafenib for patients with hepatocellular carcinoma who progressed on sorafenib treatment (RESORCE): a randomised, double-blind, placebo-controlled, phase 3 trial. *Lancet* 2017;**389**: 56-66.

161. Heo YA, Syed YY. Regorafenib: A Review in Hepatocellular Carcinoma. *Drugs* 2018.

162. Kudo M. Immune Checkpoint Inhibition in Hepatocellular Carcinoma: Basics and Ongoing Clinical Trials. *Oncology* 2017;**92 Suppl 1**: 50-62.

163. El-Khoueiry AB, Sangro B, Yau T, Crocenzi TS, Kudo M, Hsu C, Kim TY, Choo SP, Trojan J, Welling THR, Meyer T, Kang YK, et al. Nivolumab in patients with advanced hepatocellular carcinoma (CheckMate 040): an open-label, non-comparative, phase 1/2 dose escalation and expansion trial. *Lancet* 2017;**389**: 2492-502.

164. de Sousa Cavalcante L, Monteiro G. Gemcitabine: metabolism and molecular mechanisms of action, sensitivity and chemoresistance in pancreatic cancer. *Eur J Pharmacol* 2014;**741**: 8-16.

165. Dasari S, Tchounwou PB. Cisplatin in cancer therapy: molecular mechanisms of action. *Eur J Pharmacol* 2014;**740**: 364-78.

166. Bupathi M, Ahn DH, Bekaii-Saab T. Therapeutic options for intrahepatic cholangiocarcinoma. *Hepatobiliary Surg Nutr* 2017;**6**: 91-100.

167. Santos NP, Colaco AA, Oliveira PA. Animal models as a tool in hepatocellular carcinoma research: A Review. *Tumour Biol* 2017;**39**: 1010428317695923.

168. Cekanova M, Rathore K. Animal models and therapeutic molecular targets of cancer: utility and limitations. *Drug Des Devel Ther* 2014;**8**: 1911-21.

169. He L, Tian DA, Li PY, He XX. Mouse models of liver cancer: Progress and recommendations. *Oncotarget* 2015;**6**: 23306-22.

170. Aravalli RN, Golzarian J, Cressman EN. Animal models of cancer in interventional radiology. *Eur Radiol* 2009;**19**: 1049-53.

171. Kim MP, Evans DB, Wang H, Abbruzzese JL, Fleming JB, Gallick GE. Generation of orthotopic and heterotopic human pancreatic cancer xenografts in immunodeficient mice. *Nat Protoc* 2009;**4**: 1670-80.

172. Reiberger T, Chen Y, Ramjiawan RR, Hato T, Fan C, Samuel R, Roberge S, Huang P, Lauwers GY, Zhu AX, Bardeesy N, Jain RK, et al. An orthotopic mouse model of hepatocellular carcinoma with underlying liver cirrhosis. *Nat Protoc* 2015;**10**: 1264-74.

173. Yu J, Qin B, Moyer AM, Sinnwell JP, Thompson KJ, Copland JA, 3rd, Marlow LA, Miller JL, Yin P, Gao B, Minter-Dykhouse K, Tang X, et al. Establishing and characterizing patient-derived xenografts using pre-chemotherapy percutaneous biopsy and post-chemotherapy surgical samples from a prospective neoadjuvant breast cancer study. *Breast Cancer Res* 2017;**19**: 130.

174. Izumchenko E, Paz K, Ciznadija D, Sloma I, Katz A, Vasquez-Dunddel D, Ben-Zvi I, Stebbing J, McGuire W, Harris W, Maki R, Gaya A, et al. Patient-derived xenografts effectively capture responses to oncology therapy in a heterogeneous cohort of patients with solid tumors. *Ann Oncol* 2017;**28**: 2595-605.

175. Pompili L, Porru M, Caruso C, Biroccio A, Leonetti C. Patient-derived xenografts: a relevant preclinical model for drug development. *J Exp Clin Cancer Res* 2016;**35**: 189.

176. Siolas D, Hannon GJ. Patient-derived tumor xenografts: transforming clinical samples into mouse models. *Cancer Res* 2013;**73**: 5315-9.

177. Broutier L, Mastrogiovanni G, Verstegen MM, Francies HE, Gavarro LM, Bradshaw CR, Allen GE, Arnes-Benito R, Sidorova O, Gaspersz MP, Georgakopoulos N, Koo BK, et al. Human primary liver cancer-derived organoid cultures for disease modeling and drug screening. *Nat Med* 2017;**23**: 1424-35.

178. Nuciforo S, Fofana I, Matter MS, Blumer T, Calabrese D, Boldanova T, Piscuoglio S, Wieland S, Ringnalda F, Schwank G, Terracciano LM, Ng CKY, et al. Organoid Models of Human Liver Cancers Derived from Tumor Needle Biopsies. *Cell Rep* 2018;**24**: 1363-76.

179. Gao D, Vela I, Sboner A, Iaquinta PJ, Karthaus WR, Gopalan A, Dowling C, Wanjala JN, Undvall EA, Arora VK, Wongvipat J, Kossai M, et al. Organoid cultures derived from patients with advanced prostate cancer. *Cell* 2014;**159**: 176-87.

180. Boj SF, Hwang CI, Baker LA, Chio, II, Engle DD, Corbo V, Jager M, Ponz-Sarvise M, Tiriac H, Spector MS, Gracanin A, Oni T, et al. Organoid models of human and mouse ductal pancreatic cancer. *Cell* 2015;**160**: 324-38.

181. van de Wetering M, Francies HE, Francis JM, Bounova G, Iorio F, Pronk A, van Houdt W, van Gorp J, Taylor-Weiner A, Kester L, McLaren-Douglas A, Blokker J, et al. Prospective derivation of a living organoid biobank of colorectal cancer patients. *Cell* 2015;**161**: 933-45.

182. Shihab HA, Gough J, Cooper DN, Stenson PD, Barker GL, Edwards KJ, Day IN, Gaunt TR. Predicting the functional, molecular, and phenotypic consequences of amino acid substitutions using hidden Markov models. *Hum Mutat* 2013;**34**: 57-65.

183. Lee SH, Hu W, Matulay JT, Silva MV, Owczarek TB, Kim K, Chua CW, Barlow LJ, Kandoth C, Williams AB, Bergren SK, Pietzak EJ, et al. Tumor Evolution and Drug Response in Patient-Derived Organoid Models of Bladder Cancer. *Cell* 2018;**173**: 515-28 e17.

184. Baker LA, Tiriac H, Clevers H, Tuveson DA. Modeling pancreatic cancer with organoids. *Trends Cancer* 2016;**2**: 176-90.

185. Drost J, Clevers H. Organoids in cancer research. *Nat Rev Cancer* 2018;**18**: 407-18.

186. Goodspeed A, Heiser LM, Gray JW, Costello JC. Tumor-Derived Cell Lines as Molecular Models of Cancer Pharmacogenomics. *Mol Cancer Res* 2016;**14**: 3-13.

187. Barretina J, Caponigro G, Stransky N, Venkatesan K, Margolin AA, Kim S, Wilson CJ, Lehar J, Kryukov GV, Sonkin D, Reddy A, Liu M, et al. The Cancer Cell Line Encyclopedia enables predictive modelling of anticancer drug sensitivity. *Nature* 2012;**483**: 603-7.

188. Wistuba, II, Bryant D, Behrens C, Milchgrub S, Virmani AK, Ashfaq R, Minna JD, Gazdar AF. Comparison of features of human lung cancer cell lines and their corresponding tumors. *Clin Cancer Res* 1999;**5**: 991-1000.

189. Sharma SV, Haber DA, Settleman J. Cell line-based platforms to evaluate the therapeutic efficacy of candidate anticancer agents. *Nat Rev Cancer* 2010;**10**: 241-53.

190. Gillet JP, Varma S, Gottesman MM. The clinical relevance of cancer cell lines. *J Natl Cancer Inst* 2013;**105**: 452-8.

191. Gazdar AF, Minna JD. NCI series of cell lines: an historical perspective. *J Cell Biochem Suppl* 1996;**24**: 1-11.

192. Ashley N, Jones M, Ouaret D, Wilding J, Bodmer WF. Rapidly derived colorectal cancer cultures recapitulate parental cancer characteristics and enable personalized therapeutic assays. *J Pathol* 2014;**234**: 34-45.

193. Hartmann C, Kluwe L, Lucke M, Westphal M. The rate of homozygous CDKN2A/p16 deletions in glioma cell lines and in primary tumors. *Int J Oncol* 1999;**15**: 975-82.

194. Gao Q, Wang ZC, Duan M, Lin YH, Zhou XY, Worthley DL, Wang XY, Niu G, Xia Y, Deng M, Liu LZ, Shi JY, et al. Cell Culture System for Analysis of Genetic Heterogeneity Within Hepatocellular Carcinomas and Response to Pharmacologic Agents. *Gastroenterology* 2017;**152**: 232-42 e4.

195. Crystal AS, Shaw AT, Sequist LV, Friboulet L, Niederst MJ, Lockerman EL, Frias RL, Gainor JF, Amzallag A, Greninger P, Lee D, Kalsy A, et al. Patient-derived models

of acquired resistance can identify effective drug combinations for cancer. *Science* 2014;**346**: 1480-6.

196. Lee JS, Chu IS, Heo J, Calvisi DF, Sun Z, Roskams T, Durnez A, Demetris AJ, Thorgeirsson SS. Classification and prediction of survival in hepatocellular carcinoma by gene expression profiling. *Hepatology* 2004;**40**: 667-76.

197. Andersen JB, Spee B, Blechacz BR, Avital I, Komuta M, Barbour A, Conner EA, Gillen MC, Roskams T, Roberts LR, Factor VM, Thorgeirsson SS. Genomic and genetic characterization of cholangiocarcinoma identifies therapeutic targets for tyrosine kinase inhibitors. *Gastroenterology* 2012;**142**: 1021-31 e15.

198. Kotepui M, Thawornkuno C, Chavalitshewinkoon-Petmitr P, Punyarit P, Petmitr S. Quantitative real-time RT-PCR of ITGA7, SVEP1, TNS1, LPHN3, SEMA3G, KLB and MMP13 mRNA expression in breast cancer. *Asian Pac J Cancer Prev* 2012;**13**: 5879-82.

199. Watanabe J, Saito H, Miyatani K, Ikeguchi M, Umekita Y. TSLP Expression and High Serum TSLP Level Indicate a Poor Prognosis in Gastric Cancer Patients. *Yonago Acta Med* 2015;**58**: 137-43.

200. Liu C, Wang C, Wang J, Huang H. miR-1297 promotes cell proliferation by inhibiting RB1 in liver cancer. *Oncol Lett* 2016;**12**: 5177-82.

201. Ohashi T, Komatsu S, Ichikawa D, Miyamae M, Okajima W, Imamura T, Kiuchi J, Kosuga T, Konishi H, Shiozaki A, Fujiwara H, Okamoto K, et al. Overexpression of PBK/TOPK relates to tumour malignant potential and poor outcome of gastric carcinoma. *Br J Cancer* 2017;**116**: 218-26.

202. Song H, Ramus SJ, Tyrer J, Bolton KL, Gentry-Maharaj A, Wozniak E, Anton-Culver H, Chang-Claude J, Cramer DW, DiCioccio R, Dork T, Goode EL, et al. A genome-wide association study identifies a new ovarian cancer susceptibility locus on 9p22.2. *Nat Genet* 2009;**41**: 996-1000.

203. Likhitrattanapisal S, Tipanee J, Janvilisri T. Meta-analysis of gene expression profiles identifies differential biomarkers for hepatocellular carcinoma and cholangiocarcinoma. *Tumour Biol* 2016;**37**: 12755-66.

204. Woo HG, Lee JH, Yoon JH, Kim CY, Lee HS, Jang JJ, Yi NJ, Suh KS, Lee KU, Park ES, Thorgeirsson SS, Kim YJ. Identification of a cholangiocarcinoma-like gene expression trait in hepatocellular carcinoma. *Cancer Res* 2010;**70**: 3034-41.

205. Seok JY, Na DC, Woo HG, Roncalli M, Kwon SM, Yoo JE, Ahn EY, Kim GI, Choi JS, Kim YB, Park YN. A fibrous stromal component in hepatocellular carcinoma reveals a cholangiocarcinoma-like gene expression trait and epithelial-mesenchymal transition. *Hepatology* 2012;**55**: 1776-86.

206. Villanueva A, Newell P, Chiang DY, Friedman SL, Llovet JM. Genomics and signaling pathways in hepatocellular carcinoma. *Semin Liver Dis* 2007;**27**: 55-76.

207. Andersen JB, Thorgeirsson SS. Genetic profiling of intrahepatic cholangiocarcinoma. *Curr Opin Gastroenterol* 2012;**28**: 266-72.

208. Pellegrino R, Calvisi DF, Ladu S, Ehemann V, Staniscia T, Evert M, Dombrowski F, Schirmacher P, Longerich T. Oncogenic and tumor suppressive roles of polo-like kinases in human hepatocellular carcinoma. *Hepatology* 2010;**51**: 857-68.

209. Wu SY, Lan SH, Wu SR, Chiu YC, Lin XZ, Su IJ, Tsai TF, Yen CJ, Lu TH, Liang FW, Li CY, Su HJ, et al. Hepatocellular carcinoma-related cyclin D1 is selectively regulated by autophagy degradation system. *Hepatology* 2018;**68**: 141-54.

210. Humphreys EH, Williams KT, Adams DH, Afford SC. Primary and malignant cholangiocytes undergo CD40 mediated Fas dependent apoptosis, but are insensitive to direct activation with exogenous Fas ligand. *PLoS One* 2010;**5**: e14037.

211. Cardinale V, Semeraro R, Torrice A, Gatto M, Napoli C, Bragazzi MC, Gentile R, Alvaro D. Intra-hepatic and extra-hepatic cholangiocarcinoma: New insight into epidemiology and risk factors. *World J Gastrointest Oncol* 2010;**2**: 407-16.

212. Simoes AE, Rodrigues CM, Borralho PM. The MEK5/ERK5 signalling pathway in cancer: a promising novel therapeutic target. *Drug Discov Today* 2016;**21**: 1654-63.

213. Jiang W, Huang H, Ding L, Zhu P, Saiyin H, Ji G, Zuo J, Han D, Pan Y, Ding D, Ma X, Zhang Y, et al. Regulation of cell cycle of hepatocellular carcinoma by NF90 through modulation of cyclin E1 mRNA stability. *Oncogene* 2015;**34**: 4460-70.

214. Roessler S, Long EL, Budhu A, Chen Y, Zhao X, Ji J, Walker R, Jia HL, Ye QH, Qin LX, Tang ZY, He P, et al. Integrative genomic identification of genes on 8p associated with hepatocellular carcinoma progression and patient survival. *Gastroenterology* 2012;**142**: 957-66 e12.

215. Schulze K, Imbeaud S, Letouze E, Alexandrov LB, Calderaro J, Rebouissou S, Couchy G, Meiller C, Shinde J, Soysouvanh F, Calatayud AL, Pinyol R, et al. Exome sequencing of hepatocellular carcinomas identifies new mutational signatures and potential therapeutic targets. *Nat Genet* 2015;**47**: 505-11.

216. Lin DC, Mayakonda A, Dinh HQ, Huang P, Lin L, Liu X, Ding LW, Wang J, Berman BP, Song EW, Yin D, Koeffler HP. Genomic and Epigenomic Heterogeneity of Hepatocellular Carcinoma. *Cancer Res* 2017;**77**: 2255-65.

217. O'Dell MR, Huang JL, Whitney-Miller CL, Deshpande V, Rothberg P, Grose V, Rossi RM, Zhu AX, Land H, Bardeesy N, Hezel AF. Kras(G12D) and p53 mutation cause primary intrahepatic cholangiocarcinoma. *Cancer Res* 2012;**72**: 1557-67.

218. Hanahan D, Weinberg RA. Hallmarks of cancer: the next generation. *Cell* 2011;**144**: 646-74.

219. Shapiro LJ. Human genome project. *West J Med* 1993;**158**: 181.

220. Marquardt JU, Andersen JB. Next-generation sequencing: application in liver cancer-past, present and future? *Biology (Basel)* 2012;**1**: 383-94.

221. Wong D, Yip S. Machine learning classifies cancer. *Nature* 2018;**555**: 446-7.

222. Tentler JJ, Tan AC, Weekes CD, Jimeno A, Leong S, Pitts TM, Arcaroli JJ, Messersmith WA, Eckhardt SG. Patient-derived tumour xenografts as models for oncology drug development. *Nat Rev Clin Oncol* 2012;**9**: 338-50.

223. Clevers H. Modeling Development and Disease with Organoids. *Cell* 2016;**165**: 1586-97.

224. Gu Q, Zhang B, Sun H, Xu Q, Tan Y, Wang G, Luo Q, Xu W, Yang S, Li J, Fu J, Chen L, et al. Genomic characterization of a large panel of patient-derived hepatocellular carcinoma xenograft tumor models for preclinical development. *Oncotarget* 2015;**6**: 20160-76.

225. Nicolle D, Fabre M, Simon-Coma M, Gorse A, Kappler R, Nonell L, Mallo M, Haidar H, Deas O, Mussini C, Guettier C, Redon MJ, et al. Patient-derived mouse xenografts from pediatric liver cancer predict tumor recurrence and advise clinical management. *Hepatology* 2016;**64**: 1121-35.

226. Munoz-Garrido P, Andersen JB. Genetic Optimization of Liver Cancer Therapy: A Patient-Derived Primary Cancer Cell-Based Model. *Gastroenterology* 2017;**152**: 19-21.

227. Kodack DP, Farago AF, Dastur A, Held MA, Dardaei L, Friboulet L, von Flotow F, Damon LJ, Lee D, Parks M, Dicecca R, Greenberg M, et al. Primary Patient-Derived Cancer Cells and Their Potential for Personalized Cancer Patient Care. *Cell Rep* 2017;**21**: 3298-309.

228. Proungvitaya S, Klinthong W, Proungvitaya T, Limpaiboon T, Jearanaikoon P, Roytrakul S, Wongkham C, Nimboriboonporn A, Wongkham S. High expression of CCDC25 in cholangiocarcinoma tissue samples. *Oncol Lett* 2017;**14**: 2566-72.

229. Callegari E, Gramantieri L, Domenicali M, D'Abundo L, Sabbioni S, Negrini M. MicroRNAs in liver cancer: a model for investigating pathogenesis and novel therapeutic approaches. *Cell Death Differ* 2015;**22**: 46-57.

230. Qiu Z, Zou K, Zhuang L, Qin J, Li H, Li C, Zhang Z, Chen X, Cen J, Meng Z, Zhang H, Li Y, et al. Hepatocellular carcinoma cell lines retain the genomic and transcriptomic landscapes of primary human cancers. *Sci Rep* 2016;**6**: 27411.

231. Cheung PF, Yip CW, Ng LW, Lo KW, Wong N, Choy KW, Chow C, Chan KF, Cheung TT, Poon RT, Fan ST, Cheung ST. Establishment and characterization of a novel primary hepatocellular carcinoma cell line with metastatic ability in vivo. *Cancer Cell Int* 2014;**14**: 103.

232. Chen XP, Qiu FZ, Wu ZD, Zhang ZW, Huang ZY, Chen YF. Long-term outcome of resection of large hepatocellular carcinoma. *Br J Surg* 2006;**93**: 600-6.

233. Ruys AT, van Haelst S, Busch OR, Rauws EA, Gouma DJ, van Gulik TM. Long-term survival in hilar cholangiocarcinoma also possible in unresectable patients. *World J Surg* 2012;**36**: 2179-86.

234. Ribero D, Pinna AD, Guglielmi A, Ponti A, Nuzzo G, Giulini SM, Aldrighetti L, Calise F, Gerunda GE, Tomatis M, Amisano M, Berloco P, et al. Surgical Approach for Long-term Survival of Patients With Intrahepatic Cholangiocarcinoma: A Multi-institutional Analysis of 434 Patients. *Arch Surg* 2012;**147**: 1107-13.

235. Maetzel D, Denzel S, Mack B, Canis M, Went P, Benk M, Kieu C, Papior P, Baeuerle PA, Munz M, Gires O. Nuclear signalling by tumour-associated antigen EpCAM. *Nat Cell Biol* 2009;**11**: 162-71.

236. Spizzo G, Fong D, Wurm M, Ensinger C, Obrist P, Hofer C, Mazzoleni G, Gastl G, Went P. EpCAM expression in primary tumour tissues and metastases: an immunohistochemical analysis. *J Clin Pathol* 2011;**64**: 415-20.

237. Sulpice L, Rayar M, Turlin B, Boucher E, Bellaud P, Desille M, Meunier B, Clement B, Boudjema K, Coulouarn C. Epithelial cell adhesion molecule is a prognosis marker for intrahepatic cholangiocarcinoma. *J Surg Res* 2014;**192**: 117-23.

238. Blechacz B, Gores GJ. Tumor-specific marker genes for intrahepatic cholangiocarcinoma: utility and mechanistic insight. *J Hepatol* 2008;**49**: 160-2.

239. Lo RC, Leung CO, Chok KS, Ng IO. Variation of stemness markers expression in tumor nodules from synchronous multi-focal hepatocellular carcinoma - an immunohistochemical study. *Diagn Pathol* 2017;**12**: 56.

240. Zhao YJ, Ju Q, Li GC. Tumor markers for hepatocellular carcinoma. *Mol Clin Oncol* 2013;**1**: 593-8.

241. Cancer Genome Atlas Research Network. Electronic address wbe, Cancer Genome Atlas Research N. Comprehensive and Integrative Genomic Characterization of Hepatocellular Carcinoma. *Cell* 2017;**169**: 1327-41 e23.

242. Wang F, Wang R, Li Q, Qu X, Hao Y, Yang J, Zhao H, Wang Q, Li G, Zhang F, Zhang H, Zhou X, et al. A transcriptome profile in hepatocellular carcinomas based on integrated analysis of microarray studies. *Diagn Pathol* 2017;**12**: 4.

243. Dai R, Chen R, Li H. Cross-talk between PI3K/Akt and MEK/ERK pathways mediates endoplasmic reticulum stress-induced cell cycle progression and cell death in human hepatocellular carcinoma cells. *Int J Oncol* 2009;**34**: 1749-57.

244. Zhou X, Zheng R, Zhang H, He T. Pathway crosstalk analysis of microarray gene expression profile in human hepatocellular carcinoma. *Pathol Oncol Res* 2015;**21**: 563-9.

245. Waddell N, Pajic M, Patch AM, Chang DK, Kassahn KS, Bailey P, Johns AL, Miller D, Nones K, Quek K, Quinn MC, Robertson AJ, et al. Whole genomes redefine the mutational landscape of pancreatic cancer. *Nature* 2015;**518**: 495-501.

246. Nakamura H, Arai Y, Totoki Y, Shirota T, Elzawahry A, Kato M, Hama N, Hosoda F, Urushidate T, Ohashi S, Hiraoka N, Ojima H, et al. Genomic spectra of biliary tract cancer. *Nat Genet* 2015;**47**: 1003-10.

247. Sia D, Villanueva A, Friedman SL, Llovet JM. Liver Cancer Cell of Origin, Molecular Class, and Effects on Patient Prognosis. *Gastroenterology* 2017;**152**: 745-61.

248. Ben-David U, Ha G, Tseng YY, Greenwald NF, Oh C, Shih J, McFarland JM, Wong B, Boehm JS, Beroukhim R, Golub TR. Patient-derived xenografts undergo mouse-specific tumor evolution. *Nat Genet* 2017;**49**: 1567-75.

249. Yokoyama M, Ohnishi H, Ohtsuka K, Matsushima S, Ohkura Y, Furuse J, Watanabe T, Mori T, Sugiyama M. KRAS Mutation as a Potential Prognostic Biomarker of Biliary Tract Cancers. *Jpn Clin Med* 2016;**7**: 33-9.

250. Churi CR, Shroff R, Wang Y, Rashid A, Kang HC, Weatherly J, Zuo M, Zinner R, Hong D, Meric-Bernstam F, Janku F, Crane CH, et al. Mutation profiling in cholangiocarcinoma: prognostic and therapeutic implications. *PLoS One* 2014;**9**: e115383.

251. Mitra A, Mishra L, Li S. Technologies for deriving primary tumor cells for use in personalized cancer therapy. *Trends Biotechnol* 2013;**31**: 347-54.

252. Ding XX, Zhu QG, Zhang SM, Guan L, Li T, Zhang L, Wang SY, Ren WL, Chen XM, Zhao J, Lin S, Liu ZZ, et al. Precision medicine for hepatocellular carcinoma: driver mutations and targeted therapy. *Oncotarget* 2017;**8**: 55715-30.

253. Geng F, Wang Z, Yin H, Yu J, Cao B. Molecular Targeted Drugs and Treatment of Colorectal Cancer: Recent Progress and Future Perspectives. *Cancer Biother Radiopharm* 2017;**32**: 149-60.

254. Sia D, Hoshida Y, Villanueva A, Roayaie S, Ferrer J, Tabak B, Peix J, Sole M, Tovar V, Alsinet C, Cornella H, Klotzle B, et al. Integrative molecular analysis of intrahepatic cholangiocarcinoma reveals 2 classes that have different outcomes. *Gastroenterology* 2013;**144**: 829-40.

255. Masago K, Fujita S, Muraki M, Hata A, Okuda C, Otsuka K, Kaji R, Takeshita J, Kato R, Katakami N, Hirata Y. Next-generation sequencing of tyrosine kinase inhibitor-resistant non-small-cell lung cancers in patients harboring epidermal growth factor-activating mutations. *BMC Cancer* 2015;**15**: 908.

256. Silva IP, Salhi A, Giles KM, Vogelsang M, Han SW, Ismaili N, Lui KP, Robinson EM, Wilson MA, Shapiro RL, Pavlick A, Zhong J, et al. Identification of a Novel Pathogenic Germline KDR Variant in Melanoma. *Clin Cancer Res* 2016;**22**: 2377-85.

257. de Martino M, Gigante M, Cormio L, Prattichizzo C, Cavalcanti E, Gigante M, Ariano V, Netti GS, Montemurno E, Mancini V, Battaglia M, Gesualdo L, et al. JAK3 in clear cell renal cell carcinoma: mutational screening and clinical implications. *Urol Oncol* 2013;**31**: 930-7.

258. O'Hagan RC, Heyer J. KRAS Mouse Models: Modeling Cancer Harboring KRAS Mutations. *Genes Cancer* 2011;**2**: 335-43.

259. Krishnaswamy S, Kanteti R, Duke-Cohan JS, Loganathan S, Liu W, Ma PC, Sattler M, Singleton PA, Ramnath N, Innocenti F, Nicolae DL, Ouyang Z, et al. Ethnic differences and functional analysis of MET mutations in lung cancer. *Clin Cancer Res* 2009;**15**: 5714-23.

260. Wardell CP, Fujita M, Yamada T, Simbolo M, Fassan M, Karlic R, Polak P, Kim J, Hatanaka Y, Maejima K, Lawlor RT, Nakanishi Y, et al. Genomic characterization of biliary tract cancers identifies driver genes and predisposing mutations. *J Hepatol* 2018;**68**: 959-69.

261. Xue R, Li R, Guo H, Guo L, Su Z, Ni X, Qi L, Zhang T, Li Q, Zhang Z, Xie XS, Bai F, et al. Variable Intra-Tumor Genomic Heterogeneity of Multiple Lesions in Patients With Hepatocellular Carcinoma. *Gastroenterology* 2016;**150**: 998-1008.

8. Appendix

Supplementary Table 1 List of authentic HCC patients used for genomic analyses.
Cohort of 48 authentic human HCC that were on used in the genomic studies of PDCL are listed in the table below. Given are clinicopathological information of HCC tumors.

HCC patients	Gender	Size (cm)	TNM	Grading	Differentiation	Etiology
HCC2	F	8	pT2, pNx, M0, R0	G3	Poor	NASH
HCC3	M	11	pT3b, pNx, M1, R2	G3	Poor	NASH
HCC4	F	3	pT1, pNx, M0, R0	G2	Moderate	N/A
HCC5	M	9	pT2, pnX, M0, R0	G3	Poor	N/A
HCC8	M	9	pT2, pNx, M0, Rx	G2	Moderate	HBV
HCC9	F	13	pT2, pNx, M0, R0	G2-G3	Moderate to poor	NASH
HCC10	M	4,5	pT1, pNx, M0, R0	G2	Moderate	NASH
HCC11	M	9	pT1, pNx, M0; R0	G1-G2	Moderate	NASH
HCC17	M	14	pT1, pN0, M0, R0	G1	Well	NASH
HCC20	M	1,2	ypT1, pNX, M0, R0	N/A	N/A	HCV
HCC21	M	2,8	ypT1, pNX, M0, R0	G2	Moderate	HCV
HCC23	F	3	pT2, pNx, M0, R0	G2	Moderate	HCV
HCC24	F	14	pT3b, pNx, M0, R1	G2	Moderate	HCV
HCC26	M	3,5	pT3a, pN0, M0, R0	G2	Moderate	NASH
HCC27	M	5	pT1, pNx, M0, R0	G2	Moderate	EtOH
HCC31	M	2,6	pT2, pN0, M0,R0	G1	Well	EtOH
HCC32	M	6	pT2, pNx, M0, R0	G2	Moderate	Cirrhosis
HCC33	M	6,3	pT3, pNx, M0, R0	G2	Moderate	NASH
HCC34	M	7	pT4, pNX, M0, R0	G2	Moderate	HCV
HCC36	M	3,6	pT1, pNx, M0, R0	G2	Moderate	Cirrhosis
HCC37	M	11,5	pT1, pNX, M0, R0	G1-G2	Well to moderate	N/A
HCC38	M	4,5	pT1, pNx, M0, R0	G1	Well	HCV
HCC39	F	5,8	pT1, pNx, M0, R0	G1-G2	Well to moderate	N/A
HCC41	M	12,3	pT2, pN0, R0	G1	Well	HBV
HCC45	M	1,5	rpT2, rpNx, M0, R0	G2	Moderate	Cirrhosis
HCC46	M	9	pT3b, pN1, M0, R0	G3	Poor	N/A
HCC48	M	4,7	pT1, Nx, Mx, R0	G2	Moderate	N/A
HCC49	M	16	pT3b, pN0, MX, R1	G2-G3	Moderate to poor	HCV
HCC52	M	7	pT1, pN0, M0, R0	G3	Poor	N/A
HCC55	M	5,5	pT1, Nx, M0, R0	G2-G3	Moderate to poor	EtOH
HCC56	M	7	pT1, pNx, M0, R0	G1-G2	Well to moderate	HBV
HCC57	M	10	pT1, pN0, M0, R0	G1-G2	Moderate	N/A
HCC59	M	6,6	pT1, pN0, M0, R0	G2	Moderate	N/A
HCC60	M	3,5	pT3b, pN0, M0, R0	G1-G2	Well to moderate	EtOH
HCC61	M	9	pT1, pN0, Mx, R0	G2-G3	Moderate to poor	No cirrhosis
HCC62	F	3,5	pT3, pN0, R0	G1-G2	Well to moderate	N/A
HCC63	M	14,5	pT3a, pN0, M0, R0	G2	Moderate	N/A
HCC64	M	8,5	pT3b, pN0, M0, R1	G3	Poor	N/A
HCC65	M	1,8	pT1, Nx, M0; R0	G2	Moderate	Cirrhosis
HCC69	F	13,5	pT2, pN0, M0, R0	G3	Poor	N/A
HCC70	F	14	pT1, pNx, M0, R0	G2	Moderate	Cirrhosis
HCC71	M	N/A	N/A	G2-G3	Moderate to poor	N/A
HCC72	M	10	pT3a, pN0, M0, R0	G3	Poor	HCV
HCC73	M	5,8	pT3a, pNx, M0, R0	G3	Poor	N/A
HCC74	M	3,2	pT2a, pNx, M0, R0	G2	Moderate	Cirrhosis
HCC76	M	7	pT2, pNx, M0, R0	G2-G3	Moderate to poor	EtOH
HCC77	M	9	pT3a, PNx, M0, R1	G3	Poor	N/A
HCC80	M	9	N/A	N/A	N/A	N/A

Supplementary Table 2 List of authentic iCCA patients used for genomic analyses.
Cohort of 28 authentic human iCCA that were on used in the genomic studies of PDCL are listed in the table below. Given are clinicopathological information of iCCA tumors.

CCA patients	Gender	Size (cm)	TNM	Grading	Differentiation	Inflammation
CCA1	M	1,4	N/A	G2	Moderate	Yes
CCA2	F	13	pT1, pN0, M0, R0	G2	Moderate	Yes
CCA3	F	6	pT2b, pN0, M0, R0	G1-G2	Well to moderate	Yes
CCA4	F	6,5	pT2b, pN0, M0, R1	G2	Moderate	No
CCA5	F	10,3	pT1, pN0, M0, R0	G2	Moderate	Yes
CCA6	M	3,5	pT1, pN0, M0, R0	G2	Moderate	Yes
CCA7	M	12	pT2a, pN0, M0, R0	G2	Moderate	No
CCA8	F	5	pT1, pN0, M0, R0	G2	Moderate	No
CCA10	F	5,9	pT3, pN1, M0, R0	G2	Moderate	Yes
CCA11	M	8,3	R0	G2	Moderate	No
CCA12	F	0,5	pT2, R1	G3	Poor	No
CCA13	M	4,3	pT3, pN1, M0, R0	G2	Moderate	Yes
CCA14	M	3,5	N/A	G2	Moderate	Yes
CCA15	F	12	pT2b, pN0, M0, R0	G2	Moderate	Yes
CCA16	M	10	pT3, pN1, M0, R0	G3	Poor	No
CCA17	M	14,5	pT3, pN1, M0, R1	G2-G3	Poor	Yes
CCA18	F	10,2	pT2a, pN1, M0, R0	G3	Poor	Yes
CCA19	M	7,3	pT3, pN1, M0, R0	G2	Moderate	No
CCA21	M	3,5	rpT3, pN0 (0/1), R0	G2	Moderate	Yes
CCA22	M	9	pT2a, pN0, M0, R0	G3	Poor	Yes
CCA23	F	N/A	pT1, Nx, M0, R0	G2	Moderate	Yes
CCA24	M	3	pT1, pNX, M0, R0	G2	Moderate	Yes
CCA25	M	0,5	ypT1, pN0, Mx, R0	N/A	N/A	Yes
CCA28	M	9,5	N/A	N/A	N/A	No
CCA29	F	0,6	pT2b, pN0, Mx, R0	G2	Moderate	Yes
CCA30	F	14	pT2b, pN0, M0, R0	G2	Moderate	Yes
CCA31	M	7,5	pT2a, N0, M0, R0	G3	Poor	Yes
CCA33	M	8,5	pT2a, pN1, M0, R0	G3	Poor	Yes

Supplementary Table 3 cell lines.
Listed are commercial cell lines of HCC and CCA used for genomic analyses.

Hepatoma cell lines	CCA cell lines
Hep3B	EGI-1
HepG2	HuCCT-1
Huh7	RBE
KMCH	SNU-478
LECHCC	SNU-1079
PLC/PRF/5	SNU-1196
WRL68	SSP-25
	WITT

Supplementary Table 4 Commonly dysregulated genes.

Shown are the numbers of significant genes between different PDCL determined by Wald test as well as the unique genes commonly dysregulated in each PDCL

Wald-Test pvalue<0.01	ALL	CCA16	CCA33	HCC9	HCC16	HCC31	HCC68
CCA10	54	3054	2540	3055	2954	2223	2095
CCA16	205		2866	3456	3471	3490	3402
CCA33	61			2800	2721	2367	3428
HCC9	108				2545	2284	2995
HCC16	190					1964	2468
HCC31	30						2714
HCC68	77						

Unique Genes**CCA10**(log2FC)					
No.	Ensembl GeneID	Symbol	T	P5	P30
1	ENSG00000238098	ABCA17P	2.41432	2.45439	2.80946
2	ENSG00000224063	AC007319.1	4.7015	2.98897	4.3294
3	ENSG00000143429	AC027612.6	-1.2305	-2.10696	-1.15119
4	ENSG00000233006	AC034220.3	4.33508	2.39928	1.07882
5	ENSG00000267270	AC139100.2	3.92004	1.24991	0.284368
6	ENSG00000184160	ADRA2C	2.97333	5.07193	3.82671
7	ENSG00000196581	AJAP1	1.9089	5.56852	5.9915
8	ENSG00000215033	AL603965.1	4.35847	5.82004	4.83971
9	ENSG00000088448	ANKRD10	1.22394	1.31887	1.71618
10	ENSG00000162813	BPNT1	-1.18319	-1.26368	-0.874488
11	ENSG00000074410	CA12	0.0174293	-3.36153	-2.75126
12	ENSG00000147889	CDKN2A	2.64105	3.36639	3.94857
13	ENSG00000136425	CIB2	-1.17897	-3.236	-2.94765
14	ENSG00000164778	EN2	6.23294	7.83049	6.87128
15	ENSG00000119782	FKBP1B	-2.16248	-3.99712	-3.93116
16	ENSG00000174500	GCSAM	2.14029	2.30775	1.73417
17	ENSG00000104381	GDAP1	-1.54551	-4.64693	-4.77362
18	ENSG00000164949	GEM	0.790971	3.42223	1.04834
19	ENSG00000110422	HIPK3	0.531431	0.771268	0.0613949
20	ENSG00000231908	IDH1-AS1	-4.21139	-5.26842	-3.81015
21	ENSG00000105655	ISYNA1	1.47942	3.54065	4.20287
22	ENSG00000233237	LINC00472	6.22254	6.33968	4.97121
23	ENSG00000006062	MAP3K14	0.457768	1.98261	2.13432
24	ENSG00000112139	MDGA1	3.2457	6.5543	6.33459
25	ENSG00000247516	MIR4458HG	-4.11653	-7.63299	-7.75968

26	ENSG00000075975	MKRN2	-0.90971	-0.49853	-0.283895
27	ENSG00000133030	MPRIP	2.2042	3.79337	3.49739
28	ENSG00000144959	NCEH1	1.88787	2.8615	3.0803
29	ENSG00000163121	NEURL3	1.55835	5.78088	2.81771
30	ENSG00000147862	NFIB	1.51351	1.29263	1.46305
31	ENSG00000253873	PCDHGA11	6.21383	1.75395	1.09674
32	ENSG00000071994	PDCD2	-1.38338	-0.955786	-0.82456
33	ENSG00000184203	PPP1R2	-0.877538	-0.670792	-0.504274
34	ENSG00000121481	RNF2	-0.978119	-1.32691	-0.566755
35	ENSG00000258285	RP11-103B5.2	0.432467	4.16899	-0.570684
36	ENSG00000254634	RP11-231C14.3	3.78296	2.71172	0.570672
37	ENSG00000225265	RP11-378J18.3	-4.88946	-3.48706	-3.07318
38	ENSG00000231365	RP11-418J17.1	3.44205	3.51075	0.871675
39	ENSG00000235902	RP11-626E13.1	5.11054	3.18279	-2.07318
40	ENSG00000215548	RP11-764K9.4	-0.609353	-0.79965	-2.29558
41	ENSG00000239218	RPS20P22	3.96852	3.78143	2.45038
42	ENSG00000139218	SCAF11	1.36497	2.42021	2.58178
43	ENSG00000164023	SGMS2	-0.161462	0.88755	0.25432
44	ENSG00000197375	SLC22A5	1.82692	1.95344	1.28671
45	ENSG00000137968	SLC44A5	-1.75196	-2.80899	-4.81015
46	ENSG00000205571	SMN2	-0.474424	1.71647	0.589781
47	ENSG00000171148	TADA3	-1.88681	-1.33178	-1.42087
48	ENSG00000028839	TBPL1	-1.62329	-1.10059	-0.683113
49	ENSG00000029639	TFB1M	-1.19556	-2.30603	-1.82973
50	ENSG00000231770	TMEM44-AS1	-1.3947	-2.31846	-1.83218
51	ENSG00000056558	TRAF1	1.92324	1.1384	2.32951
52	ENSG00000132549	VPS13B	3.28168	2.81381	2.97896
53	ENSG00000105875	WDR91	3.09982	4.02384	3.27057
54	ENSG00000171307	ZDHHC16	-1.26694	-1.77772	-1.34038

Unique Genes CCA16 (log2FC)

No.	Ensembl GeneID	Symbol	T	P5	P30
1	ENSG00000109576	AADAT	-10.1804	-10.3797	-11.1208
2	ENSG00000023839	ABCC2	-8.92619	-10.4151	-8.49317
3	ENSG00000136379	ABHD17C	3.62504	3.99509	2.04631
4	ENSG00000127220	ABHD8	-2.76785	-1.76141	-1.889
5	ENSG00000226363	AC009336.24	4.29426	6.06769	5.32544
6	ENSG00000224769	AC069213.1	8.03921	5.45943	0.693694
7	ENSG00000078124	ACER3	1.11588	2.18276	1.75493
8	ENSG00000112304	ACOT13	-4.1074	-3.79279	-3.38792
9	ENSG00000100591	AHSA1	1.4527	0.893817	1.97109
10	ENSG00000189366	ALG1L	5.97194	5.29161	5.8673
11	ENSG00000148677	ANKRD1	-3.088	-2.28739	-1.44348
12	ENSG00000166825	ANPEP	-7.55656	-8.17907	-9.05008
13	ENSG00000164144	ARFIP1	1.28543	1.62753	0.399497
14	ENSG00000137962	ARHGAP29	-4.13963	-6.06339	-5.44264
15	ENSG00000157399	ARSE	-7.79057	-9.405	-11.316
16	ENSG00000148219	ASTN2	-0.820521	-2.34183	-2.96741
17	ENSG00000181652	ATG9B	8.59067	8.39391	2.64162
18	ENSG00000095739	BAMBI	-2.06539	-3.42705	-3.30303
19	ENSG00000132840	BHMT2	-11.3697	-11.1767	-12.7251
20	ENSG00000166619	BLCAP	0.323342	1.00109	1.36582
21	ENSG00000125999	BPIFB1	11.8529	7.89989	4.43576

22	ENSG00000177627	C12orf54	1.3494	6.95802	4.73089
23	ENSG00000169609	C15orf40	0.847876	1.30261	0.842232
24	ENSG00000171984	C20orf196	4.60037	2.62251	2.55301
25	ENSG00000183287	CCBE1	-5.76694	-4.57401	-7.70738
26	ENSG00000170558	CDH2	-7.32156	-6.30211	-9.41954
27	ENSG00000147889	CDKN2A	2.3069	1.83823	1.57992
28	ENSG00000105388	CEACAM5	9.97037	8.86185	7.14377
29	ENSG00000086548	CEACAM6	9.2549	7.8354	3.88558
30	ENSG00000170835	CEL	5.62951	8.2748	4.24835
31	ENSG00000064886	CHI3L2	-1.97252	-2.58695	-4.91296
32	ENSG00000117971	CHRNB4	3.78236	7.5294	5.40896
33	ENSG00000137975	CLCA2	5.49508	9.95778	7.41683
34	ENSG00000070371	CLTCL1	-2.0324	-2.50709	-1.11401
35	ENSG00000117519	CNN3	-3.02554	-4.07312	-2.77732
36	ENSG00000230183	CNOT6LP1	1.61244	4.05953	2.41551
37	ENSG00000065618	COL17A1	4.26482	7.91373	7.60525
38	ENSG00000093010	COMT	-3.866	-3.8618	-4.18782
39	ENSG00000196353	CPNE4	4.66651	5.77646	3.13143
40	ENSG00000143320	CRABP2	10.4276	9.30484	5.75059
41	ENSG00000108342	CSF3	-3.97252	8.77678	5.39822
42	ENSG00000121552	CSTA	1.31582	2.95399	2.06978
43	ENSG00000134030	CTIF	-2.06053	-0.572787	-1.70345
44	ENSG00000112514	CUTA	-1.85538	-2.73348	-2.47134
45	ENSG00000019186	CYP24A1	6.64018	9.77782	6.26162
46	ENSG00000170456	DENND5B	-5.23767	-5.17718	-3.48743
47	ENSG00000134757	DSG3	2.31288	6.88777	8.77703
48	ENSG00000140254	DUOXA1	9.54711	9.16292	7.93566
49	ENSG00000119718	EIF2B2	1.19938	0.681457	1.28973
50	ENSG00000145191	EIF2B5	0.600661	0.564016	1.2144
51	ENSG00000012660	ELOVL5	-5.08761	-5.89612	-7.60296
52	ENSG00000079819	EPB41L2	-0.672964	-1.32845	-0.321975
53	ENSG00000134398	ERN2	9.84499	7.58964	0.502074
54	ENSG00000117036	ETV3	2.70052	3.18012	2.14602
55	ENSG00000104313	EYA1	7.64586	7.16125	7.43798
56	ENSG00000196937	FAM3C	1.50418	1.74274	1.90923
57	ENSG00000152767	FARP1	-2.62667	-3.5426	-3.0495
58	ENSG00000086570	FAT2	4.43032	7.94218	9.38712
59	ENSG00000178974	FBXO34	2.30951	1.63828	1.36552
60	ENSG00000182263	FIGN	-2.93936	-3.08247	-1.99938
61	ENSG00000115226	FNDC4	-7.30821	-6.5816	-7.04702
62	ENSG00000176920	FUT2	7.68807	6.65781	3.70175
63	ENSG00000010361	FUZ	1.40519	1.16897	1.17939
64	ENSG00000183347	GBP6	2.2754	6.14437	7.45772
65	ENSG00000084734	GCKR	-10.7185	-10.3329	-11.2439
66	ENSG00000174500	GCSAM	3.66306	5.00016	4.05117
67	ENSG00000167741	GGT6	8.38173	6.74621	6.13143
68	ENSG00000189280	GJB5	4.2173	5.50757	6.88901
69	ENSG00000182963	GJC1	0.300494	-0.648348	-2.328
70	ENSG00000178445	GLDC	-9.21808	-11.8325	-9.35116
71	ENSG00000183098	GPC6	-5.69134	-6.17084	-8.98228
72	ENSG00000173890	GPR160	5.48111	2.94214	2.59576
73	ENSG00000130956	HABP4	-1.65346	-3.4378	-1.45223
74	ENSG00000113070	HBEGF	2.51744	6.93625	4.67341

75	ENSG00000196917	HCAR1	7.2173	7.13757	5.84637
76	ENSG00000164683	HEY1	2.80178	0.684857	5.2667
77	ENSG00000156510	HKDC1	-0.972524	-3.73895	-4.23489
78	ENSG00000105996	HOXA2	5.72096	5.68918	4.54647
79	ENSG00000105997	HOXA3	4.57927	6.73293	6.01831
80	ENSG00000118960	HS1BP3	-1.39545	-1.62743	-1.41078
81	ENSG00000030419	IKZF2	3.64571	3.96477	3.00096
82	ENSG00000145103	ILDR1	7.92229	7.06141	6.24943
83	ENSG00000115221	ITGB6	6.74292	6.19783	7.42495
84	ENSG00000173801	JUP	1.36025	1.98285	2.37816
85	ENSG00000213859	KCTD11	3.65233	4.00698	3.14606
86	ENSG00000120549	KIAA1217	-0.21553	0.581893	0.780452
87	ENSG00000179454	KLHL28	0.697186	1.38436	0.862274
88	ENSG00000133703	KRAS	0.765081	0.988386	1.22788
89	ENSG00000186081	KRT5	5.78093	7.66791	9.78891
90	ENSG00000148346	LCN2	6.28174	8.33639	6.16595
91	ENSG00000259974	LINC00261	-10.9901	-12.983	-14.046
92	ENSG00000232931	LINC00342	8.34912	6.18784	3.16385
93	ENSG00000232229	LINC00865	3.66168	2.45745	1.92834
94	ENSG00000079435	LIPE	8.7409	3.85521	2.55581
95	ENSG00000176454	LPCAT4	6.08418	6.39268	4.76085
96	ENSG00000160285	LSS	-3.23795	-2.28826	-1.24812
97	ENSG00000167656	LY6D	6.35121	8.27093	2.87711
98	ENSG00000013619	MAMLD1	-2.39574	-4.46959	-1.43806
99	ENSG00000104774	MAN2B1	-0.962583	-1.24939	-1.85552
100	ENSG00000198909	MAP3K3	-1.71344	-2.68479	-0.90471
101	ENSG00000129680	MAP7D3	-4.97815	-6.27064	-8.91859
102	ENSG00000165406	MARCH8	-1.87941	-1.90256	-1.89161
103	ENSG00000133997	MED6	1.16354	1.3072	1.61473
104	ENSG00000176624	MEX3C	-4.33627	-5.06853	-8.94914
105	ENSG00000198948	MFAP3L	-10.4268	-8.28636	-12.3673
106	ENSG00000198788	MUC2	6.03995	8.94498	4.38675
107	ENSG00000176945	MUC20	6.81292	3.99533	-0.829709
108	ENSG00000145113	MUC4	8.39094	6.88535	3.41174
109	ENSG00000215182	MUC5AC	9.30152	6.80752	-0.228466
110	ENSG00000114503	NCBP2	1.2857	1.48054	1.7713
111	ENSG00000188505	NCCRP1	8.70608	7.32069	0.479353
112	ENSG00000182636	NDN	-1.22045	-1.80513	-5.16089
113	ENSG00000173848	NET1	1.58196	2.06182	2.43013
114	ENSG00000204386	NEU1	-1.83373	-2.11503	-1.66592
115	ENSG00000089723	OTUB2	2.16498	5.4144	5.30582
116	ENSG00000142623	PADI1	7.06195	6.02811	3.83171
117	ENSG00000198682	PAPSS2	-5.01815	-5.11279	-6.72876
118	ENSG00000198807	PAX9	9.84366	8.2648	8.7173
119	ENSG00000249915	PDCD6	1.30255	1.20496	0.8038
120	ENSG00000090470	PDCD7	0.526349	1.90138	1.52187
121	ENSG00000174827	PDZK1	-8.08039	-9.52489	-9.11394
122	ENSG00000049246	PER3	-3.62109	-4.36849	-5.41498
123	ENSG00000154864	PIEZO2	-3.97671	-5.84748	-6.64298
124	ENSG00000081277	PKP1	1.52998	4.5923	8.55219
125	ENSG00000104368	PLAT	4.48493	8.32242	6.01038
126	ENSG00000189266	PNRC2	-3.31492	-4.41477	-4.06271
127	ENSG00000167653	PSCA	11.5416	7.9557	1.22454

128	ENSG00000144724	PTPRG	-2.40072	-4.5702	-4.34873
129	ENSG00000106278	PTPRZ1	3.88546	1.93661	8.77178
130	ENSG00000112531	QKI	-2.29834	-1.88325	-1.938
131	ENSG00000166349	RAG1	3.09727	2.81834	2.43973
132	ENSG00000079337	RAPGEF3	5.3221	5.24639	2.25839
133	ENSG00000108352	RAPGEFL1	3.09844	3.97479	3.34882
134	ENSG00000160439	RDH13	4.00267	2.82134	2.49356
135	ENSG00000168476	REEP4	3.136	4.04175	3.79
136	ENSG00000204618	RNF39	7.81211	7.12386	2.63547
137	ENSG00000263006	ROCK1P1	-1.55749	-3.17191	-1.91296
138	ENSG00000205293	RP11-1112C15.1	5.98167	6.80322	5.44459
139	ENSG00000249550	RP11-438N16.1	7.2296	7.31543	4.99993
140	ENSG00000233901	RP11-65J3.1	2.66168	3.62007	3.06241
141	ENSG00000235142	RP1-60O19.1	-9.19492	-10.3943	-11.7203
142	ENSG00000235501	RP4-639F20.1	-3.51849	-4.38445	-4.64336
143	ENSG00000258545	RP4-755D9.1	8.83201	8.381	6.94735
144	ENSG00000259153	RP6-65G23.3	3.55104	7.56483	5.55952
145	ENSG00000215030	RPL13P12	-0.128099	-0.134281	-0.342792
146	ENSG00000100784	RPS6KA5	1.951	2.5243	2.35138
147	ENSG00000185924	RTN4RL1	-5.76694	-8.38136	-8.70738
148	ENSG00000186907	RTN4RL2	-6.25793	-3.80196	-6.27237
149	ENSG00000196754	S100A2	4.68378	7.50175	9.00635
150	ENSG00000185033	SEMA4B	2.84415	3.9097	3.06549
151	ENSG00000057149	SERPINB3	5.19071	8.99174	4.03345
152	ENSG00000163406	SLC15A2	6.15957	3.92085	4.04967
153	ENSG00000204385	SLC44A4	9.00878	4.94373	-0.912964
154	ENSG00000184564	SLITRK6	7.57774	4.19441	7.18078
155	ENSG00000141646	SMAD4	-2.87796	-3.10818	-3.70125
156	ENSG00000198732	SMOC1	-9.05928	-9.18828	-8.77733
157	ENSG00000224078	SNHG14	-3.54699	-5.22555	-6.42603
158	ENSG00000129194	SOX15	2.45374	6.21233	6.8285
159	ENSG00000181449	SOX2	6.15933	4.44648	9.96614
160	ENSG00000204335	SP5	-3.87941	-7.0788	-4.40482
161	ENSG00000241794	SPRR2A	0.612438	7.15901	5.16385
162	ENSG00000163209	SPRR3	6.2754	8.55516	7.78921
163	ENSG00000128039	SRD5A3	3.75925	3.69333	0.215442
164	ENSG00000249700	SRD5A3-AS1	4.70696	4.57292	0.334964
165	ENSG00000188529	SRSF10	-4.81383	-4.20586	-2.20995
166	ENSG00000124783	SSR1	-2.06563	-1.80834	-1.29769
167	ENSG00000157350	ST3GAL2	-2.51877	-1.75313	-2.14268
168	ENSG00000165283	STOML2	0.72049	0.770407	1.60217
169	ENSG00000137868	STRA6	7.23578	8.4395	6.16259
170	ENSG00000161860	SYCE2	-0.972524	-2.58695	-0.175998
171	ENSG00000142765	SYTL1	6.42713	6.95691	5.88978
172	ENSG00000143498	TAF1A	2.53923	3.02592	2.89439
173	ENSG00000134827	TCN1	9.49695	6.94248	3.23678
174	ENSG00000159648	TEPP	4.68569	5.31994	1.54647
175	ENSG00000144115	THNSL2	-7.82271	-8.62978	-9.76315
176	ENSG00000164180	TMEM161B	1.14026	1.48546	1.033
177	ENSG00000187049	TMEM216	1.88071	2.1214	2.33677
178	ENSG00000163472	TMEM79	2.00338	1.98638	2.10539
179	ENSG00000137648	TMPRSS4	9.56736	9.45437	7.35923
180	ENSG00000131746	TNS4	4.88177	7.23146	7.96866

181	ENSG00000073282	TP63	4.98748	7.33452	8.61017
182	ENSG00000140391	TSPAN3	4.05598	2.52632	1.62459
183	ENSG00000100154	TTC28	-5.15532	-6.33162	-6.46499
184	ENSG00000182247	UBE2E2	-3.36484	-4.64223	-5.55321
185	ENSG00000135220	UGT2A3	-9.04399	-10.6584	-9.98443
186	ENSG00000174607	UGT8	6.56016	6.66729	7.28753
187	ENSG00000147679	UTP23	0.885457	1.72557	1.69229
188	ENSG00000168140	VASN	-2.30035	-2.63041	-3.75115
189	ENSG00000184056	VPS33B	1.08451	2.23255	1.35281
190	ENSG00000101443	WFDC2	10.1865	9.29305	5.34805
191	ENSG00000134744	ZCCHC11	-3.94431	-5.00804	-6.71257
192	ENSG00000148516	ZEB1	-2.18141	-3.65643	-7.14291
193	ENSG00000120784	ZFP30	-3.84699	-5.04638	-7.95736
194	ENSG00000187801	ZFP69B	-1.87941	-4.49384	-4.81985
195	ENSG00000198315	ZKSCAN8	-3.39337	-4.71406	-8.288
196	ENSG00000125846	ZNF133	1.33383	2.07729	2.02142
197	ENSG00000168661	ZNF30	-2.23556	-6.49384	-5.23489
198	ENSG00000181894	ZNF329	-5.25456	-6.52106	-7.65443
199	ENSG00000177932	ZNF354C	-0.585501	-1.96546	-1.91296
200	ENSG00000161642	ZNF385A	2.87444	4.69218	3.85637
201	ENSG00000196437	ZNF569	-6.90326	-7.51768	-6.25874
202	ENSG00000188227	ZNF793	0.197401	-2.26502	-3.91296
203	ENSG00000223547	ZNF844	-3.95156	-6.45907	-8.59244
204	ENSG00000121413	ZSCAN18	-3.17246	-5.41138	-8.32236
205	ENSG00000203995	ZYG11A	-5.75388	-5.36831	-3.60686

Unique Genes**CCA33**(log2FC)

No.	Ensembl GeneID	Symbol	T	P5	P30
1	ENSG00000226856	AC093901.1	0.561082	0.271033	0.0859771
2	ENSG00000169129	AFAP1L2	5.66296	5.85383	5.89043
3	ENSG00000110497	AMBRA1	-0.568686	-3.71779	-3.01329
4	ENSG00000206560	ANKRD28	0.741587	1.5825	1.65363
5	ENSG00000152056	AP1S3	5.3555	7.98137	7.03088
6	ENSG00000144746	ARL6IP5	1.09607	1.95932	1.71753
7	ENSG00000206190	ATP10A	5.93751	7.11376	6.15111
8	ENSG00000135407	AVIL	-3.09788	-4.32148	-3.115
9	ENSG00000155096	AZIN1	1.33815	1.66651	2.54332
10	ENSG00000106635	BCL7B	0.940403	1.33181	0.66853
11	ENSG00000091317	CMTM6	0.414895	0.33367	0.620144
12	ENSG00000197813	CTC-301O7.4	-4.40239	-3.03014	-4.63101
13	ENSG00000105928	DFNA5	0.735112	-2.45898	0.123874
14	ENSG00000170464	DNAJC18	-0.327557	-0.644011	-0.708182
15	ENSG00000167968	DNASE1L2	-3.50931	-2.03752	-2.416
16	ENSG00000178852	EFCAB13	-4.36492	-2.68454	-2.47806
17	ENSG00000102287	GABRE	-1.21215	-2.83366	-4.9002
18	ENSG00000111846	GCNT2	0.914719	1.89525	2.13101
19	ENSG00000170604	IRF2BP1	-0.910818	-1.55209	-1.39524
20	ENSG00000120071	KANSL1	-0.555672	-0.328633	-0.00640549
21	ENSG00000104863	LIN7B	-2.00861	-1.28225	-2.12761
22	ENSG00000238266	LINC00707	6.88301	8.2515	7.33738
23	ENSG00000088899	LZTS3	-1.18854	-1.42236	-3.15685
24	ENSG00000078018	MAP2	3.14638	3.83734	3.40553

25	ENSG00000143995	MEIS1	-1.55439	-1.91149	-2.18476
26	ENSG00000203791	METTL10	0.32059	0.735351	0.502806
27	ENSG00000002079	MYH16	3.15603	4.44791	6.58611
28	ENSG00000144959	NCEH1	4.5271	6.36807	5.82431
29	ENSG00000160209	PDXK	2.3648	3.29921	3.67216
30	ENSG00000172531	PPP1CA	1.12685	1.21244	1.27459
31	ENSG00000183255	PTTG1IP	1.79231	2.56133	3.04519
32	ENSG00000137502	RAB30	-1.44561	-0.971586	-2.87168
33	ENSG00000144118	RALB	1.62669	2.35048	2.01801
34	ENSG00000108375	RNF43	-0.239609	-0.251694	-3.1745
35	ENSG00000251003	RP11-152P17.2	-0.701952	-1.13705	-1.93057
36	ENSG00000234840	RP11-399D6.2	-4.02388	-2.87402	-2.55206
37	ENSG00000260329	RP11-412D9.4	-2.50931	-2.62248	-3.00096
38	ENSG00000226824	RP4-756H11.3	-0.583308	0.566555	0.741043
39	ENSG00000226102	SEPT7P3	-0.106342	-0.137052	0.0774187
40	ENSG00000042317	SPATA7	-1.72081	-2.23391	-1.568
41	ENSG00000152582	SPEF2	-1.88416	-2.34727	-0.574812
42	ENSG00000137767	SQRDL	0.919371	1.36259	0.733205
43	ENSG00000100321	SYNGR1	-1.76496	-3.05322	-5.63101
44	ENSG00000104946	TBC1D17	-0.955768	-1.28632	-1.16522
45	ENSG00000198933	TBKBP1	-0.386856	-2.15995	-2.54422
46	ENSG00000134490	TMEM241	2.50537	3.55479	3.55544
47	ENSG00000130598	TNNI2	4.08232	5.8152	6.7532
48	ENSG00000141510	TP53	-0.579095	-1.9947	-1.58673
49	ENSG00000165699	TSC1	-0.958727	-0.321877	-0.219319
50	ENSG00000102904	TSNAXIP1	-2.74148	-3.17658	-7.14003
51	ENSG00000015532	XYLT2	-0.223905	-0.912558	0.162938
52	ENSG00000166793	YPEL4	-2.87188	-3.98505	-2.51554
53	ENSG00000149050	ZNF214	-1.65615	-4.50629	-2.71485
54	ENSG00000165804	ZNF219	-0.119384	-0.254773	-1.73614
55	ENSG00000197935	ZNF311	-2.50931	-3.94441	-2.2785
56	ENSG00000083812	ZNF324	-0.578377	-0.822178	-0.817806
57	ENSG00000256087	ZNF432	-1.34965	-1.09918	-0.777804
58	ENSG00000197701	ZNF595	1.8341	2.49522	2.28666
59	ENSG00000142556	ZNF614	-1.05889	-6.32688	-4.21351
60	ENSG00000197619	ZNF615	-1.7258	-2.98033	-1.85008
61	ENSG00000182318	ZSCAN22	-0.778303	-1.25315	-1.19957

Unique Genes**HCC9**(log2FC)

No.	Ensembl GeneID	Symbol	T	P5	P30
1	ENSG00000213225	AC018804.7	3.16647	3.38302	3.6791
2	ENSG00000075340	ADD2	3.72615	0.730814	4.01744
3	ENSG00000138138	ATAD1	-5.17297	-4.84	-7.11818
4	ENSG00000105146	AURKC	2.71658	3.73425	3.12263
5	ENSG00000118276	B4GALT6	2.95968	3.72899	3.64515
6	ENSG00000273045	C2ORF15	-0.0841135	-1.33808	-0.403712
7	ENSG00000165181	C9orf84	-2.23612	-2.33808	0.0881413
8	ENSG00000158941	CCAR2	-0.286294	0.201036	0.183907
9	ENSG00000186567	CEACAM19	-2.60576	-4.31845	-5.61626
10	ENSG00000111642	CHD4	1.93729	2.64024	2.44673
11	ENSG00000164695	CHMP4C	-0.119077	-1.35855	-2.21361
12	ENSG00000113946	CLDN16	-3.62843	-3.06743	-3.30418

13	ENSG00000109472	CPE	1.26344	2.84605	1.7666
14	ENSG00000139117	CPNE8	-2.72726	-1.41418	-2.58742
15	ENSG00000177738	CTD-2201E18.3	2.2407	2.97177	2.68269
16	ENSG00000273018	CTD-2303H24.2	1.47502	1.27758	0.800702
17	ENSG00000253982	CTD-2336O2.1	-3.18665	-3.28861	-3.39327
18	ENSG00000100523	DDHD1	2.35095	3.08995	2.68403
19	ENSG00000181381	DDX60L	-0.887538	2.59536	2.38951
20	ENSG00000134755	DSC2	-2.55629	-2.86471	-1.80655
21	ENSG00000134769	DTNA	0.241931	-0.40847	-0.0562486
22	ENSG00000125971	DYNLRB1	-1.29738	-1.29149	-1.13762
23	ENSG00000084710	EFR3B	4.20683	6.97253	8.30828
24	ENSG00000115504	EHBP1	-2.01971	-3.50019	-4.19256
25	ENSG00000119888	EPCAM	2.55712	-0.451738	-1.21209
26	ENSG00000198324	FAM109A	1.62866	1.49147	2.06711
27	ENSG00000183114	FAM43B	-0.499151	6.99358	7.65546
28	ENSG00000168672	FAM84B	-1.95583	-1.50686	-2.06898
29	ENSG00000173295	FAM86B3P	-6.71332	-4.60229	-5.9225
30	ENSG00000066468	FGFR2	-4.19508	-4.4327	-5.92356
31	ENSG00000136877	FPGS	-1.04664	-2.08765	-1.7518
32	ENSG00000131067	GGT7	-0.870681	-1.33236	-1.74468
33	ENSG00000173905	GOLIM4	2.51687	0.123506	0.876059
34	ENSG00000233276	GPX1	-3.52349	-5.26153	-10.3249
35	ENSG00000181333	HEPHL1	1.71808	5.80403	6.96956
36	ENSG00000078399	HOXA9	6.84603	7.03696	6.82691
37	ENSG00000226742	HSBP1L1	-1.92166	-4.02791	-4.29357
38	ENSG00000126803	HSPA2	2.66605	3.45097	4.20362
39	ENSG00000003147	ICA1	-3.3557	-6.09707	-8.69322
40	ENSG00000244242	IFITM10	-3.07627	-4.4654	-4.70903
41	ENSG00000148798	INA	-1.23612	7.43065	8.24566
42	ENSG00000257093	KIAA1147	-1.40232	-2.47777	-3.35391
43	ENSG00000137177	KIF13A	0.346726	2.24304	2.50119
44	ENSG00000166796	LDHC	1.0369	1.18548	1.60752
45	ENSG00000138131	LOXL4	0.689883	0.805965	-2.87764
46	ENSG00000148356	LRSAM1	-1.60276	-1.75226	-1.72961
47	ENSG00000185247	MAGEA11	7.1313	7.99115	8.17295
48	ENSG00000156009	MAGEA8	7.36973	8.0313	8.11936
49	ENSG00000185090	MANEAL	-4.25848	-3.50247	-2.30196
50	ENSG00000175130	MARCKSL1	-0.777331	-3.25746	-5.7292
51	ENSG00000141644	MBD1	-0.696817	-0.414659	-0.549315
52	ENSG00000014641	MDH1	-5.48611	-5.78072	-9.42238
53	ENSG00000163975	MFI2	-0.531021	-1.38741	-3.17441
54	ENSG00000037757	MRI1	-1.63436	-4.49121	-5.27144
55	ENSG00000173272	MZT2A	-0.392692	-0.818495	-0.261443
56	ENSG00000078177	N4BP2	-2.87323	-2.1998	-2.52614
57	ENSG00000100285	NEFH	1.68275	6.27387	6.6435
58	ENSG00000184613	NELL2	7.79262	8.11334	7.16581
59	ENSG00000107833	NPM3	0.0772155	-1.03051	-0.534446
60	ENSG00000189223	PAX8-AS1	-3.01256	-0.652557	-0.429929
61	ENSG00000078674	PCM1	-1.42153	-0.913502	-0.816046
62	ENSG00000121892	PDS5A	-1.49599	-1.98079	-1.98091
63	ENSG00000162366	PDZK1IP1	1.43848	2.0856	-0.98003
64	ENSG00000101464	PIGU	-0.362334	-0.208151	-0.0832952
65	ENSG00000057294	PKP2	-2.20558	-2.29707	-2.68552

66	ENSG00000110841	PPFIBP1	0.117568	2.28093	2.04913
67	ENSG00000135406	PRPH	1.34885	7.60443	6.90064
68	ENSG00000171862	PTEN	-4.42956	-5.49941	-8.00756
69	ENSG00000050628	PTGER3	4.07222	8.02715	8.85003
70	ENSG00000148334	PTGES2	-0.847132	-0.929812	-1.26917
71	ENSG00000118849	RARRES1	-1.86999	-3.82993	-4.14068
72	ENSG00000169733	RFNG	-1.78307	-2.67783	-3.00689
73	ENSG00000225465	RFPL1S	-2.58007	1.79245	2.80397
74	ENSG00000131941	RHPN2	-1.51524	-1.97858	-2.98833
75	ENSG00000257718	RP11-396F22.1	-4.78044	-4.14544	-4.36307
76	ENSG00000247903	RP11-421F16.3	-1.68132	-2.97883	-1.95426
77	ENSG00000259985	RP11-549B18.1	3.01938	3.52982	3.95604
78	ENSG00000231345	RP11-564C4.6	1.39615	-0.95957	-1.55571
79	ENSG00000249741	RP11-673E1.3	2.67077	2.90985	1.76621
80	ENSG00000272005	RP11-91J19.4	-4.08161	-2.20629	-3.75735
81	ENSG00000272841	RP3-428L16.2	2.26031	5.03944	4.00325
82	ENSG00000129197	RPAIN	-1.09502	-1.56597	-1.36112
83	ENSG00000220793	RPL21P119	-7.62557	-0.785019	-0.815884
84	ENSG00000105372	RPS19	-1.03184	-1.3229	-1.93943
85	ENSG00000081019	RSBN1	-0.594099	-1.3473	-1.29
86	ENSG00000164764	SBSPON	4.76908	5.3538	3.16906
87	ENSG00000138623	SEMA7A	-0.711026	-1.86274	-2.54694
88	ENSG00000175793	SFN	4.90087	1.05424	2.77744
89	ENSG00000111252	SH2B3	1.03569	2.79116	2.48745
90	ENSG00000116991	SIPA1L2	4.90321	3.70738	4.26464
91	ENSG00000070915	SLC12A3	2.67077	8.62337	9.35914
92	ENSG00000214617	SLC6A10P	9.08073	6.50741	6.32846
93	ENSG00000077935	SMC1B	5.43631	6.00066	6.10829
94	ENSG00000067221	STOML1	-0.915386	-1.43079	-1.53197
95	ENSG00000028839	TBPL1	1.58938	0.85938	0.551343
96	ENSG00000240280	TCAM1P	1.67077	6.11725	5.25807
97	ENSG00000120889	TNFRSF10B	-2.09394	-1.9243	-2.14728
98	ENSG00000125657	TNFSF9	2.421	7.51102	8.41561
99	ENSG00000115129	TP53I3	2.37689	2.16102	2.55559
100	ENSG00000156521	TYSND1	-1.86131	-2.40199	-1.70772
101	ENSG00000130985	UBA1	0.807591	1.57506	1.43272
102	ENSG00000078140	UBE2K	-2.27226	-2.7344	-2.96828
103	ENSG00000177414	UBE2U	7.00706	5.55674	6.43864
104	ENSG00000101019	UQCC1	-1.52864	-0.873413	-0.829397
105	ENSG00000139190	VAMP1	2.3112	2.48604	1.66081
106	ENSG00000143951	WDPCP	-2.14054	-4.20598	-3.61626
107	ENSG00000124343	XG	-1.18167	3.53323	2.25313
108	ENSG00000235109	ZSCAN31	4.39964	3.84461	3.30822

Unique Genes**HCC16**(log2FC)

No.	Ensembl GeneID	Symbol	T	P5
1	ENSG00000103222	ABCC1	-0.360751	-0.282103
2	ENSG00000183260	ABHD16B	-1.51837	-2.00929
3	ENSG00000136379	ABHD17C	-2.94628	-1.51412
4	ENSG00000120437	ACAT2	0.958777	0.626383
5	ENSG00000126705	AHDC1	-0.787993	-0.811939
6	ENSG00000185567	AHNAK2	-5.31746	-2.62699
7	ENSG00000161618	ALDH16A1	-1.58743	-3.12952

8	ENSG00000178038	ALS2CL	-3.06648	-3.19515
9	ENSG00000138772	ANXA3	-3.53985	-1.02523
10	ENSG00000142192	APP	-3.71471	-3.51217
11	ENSG00000071205	ARHGAP10	-2.51786	-3.17317
12	ENSG00000225485	ARHGAP23	-2.24968	-0.971849
13	ENSG00000142632	ARHGEF19	-2.26301	-2.3878
14	ENSG00000204959	ARHGEF34P	-3.51386	-3.99923
15	ENSG00000050327	ARHGEF5	-5.38785	-3.04315
16	ENSG00000072444	ASAH2C	-3.53985	3.23947
17	ENSG00000145246	ATP10D	4.41766	3.17444
18	ENSG00000174684	B3GNT1	2.16565	1.76668
19	ENSG00000179913	B3GNT3	-6.16713	-4.12199
20	ENSG00000182240	BACE2	-2.42927	-2.58114
21	ENSG00000121753	BAI2	0.267502	3.00452
22	ENSG00000175866	BAIAP2	-4.97457	-6.50024
23	ENSG00000226137	BAIAP2-AS1	-3.05443	-2.01671
24	ENSG00000163093	BBS5	-2.24707	-1.65083
25	ENSG00000116985	BMP8B	-2.39546	-2.63573
26	ENSG00000169758	C15orf27	6.13787	5.02159
27	ENSG00000154102	C16orf74	-3.05443	-1.5398
28	ENSG00000143633	C1orf131	2.35595	1.92572
29	ENSG00000187642	C1orf170	-1.31746	-0.165407
30	ENSG00000198715	C1orf85	1.95462	1.82441
31	ENSG00000197261	C6orf141	-4.43294	-4.08824
32	ENSG00000182389	CACNB4	8.08128	7.90337
33	ENSG00000181982	CCDC149	-2.91383	-3.16703
34	ENSG00000107443	CCNJ	-2.50509	-3.22179
35	ENSG00000105369	CD79A	2.6146	-4.18366
36	ENSG00000075275	CELSR1	-2.73724	-2.27414
37	ENSG00000166582	CENPV	2.03547	1.87473
38	ENSG00000099814	CEP170B	-2.62499	-0.883598
39	ENSG00000189143	CLDN4	-6.01327	-6.20914
40	ENSG00000154529	CNTNAP3B	-4.12481	-3.78012
41	ENSG00000175029	CTBP2	-2.04028	-1.98705
42	ENSG00000267575	CTC-459F4.3	-0.0735347	-0.728836
43	ENSG00000118197	DDX59	1.31203	0.487452
44	ENSG00000153933	DGKE	-2.32705	-2.26865
45	ENSG00000130829	DUSP9	10.0523	5.45901
46	ENSG00000184349	EFNA5	-2.46946	-2.90237
47	ENSG00000115211	EIF2B4	1.32893	0.98571
48	ENSG00000100908	EMC9	-1.71785	-4.75458
49	ENSG00000173818	ENDOV	-2.65059	-1.70231
50	ENSG00000129595	EPB41L4A	-4.17728	-5.00251
51	ENSG00000110723	EXPH5	-7.5717	-6.64204
52	ENSG00000092820	EZR	-1.24873	-2.28431
53	ENSG00000184731	FAM110C	-7.34884	-8.58911
54	ENSG00000160752	FDPS	1.5358	1.58957
55	ENSG00000180263	FGD6	-1.25643	-1.34107
56	ENSG00000066468	FGFR2	-8.35211	-7.68548
57	ENSG00000135723	FHOD1	-0.814491	-1.25102
58	ENSG00000162769	FLVCR1	4.53239	4.29769
59	ENSG00000198468	FLVCR1-AS1	3.77259	3.95682
60	ENSG00000186564	FOXD2	-3.94195	-2.42733

61	ENSG00000204681	GABBR1	-2.89093	-2.62566
62	ENSG00000166206	GABRB3	-5.94195	-4.01229
63	ENSG00000182890	GLUD2	2.23796	3.36154
64	ENSG00000116906	GNPAT	1.75182	1.51665
65	ENSG00000147257	GPC3	8.40414	5.74214
66	ENSG00000152749	GPR180	-2.61797	-4.1707
67	ENSG00000160360	GPSM1	-2.16743	-1.53323
68	ENSG00000188290	HES4	-2.13725	-3.00406
69	ENSG00000029993	HMGB3	-4.11204	-6.29983
70	ENSG00000113161	HMGCR	2.99151	2.30257
71	ENSG00000214578	HMGN2P15	3.18504	1.90171
72	ENSG00000132196	HSD17B7	1.95765	1.61875
73	ENSG00000164270	HTR4	5.91376	1.69966
74	ENSG00000164136	IL15	-1.14189	-3.47526
75	ENSG00000134470	IL15RA	-1.96382	-3.28471
76	ENSG00000100605	ITPK1	-2.85507	-3.02619
77	ENSG00000096433	ITPR3	-0.344981	0.826181
78	ENSG00000177807	KCNJ10	0.856159	2.48843
79	ENSG00000100441	KHNYN	-2.47225	-3.66054
80	ENSG00000120549	KIAA1217	-2.09583	-1.84059
81	ENSG00000102554	KLF5	-4.10173	-1.22652
82	ENSG00000167487	KLHL26	-3.68003	-2.55772
83	ENSG00000119771	KLHL29	-3.87	-2.07464
84	ENSG00000167767	KRT80	-4.13105	-0.706622
85	ENSG00000170442	KRT86	-3.19193	-1.5253
86	ENSG00000126777	KTN1	-1.32664	-1.13136
87	ENSG00000058085	LAMC2	-4.53985	-2.40856
88	ENSG00000188636	LDOC1L	-2.22092	-1.57973
89	ENSG00000108679	LGALS3BP	-1.79842	-2.98856
90	ENSG00000237523	LINC00857	-5.27682	-1.3878
91	ENSG00000137821	LRRC49	-0.95489	-1.49471
92	ENSG00000124831	LRRFIP1	-1.39137	-1.22609
93	ENSG00000090006	LTBP4	-4.35917	-5.14073
94	ENSG00000187123	LYPD6	-3.05443	-3.12476
95	ENSG00000135525	MAP7	-5.77353	-7.32191
96	ENSG00000085276	MECOM	-1.0179	-1.99138
97	ENSG00000178053	MLF1	-3.00552	-4.66082
98	ENSG00000143674	MLK4	-5.32495	-3.98026
99	ENSG00000115648	MLPH	-4.36053	-8.7383
100	ENSG00000167508	MVD	1.91855	1.94827
101	ENSG00000157483	MYO1E	-2.86301	-3.97715
102	ENSG00000078177	N4BP2	1.27655	1.16741
103	ENSG00000050344	NFE2L3	0.811823	0.615953
104	ENSG00000147862	NFIB	-4.79351	-4.03643
105	ENSG00000167693	NXN	-3.34255	-3.46442
106	ENSG00000145247	OCIAD2	-5.43195	-8.57267
107	ENSG00000144645	OSBPL10	-1.26043	0.344505
108	ENSG00000141447	OSBPL1A	-2.1346	-3.27532
109	ENSG00000120327	PCDHB14	-3.19193	-3.26227
110	ENSG00000078674	PCM1	0.625643	1.96242
111	ENSG00000106333	PCOLCE	2.57151	1.25852
112	ENSG00000197461	PDGFA	-3.33736	-1.15136
113	ENSG00000162366	PDZK1IP1	-4.94195	-4.67125

114	ENSG00000170525	PFKFB3	-0.771518	-3.70877
115	ENSG00000107959	PITRM1	-1.82927	-1.19211
116	ENSG00000184363	PKP3	-3.21792	-3.45819
117	ENSG00000161714	PLCD3	-0.0262289	2.0367
118	ENSG00000187583	PLEKHN1	-0.147535	1.8976
119	ENSG00000088970	PLK1S1	1.95973	4.57429
120	ENSG00000102007	PLP2	-0.0386009	-1.37723
121	ENSG00000196576	PLXNB2	-1.98359	-1.50687
122	ENSG00000198883	PNMA5	9.47863	8.31221
123	ENSG00000125534	PPDPF	-3.07678	-3.77012
124	ENSG00000158528	PPP1R9A	-2.48739	-3.97276
125	ENSG00000067606	PRKCZ	-4.93217	-9.58747
126	ENSG00000172382	PRSS27	-3.31746	-1.16541
127	ENSG00000166450	PRTG	6.62681	6.6664
128	ENSG00000185920	PTCH1	-1.63494	-2.02721
129	ENSG00000183134	PTGDR2	5.45096	0.57303
130	ENSG00000060656	PTPRU	-4.90242	-4.84313
131	ENSG00000171813	PWWP2B	-3.00698	-4.99486
132	ENSG00000124839	RAB17	-8.60132	-8.19773
133	ENSG00000108352	RAPGEFL1	1.8461	0.859794
134	ENSG00000172819	RARG	-1.85861	-1.25435
135	ENSG00000146282	RARS2	1.33911	1.05495
136	ENSG00000100461	RBM23	-3.06197	-4.41692
137	ENSG00000072422	RHOBTB1	3.9087	2.40671
138	ENSG00000272327	RP11-1002K11.1	-4.63939	-4.29469
139	ENSG00000260296	RP11-395I6.3	3.08768	1.58948
140	ENSG00000205664	RP11-706O15.1	-4.03628	-2.46276
141	ENSG00000204117	RP4-640H8.2	6.09405	-1.3878
142	ENSG00000177189	RPS6KA3	1.17684	0.998945
143	ENSG00000040608	RTN4R	-3.79361	-7.14935
144	ENSG00000163191	S100A11	-0.434296	-1.10439
145	ENSG00000154447	SH3RF1	-2.1628	-0.303019
146	ENSG00000185187	SIGIRR	-3.41919	-5.29469
147	ENSG00000197119	SLC25A29	-2.91182	-1.21996
148	ENSG00000101276	SLC52A3	-0.995532	-1.16541
149	ENSG00000108576	SLC6A4	4.5997	0.759042
150	ENSG00000090020	SLC9A1	-0.691856	-0.821274
151	ENSG00000172123	SLFN12	-1.7325	-1.28088
152	ENSG00000124107	SLPI	-7.86749	-8.5228
153	ENSG00000227906	SNAP25-AS1	5.88411	3.66082
154	ENSG00000167780	SOAT2	5.12003	5.06135
155	ENSG00000168502	SOGA2	-3.97535	-1.1977
156	ENSG00000124766	SOX4	-3.25724	-0.0498778
157	ENSG00000134278	SPIRE1	-2.83633	-2.63886
158	ENSG00000144228	SPOPL	1.9966	1.10544
159	ENSG00000235374	SSR4P1	-4.05443	-4.70973
160	ENSG00000137868	STRA6	-3.7325	-2.06587
161	ENSG00000143502	SUSD4	-2.19193	-2.26227
162	ENSG00000197321	SVIL	-3.7747	-2.12258
163	ENSG00000101190	TCFL5	-2.84798	-3.21377
164	ENSG00000095627	TDRD1	4.74324	5.37109

165	ENSG00000029639	TFB1M	1.28131	1.51698
166	ENSG00000187720	THSD4	-7.10464	-4.25744
167	ENSG00000105289	TJP3	-6.00396	-6.33733
168	ENSG00000104953	TLE6	-4.12481	-5.78012
169	ENSG00000117500	TMED5	0.568013	0.992343
170	ENSG00000144120	TMEM177	0.98988	0.694703
171	ENSG00000106771	TMEM245	3.21037	2.62369
172	ENSG00000127863	TNFRSF19	5.90548	4.94114
173	ENSG00000158882	TOMM40L	1.62164	2.21163
174	ENSG00000115129	TP53I3	2.8356	3.85097
175	ENSG00000122779	TRIM24	2.2069	2.33593
176	ENSG00000163462	TRIM46	0.267502	0.727678
177	ENSG00000099282	TSPAN15	-1.50899	-2.85309
178	ENSG00000100300	TSPO	-1.56516	-1.26697
179	ENSG00000133985	TTC9	-3.83683	-4.29949
180	ENSG00000101162	TUBB1	0.621139	3.57156
181	ENSG00000198680	TUSC1	-4.15876	-4.86653
182	ENSG00000184787	UBE2G2	-1.43625	-1.46841
183	ENSG00000154914	USP43	-7.47396	-6.12927
184	ENSG00000155975	VPS37A	0.364799	1.74255
185	ENSG00000165171	WBSCR27	-5.43294	-3.50328
186	ENSG00000188064	WNT7B	-2.19193	-3.84723
187	ENSG00000160062	ZBTB8A	-3.05443	-2.97276
188	ENSG00000159733	ZFYVE28	-3.30235	-4.1503
189	ENSG00000122515	ZMIZ2	-0.586376	-0.127017
190	ENSG00000168916	ZNF608	-2.69597	-2.35127

Unique Genes**HCC31**(log2FC)

No.	Ensembl GeneID	Symbol	T	P5	P30
1	ENSG00000236078	AC095067.1	2.21046	2.68232	1.64289
2	ENSG00000008277	ADAM22	-1.0936	-0.0336044	-0.737331
3	ENSG00000102181	CD99L2	1.70832	2.02333	0.236686
4	ENSG00000176410	DNAJC30	0.541641	-0.372347	0.0931523
5	ENSG00000178498	DTX3	-1.55346	-1.86868	-3.18325
6	ENSG00000102034	ELF4	-0.940192	-5.30869	-5.83185
7	ENSG00000158220	ESYT3	-2.3045	-2.27307	-3.27016
8	ENSG00000175170	FAM182B	-1.24561	0.370786	-0.889335
9	ENSG00000133136	GNG5P2	1.39381	-1.00773	-0.55415
10	ENSG00000126945	HNRNPH2	0.704664	0.50155	0.889887
11	ENSG00000123496	IL13RA2	-2.12007	6.51609	4.6308
12	ENSG00000187242	KRT12	1.07632	7.95875	11.0274
13	ENSG00000005893	LAMP2	1.5192	0.346245	-0.565795
14	ENSG00000198786	MT-ND5	-1.19788	-2.96912	-1.2515
15	ENSG00000124479	NDP	-2.83057	4.69752	3.66321
16	ENSG00000196865	NHLRC2	-0.847521	-1.04875	-1.82861
17	ENSG00000125841	NRSN2	-1.44517	-1.69272	-1.78934
18	ENSG00000255642	PABPC1P4	1.93882	2.50829	1.74716
19	ENSG00000106443	PHF14	-0.649604	-1.24781	-1.26776
20	ENSG00000232160	RAP2C-AS1	2.222	2.13632	-0.145173
21	ENSG00000227354	RBM26-AS1	0.723589	0.147038	0.610534
22	ENSG00000047936	ROS1	1.84186	6.37259	-1.72584
23	ENSG00000267390	RP11-635N19.1	-0.151891	-2.88491	-3.26051

24	ENSG00000139508	SLC46A3	0.837206	-1.43352	-2.66879
25	ENSG00000135913	USP37	0.537771	0.692714	-1.07881
26	ENSG00000165238	WNK2	-4.94604	-4.25926	-3.32674
27	ENSG00000141040	ZNF287	-3.05296	-2.7585	-6.01862
28	ENSG00000151789	ZNF385D	-2.70504	3.63927	6.19039
29	ENSG00000197701	ZNF595	0.610005	-0.0580574	-1.14415
30	ENSG00000184635	ZNF93	-0.567533	-2.27307	-2.53319

Unique Genes**HCC68**(log2FC)

No.	Ensembl GeneID	Symbol	T	P5	P30
1	ENSG00000232320	AC009299.5	2.10122	1.46892	1.62766
2	ENSG00000001629	ANKIB1	3.1026	3.72782	3.22252
3	ENSG00000221838	AP4M1	3.51463	3.09443	2.14973
4	ENSG00000169188	APEX2	-1.76287	-0.924441	-1.15617
5	ENSG00000101844	ATG4A	-4.20977	-4.17465	-3.61443
6	ENSG00000106635	BCL7B	-1.97821	-1.40823	-1.75998
7	ENSG00000198908	BHLHB9	-0.443873	-0.704206	-2.69222
8	ENSG00000157456	CCNB2	2.6365	-1.19018	-0.641596
9	ENSG00000215039	CD27-AS1	-3.2898	-1.04378	-2.19068
10	ENSG00000130177	CDC16	-2.43024	-1.4065	-1.57687
11	ENSG00000181789	COPG1	-0.749147	-0.872021	-0.299222
12	ENSG00000261780	CTD-2354A18.1	8.22636	9.13313	9.70508
13	ENSG00000144677	CTDSPL	0.164566	1.50554	1.40524
14	ENSG00000008283	CYB561	-0.403516	-1.18343	-1.36329
15	ENSG00000136986	DERL1	-2.74996	-1.47349	-1.53498
16	ENSG00000088387	DOCK9	-1.43174	-2.56654	-2.74175
17	ENSG00000132394	EEFSEC	-1.35877	-2.23831	-1.47764
18	ENSG00000118407	FILIP1	3.26772	-3.67912	4.36196
19	ENSG00000157240	FZD1	4.85771	6.41535	6.35711
20	ENSG00000198746	GPATCH3	0.683067	0.439833	0.349023
21	ENSG00000134202	GSTM3	0.954676	-2.93501	-3.87863
22	ENSG00000110422	HIPK3	-1.80449	-1.71287	-2.29034
23	ENSG00000106211	HSPB1	-1.29606	-1.4266	-1.77434
24	ENSG00000063241	ISOC2	-4.82101	-12.5408	-10.2917
25	ENSG00000184611	KCNH7	3.05154	4.09047	4.4173
26	ENSG00000104731	KLHDC4	1.96352	0.169901	0.0353021
27	ENSG00000103550	KNOP1	3.90166	1.89209	2.59138
28	ENSG00000001631	KRIT1	2.57215	2.57871	1.68
29	ENSG00000188825	LINC00910	3.39102	2.1928	3.02137
30	ENSG00000164715	LMTK2	2.92523	2.22792	2.39972
31	ENSG00000161036	LRWD1	2.87427	1.07596	0.694287
32	ENSG00000180155	LYNX1	-3.43138	-7.15115	-5.90212
33	ENSG00000172264	MACROD2	3.07015	4.0427	4.61184
34	ENSG00000187601	MAGEH1	-4.81471	-6.94951	-5.11553
35	ENSG00000111196	MAGOHB	-1.85033	-1.31743	-1.87813
36	ENSG00000165175	MID1IP1	-2.45214	-4.68077	-5.37034
37	ENSG00000123562	MORF4L2	-1.53594	-2.36723	-1.54927
38	ENSG00000101888	NXT2	-1.99867	-2.18239	-1.72525
39	ENSG00000138617	PARP16	-2.71223	-2.06442	-1.83045
40	ENSG00000127980	PEX1	1.28371	1.85911	1.69363
41	ENSG00000101856	PGRMC1	-4.47208	-3.7759	-5.10689
42	ENSG00000136147	PHF11	-3.19765	-1.6173	-2.8204

43	ENSG00000099256	PRTFDC1	-0.871294	-0.52497	-0.364756
44	ENSG00000127993	RBM48	2.93348	2.88109	1.76893
45	ENSG00000013561	RNF14	-1.96562	-1.4791	-1.68148
46	ENSG00000231841	RP11-206F17.2	5.82915	0.431309	2.26529
47	ENSG00000261613	RP11-20I23.13	2.738	-3.41787	-6.25631
48	ENSG00000230291	RP11-244J10.1	-1.30014	-0.113012	0.136012
49	ENSG00000180211	RP1-278E11.3	-0.443873	0.782781	0.533846
50	ENSG00000102218	RP2	-2.26255	-1.24626	-1.62896
51	ENSG00000260121	RP5-1142A6.9	2.4003	-0.219003	-0.715596
52	ENSG00000235174	RPL39P3	-3.13279	-1.06901	-0.957269
53	ENSG00000224094	RPS24P8	-2.69442	0.875837	0.840467
54	ENSG00000185669	SNAI3	2.6365	-0.398766	1.92446
55	ENSG00000144867	SRPRB	-2.09907	-2.10664	-1.38378
56	ENSG00000235082	SUMO1P3	-0.755817	-0.171801	-0.0972752
57	ENSG00000133138	TBC1D8B	-2.38738	-8.56658	-6.85812
58	ENSG00000106638	TBL2	-0.34078	-0.753883	-1.09174
59	ENSG00000172465	TCEAL1	-1.13168	-4.95836	-4.50289
60	ENSG00000205356	TECPR1	3.28687	1.66775	1.35224
61	ENSG00000139173	TMEM117	-0.775717	-3.55688	-4.24646
62	ENSG00000175606	TMEM70	-3.0226	-2.36155	-2.05317
63	ENSG00000141510	TP53	-2.92574	-2.75179	-3.05502
64	ENSG00000167614	TTYH1	7.65696	1.12135	5.45784
65	ENSG00000175063	UBE2C	2.12871	-1.42113	-1.34204
66	ENSG00000094841	UPRT	-1.83619	-1.80107	-1.43041
67	ENSG00000187555	USP7	-1.25085	-1.02215	-0.590144
68	ENSG00000078668	VDAC3	-1.39486	-1.32427	-0.931907
69	ENSG00000131871	VIMP	-1.94993	-2.18343	-2.37818
70	ENSG00000006715	VPS41	1.33392	2.08283	1.65948
71	ENSG00000177485	ZBTB33	-2.96383	-1.98007	-2.08093
72	ENSG00000136247	ZDHHC4	-1.7767	-5.39213	-5.39945
73	ENSG00000063587	ZNF275	-3.37473	-7.20141	-4.84547
74	ENSG00000169955	ZNF747	-1.57295	-4.31871	-4.99307
75	ENSG00000196453	ZNF777	-0.540089	-0.537995	-0.723374
76	ENSG00000198556	ZNF789	3.13825	2.12525	1.68924
77	ENSG00000197037	ZSCAN25	4.05821	2.36125	1.63658